SLAM/SAP signaling regulates discrete γδ T cell developmental checkpoints and shapes the innate-like γδ TCR repertoire

Somen K Mistri[1], Brianna M. Hilton[1], Katherine J. Horrigan[1], Emma S. Andretta[1], Remi Savard[1], Oliver Dienz[1], Kenneth J Hampel[2], Diana L. Gerrard[2], Joshua T. Rose[2], Nikoletta Sidiropoulos[2], Devdoot Majumdar[1], and Jonathan E. Boyson[*1]

[1]Department of Surgery, Larner College of Medicine, University of Vermont, Burlington, Vermont 05405, USA

[2]Department of Pathology and Laboratory Medicine, Larner College of Medicine, University of Vermont Medical Center, Burlington, Vermont 05405, USA

*Corresponding Author

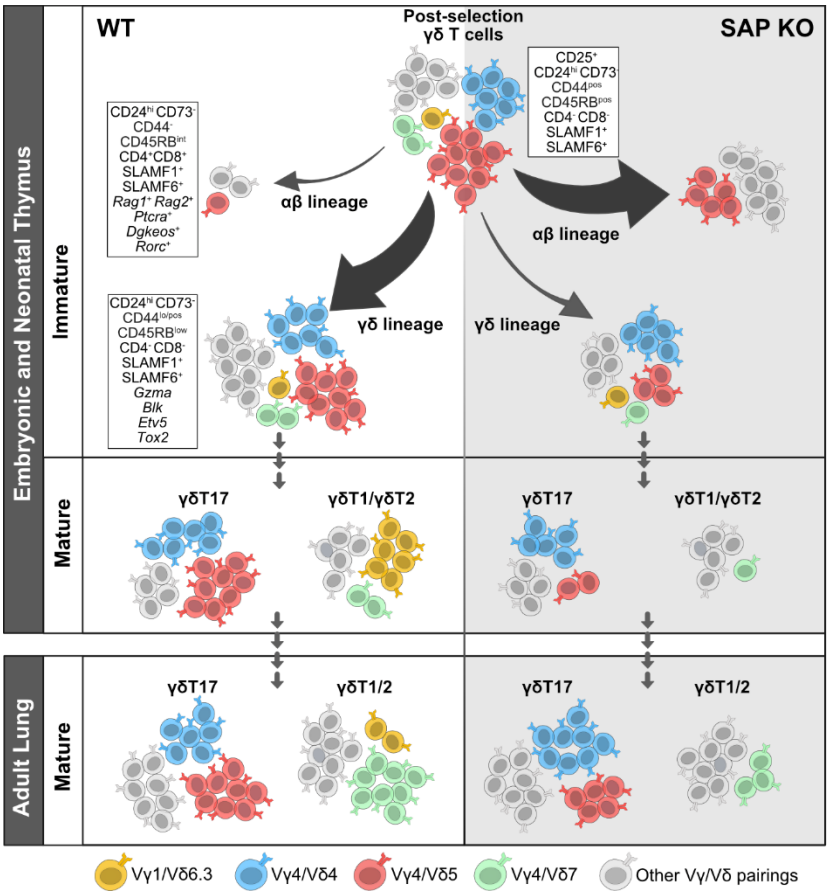

- SAP deficiency results in diversion of γδ T cells to the αβ T cell lineage
- SAP deficiency results in a loss of immature *Gzma*⁺*Blk*⁺*Etv5*⁺*Tox2*⁺ γδT17 precursors
- Identification of Vγ4/Vδ7 γδT1 cells as a novel SAP-dependent innate-like T cell subset

15

16 **Abstract**

17 During thymic development, most γδ T cells acquire innate-like characteristics that are critical for
18 their function in tumor surveillance, infectious disease, and tissue repair. The mechanisms,
19 however, that regulate γδ T cell developmental programming remain unclear. Recently, we
20 demonstrated that the SLAM-SAP signaling pathway regulates the development and function of
21 multiple innate-like γδ T cell subsets. Here, we used a single-cell proteogenomics approach to
22 identify SAP-dependent developmental checkpoints and to define the SAP-dependent γδ TCR
23 repertoire. SAP deficiency resulted in both a significant loss of an immature
24 *Gzma*$^{+}$*Blk*$^{+}$*Etv5*$^{+}$*Tox2*$^{+}$ γδT17 precursor population, and a significant increase in *Cd4*$^{+}$*Cd8*$^{+}$
25 *Rorc*$^{+}$*Ptcra*$^{+}$*Rag1*$^{+}$ thymic γδ T cells. SAP-dependent diversion of embryonic day 17 thymic γδ T
26 cell clonotypes into the αβ T cell developmental pathway was associated with a decreased
27 frequency of mature clonotypes in neonatal thymus, and an altered γδ TCR repertoire in the
28 periphery. Finally, we identify TRGV4/TRAV13-4(DV7)-expressing T cells as a novel, SAP-
29 dependent Vγ4 γδT1 subset. Together, the data suggest that SAP-dependent γδ/αβ T cell lineage
30 commitment regulates γδ T cell developmental programming and shapes the γδ TCR repertoire.

31 **Introduction**

32 Like αβ T cells, γδ T cells can be broadly grouped into innate-like IFN-γ-producing γδT1,
33 IL-4-producing γδT2, or IL-17-producing γδT17 subsets that are programmed during thymic
34 development[1, 2, 3, 4], or inducible subsets that differentiate in the periphery[5]. The innate-like γδ T
35 cells are unconventional T cells that are highly enriched in mucosal tissues such as the skin, gut,
36 and lung and that play critical roles in the host response to pathogens, in tumor surveillance, and
37 in autoimmunity[6]. The mechanisms, however, that determine whether a developing γδ T cell
38 acquires an innate-like phenotype during thymic development remain unclear.

39 A significant body of data supports a model in which weak or strong TCR signal strength
40 might contribute to the development of innate-like γδT17 (weak signal) and γδT1 (strong signal)
41 subsets[4, 7, 8, 9, 10], and a strong TCR signal has been suggested to be necessary for the development
42 of the IFN-γ and IL-4 producing γδNKT cell subset[11]. However, there is also evidence of a TCR-
43 independent model in which pre-existing hard-wired transcriptional programs regulate the
44 development of some innate-like γδT17 subsets[12], and accumulating data suggest that γδT17
45 programming is associated with the use of distinct signaling pathways[13, 14, 15].

46 SLAM family receptors comprise a family of nine receptors, SLAMF1 (SLAM; CD150),
47 SLAMF2 (CD48), SLAMF3 (Ly9; CD229), SLAMF4 (2B4; CD244), SLAMF5 (CD84),
48 SLAMF6 (Ly108; CD352), SLAMF7 (CRACC; CD319), SLAMF8 (BLAME), and SLAMF9
49 (SF2001; CD84H), that are expressed primarily on hematopoietic cells and which play diverse
50 roles in immune development and function[16]. Most SLAM family receptors interact in a
51 homophilic manner, the exception to this rule being SLAMF4 which serves as the ligand for
52 SLAMF2. SLAM family receptor signals can be both activating or inhibitory, depending on the
53 recruitment of the cytosolic signaling adapter proteins SAP and EAT-2, and inhibitory SHP-1,

54 SHP-2, or SHIP phosphatases to immunoreceptor tyrosine switch motifs in the SLAM family
55 receptor cytoplasmic domain[16]. Although SLAM/SAP signaling has long been known to play a
56 role in innate-like NKT[17] and γδNKT[11] cell development, recent findings from multiple groups
57 demonstrating that this pathway is also involved in the development of innate-like γδT1, γδT17[18]
58 and innate-like MAIT cells[19, 20] indicates that SLAM/SAP signaling plays a fundamental role in
59 the development of a majority of the innate-like T cell lineages.

60 In this study, we set out to define the stage of thymic development during which SAP
61 mediates its effect on γδ T cell developmental programming and to define SAP-dependent changes
62 in the γδ T cells transcriptional program during their development. Finally, since SAP-dependent
63 innate-like T cell subsets are often characterized by highly restricted TCRs (e.g., $V\gamma1^+/V\delta6.3^+$
64 γδNKT[21]), we wished to identify whether specific TCR clonotypes were also associated with SAP-
65 dependent γδT1 and γδT17 T cells. Therefore, we utilized a single-cell proteogenomics approach
66 with V(D)J profiling that allowed us to simultaneously compare cell surface protein expression,
67 gene expression, and TCR clonotypes between B6 and B6.$SAP^{-/-}$ γδ T cells from embryonic,
68 neonatal, and adult thymus, as well as from peripheral lung γδ T cells. Collectively, these data
69 provide a comprehensive map of the SAP-dependent γδ T cell subsets and their developmental
70 checkpoints in perinatal and adult thymus.

71 **Results**

72 *SLAM family receptor expression marks transcriptionally distinct developmental stages among*
73 *E17 γδ T cells*

74 γδT17 developmental programming is thought to occur primarily during
75 embryonic/neonatal thymic development[2, 12, 22], and is tightly linked to the expression of discrete
76 TCR gamma and delta pairings[23]. To identify the specific developmental stages of thymic
77 development during which SLAM/SAP signaling pathway exerts its effects, we employed a single-
78 cell RNAseq approach coupled with feature barcoding (i.e., CITEseq[24]) and V(D)J profiling to
79 compare embryonic day 17 (E17) B6 and B6.SAP$^{-/-}$ thymic γδ T cells (**Fig. 1A**). FACS-sorted
80 thymic γδ T cells (**Suppl. Fig. 1**) from individual embryos (n = 4 B6 and 4 B6.SAP$^{-/-}$ mice) were
81 identified using hashtags, and Vγ1^{+} and Vγ4^{+} γδ T cells were identified using barcoded antibodies
82 (ADTs). To help define the developmental trajectories of the E17 γδ T cells, we also stained cells
83 with barcoded antibodies specific for CD24, CD73, CD44, and CD45RB which define distinct
84 developmental pathways of γδT17 and γδT1 cells in the thymus[4, 25, 26], as well as for SLAMF1 and
85 SLAMF6. After data filtering and QC, we verified that clusters were evenly distributed among the
86 biological replicates (**Suppl. Fig. 1**). The resulting dataset represented a total of 5278 thymic γδ T
87 cells from B6 (n = 2597) and B6.SAP$^{-/-}$ (n = 2681) γδ T cells. Data were visualized using uniform
88 manifold approximation and projection (UMAP) for dimensionality reduction and a graph-based
89 clustering approach[27].

90 First, we annotated the B6 dataset using a combination of cell surface protein expression,
91 gene expression, and TCR clonotype sequence. This analysis revealed 11 B6 E17 γδ T cell clusters,
92 mostly distributed between two major branches (**Fig. 1B**). We observed the presence of
93 CD24^{low}73^{low}44^{high}45RB^{low}SLAMF1^{pos} (c8) and CD24^{low}73^{high}44^{high}45RB^{high}SLAMF6$^{low/pos}$ (c0,

94 c9) clusters, consistent with mature γδT17 phenotype and γδT1 phenotypes, respectively (**Fig. 1C,**
95 **Suppl. Fig. 1).** In support of this annotation, the c8 cluster was enriched in *Il17a*, *Il17f, Il23r,*
96 *Rorc*, and TRGV6/TRDV4 (IMGT nomenclature; encoding Vγ6/Vδ1) transcripts with limited
97 CDR3 diversity, while the c0/c9 cluster was enriched in *Ifng*, *Tbx21, Klrd1*, *Il2rb, Xcl1,* and
98 TRGV5/TRDV4 (encoding Vγ5/Vδ1) transcripts also with little to no diversity (**Figs. 1D – F,**
99 **Suppl. Fig. 2, Suppl. Tables 1 and 2**)[28, 29]. Consistent with previous observations[18], we noted that
100 the c0/c9 cluster was highly enriched in *Cd244a* (*Slamf4*), and was also enriched in transcripts
101 from another SLAM family member, *Slamf7* (**Figs. 1D - E**). Flow cytometric analysis confirmed
102 that SLAMF7 was expressed primarily on mature γδ T cells and that its expression was mostly
103 confined to γδ T cells expressing the canonical $CD44^{+}CD45RB^{+}$ markers of γδT1 cells (**Suppl.**
104 **Fig. 1**)[4, 30].

105 We identified a small $CD24^{low/int}73^{high}44^{high}45RB^{pos}$ c3 cluster characterized by enrichment
106 in *Cd200* (whose expression is upregulated upon TCR ligation[31]), *Il2rb, Nr4a1, Cd244a*, *Xcl1,* and
107 *Tnfrsf9* (encoding 4-1bb receptor). A high frequency of invariant TRGV5/TRDV4 clonotypes and
108 decreased TCR clonotype diversity (**Suppl. Fig. 2, Suppl. Table 2)** suggested that c3 represented
109 an immature γδT1 population. The $CD24^{low/pos}CD73^{low/pos}44^{low/pos}CD45RB^{low/pos}$ c4 cluster was
110 enriched in *Ms4a4b and Ms4a6b (*encoding CD20 homologues that modulate T cell activation[32,
111 33]), *S1pr1*, *Il6ra, Cd8a, Cd8b1,* and *Ccr9,* suggesting that the c4 cluster represents the previously
112 described emigrating thymic $Ccr9^{+}$ $S1pr1^{+}$ γδ T cells[34] (**Fig. 1C and 1E**). Consistent with the c4
113 cluster representing naïve emigrating thymic γδ T cells, the diversity of the c4 TCR clonotypes
114 was the highest among the $CD24^{low/int}$ (c0/c9, c8, c3) clusters (**Suppl. Fig. 2).**

115 We identified several immature $CD24^{high}CD73^{neg}$ ADT clusters (c1, c2, c7, c5, c6, and c10)
116 that also expressed SLAMF1 and/or SLAMF6 (**Fig. 1B and Suppl. Fig 1**). The c1 and c2 clusters

117 were enriched in γδT17-associated genes such as *Blk, Maf, Sox13, Ccr2, Tcf12, and Rorc*[26, 35, 36,
118 37, 38], as well as *Sh2d1a* (encoding SAP) and *Ccr9*[10] **(Fig. 1E, Suppl. Table 1)**. Within these two
119 clusters, the CD44$^{low/pos}$CD45RB^{low} c2 cluster was especially enriched in genes previously
120 implicated in γδ T cell development such as *Etv5, Tox, Sox4, Tcf7*, *Zbtb16* [38, 39, 40, 41, 42], *Igfbp4* and
121 *Igf1r* which were recently implicated in Th17 differentiation[43], *Tnfsf11* (RANKL) which regulates
122 Aire^{+} mTEC development [44], as well as *Themis* and *Tox2* **(Fig. 1E, Suppl. Fig. 1)**. A high level of
123 *Gzma* expression identified c2 as the previously described *Gzma*$^{+}$ γδ T cell subset[34]. Interestingly,
124 although enriched in genes associated with a γδT17 signature, the c2 cluster was also enriched in
125 γδT2-associated *Gata3* and *Il4* transcripts (**Fig. 1D – E, Suppl. Table 1**). The
126 CD44$^{low/pos}$CD45RB^{neg} c1 cluster, in contrast, exhibited significantly higher levels of *Il17a, Il17f,*
127 *Rorc*, *Maf* [36], as well as *Ifngr1,* consistent with the c1 cluster representing immature γδT17 cells
128 (**Fig. 1D – E, 1G, and Suppl. Fig. 1**).

129 Analysis of the c1 and c2 TCR transcripts revealed that the c2 cluster was notably enriched
130 in TRGV4-expressing cells and that 87% of Vγ4 T cells utilized just 3 TRDV chains (50%
131 TRDV5, 24% TRDV2-2, and 12% TRAV13-4/DV7) (**Fig. 1F, Suppl. Table 2**). Clonotype
132 analysis revealed a high frequency of semi-invariant TRGV4/TRDV5 and TRGV4/TRDV2-2
133 clonotypes previously associated with γδT17[45, 46, 47] (**Suppl. Fig. 2, Suppl. Table 2**). In contrast,
134 the c1 cluster possessed comparatively fewer of these TRGV4 clonotypes, and was enriched in
135 TRGV6, TRGV5, and TRGV1 paired with TRDV4 (**Suppl. Fig. 2, Suppl. Table 2)**. Indeed, we
136 noted that the Vγ1 repertoire, which is diverse in adult tissues, was dominated by TRGV1/TRDV4
137 clonotypes (35% of all TRGV1) in E17 thymus, and just two closely related semi-invariant
138 TRGV1/TRDV4 clonotypes comprised 17.4% of all TRGV1. The location of these clonotypes in

139 the immature γδT17-related clusters (**Suppl. Fig. 2)** suggested that they represent the dominant
140 IL-17-producing Vγ1 clonotypes at E17, which we verified using flow cytometry (**Suppl. Fig. 3**).
141 Since the IL-4-producing Vγ1/Vδ6.3 γδNKT cell subset has been shown to develop in fetal
142 thymus[1], we asked whether the *Il4*-enriched γδ T cells in cluster 2 (**Fig. 1D**) were immature Vγ1
143 γδNKT cells with previously identified canonical Vδ6.3 sequences[21]. Interestingly, while we did
144 identify a small number of Vγ1 T cells with these canonical sequences (encoded by TRAV15-
145 1/DV6-1 or TRAV15N-1) in our dataset, these were not present in the *Il4*-enriched c2 cluster.
146 The $CD44^{pos}CD45RB^{pos}$ c5 cluster was enriched in *Il2ra*, *Scin, Bex6, Cd5, Slamf6, Cd28,*
147 *Hivep3*, and cell-cycle/metabolism genes, consistent with γδ T cells that have recently developed
148 from DN2/DN3[34, 48, 49]. Within the c5 and c7 clusters, we noted that while there was expression of
149 γδT17-associated genes such as *Blk, Maf, Sox13,* and *Etv5*, there was relatively little *Rorc*
150 expression. *Rorc* expression became apparent in the c2 cluster (*Rorc*^{low}) and was significantly
151 increased in the c1 cluster (**Suppl. Fig. 1)**. Flow cytometric analysis confirmed BLK and PLZF
152 expression in $CD25^{high}$ E17 Vγ4 T cells, while RORγt expression was primarily observed in the
153 $CD25^{neg}$ population, suggesting that BLK is expressed soon after γδ T cell selection, followed by
154 RORγt (**Suppl. Fig. 3)**. These data were consistent with MAF-directed expression of *Rorc*[34, 36]
155 and suggested a c5 – c7 – c2 – c10 / c1 – c8 γδT17 developmental trajectory, which was supported
156 by trajectory inference analysis **(Fig. 1H).**
157 Finally, analysis of the $CD24^{high}73^{neg}44^{neg}45RB^{int}SLAMF1^{pos}SLAMF6^{pos}$ c6 population
158 revealed that it was highly enriched in *Cd8a, Cd8b1, Cd4, Rag1, Rag2, Ptcra, Arpp21, and*
159 *Dgkeos,* consistent with cells developing along the αβ T cell lineage **(Figs. 1E, 1G, Suppl. Fig. 1,**
160 **and Suppl. Table 1**)[50]. Analysis of the Vγ1 and Vγ4 ADTs confirmed that c6 cells were not simply
161 contaminating αβ T cells as both Vγ1- and Vγ4-expressing cells were present in the c6 cluster

162 **(Suppl. Fig. 3**) and analysis of the c6 TCR clonotypes revealed the presence of TRGV1, GV4,
163 GV5, GV6, and GV7 clonotypes, none of which appeared to be specific to the c6 cluster (**Suppl.**
164 **Table 2)**.

165 Since trajectory inference analysis suggested a strong relationship between the *Il2ra*$^{+}$ c5
166 and c6 clusters (**Fig. 1H**), we conducted differential gene expression analysis between the c5 and
167 c6 from B6 mice. Interestingly, we found that the c6 cluster was highly enriched in *Rorc,*
168 suggestive of a γδT17 phenotype, but was mostly lacking in the expression of *Maf, Blk, Ccr2*, and
169 other canonical γδT17-associated transcripts (**Fig. 1E, 1G, and Suppl. Fig. 1**). Indeed, flow
170 cytometric analysis of E17 TCRβ^{neg}TCRδ^{pos} γδ T cells confirmed that CD4CD8 DP γδ T cells
171 exhibited an immature CD44^{low}CD25^{low}MAF^{neg}BLK^{neg}RORγt^{pos} phenotype (**Suppl. Fig. 3**), and
172 that RORγt expression in the absence of BLK or MAF is a characteristic of Lin^{neg} DN thymocytes
173 as they progress from CD44^{low}25^{high} DN3 to CD44^{low}25^{low} DN4 (**Suppl. Fig. 3**). Together, these
174 data suggested that the c6 cluster γδ T cells represented previously described CD4CD8 DP γδ T
175 cells that were developing along an alternative αβ T cell pathway[51, 52, 53].

176

177 *SAP regulates γδ T cell clonotype diversion into both the γδT17 and the αβ T cell developmental*
178 *pathways.*

179 To identify SAP-dependent developmental checkpoints, we next compared the hashtag-
180 separated B6 and B6.SAP$^{-/-}$ E17 γδ T cell datasets. A comparison of the cluster frequencies
181 between B6 and B6.SAP$^{-/-}$ γδ T cells revealed significantly decreased frequencies of the
182 CD24^{high}73^{neg}44^{int}45RB^{int}SLAMF1^{pos}SLAMF6^{pos} c2 and c1 clusters in B6.SAP$^{-/-}$ mice, and a
183 striking increase in the frequency of the CD24^{high}73^{neg}44^{neg}45RB^{neg}SLAMF1^{high}SLAMF6^{high} c6
184 cluster (**Fig. 2A)**. A comparison of differentially expressed genes among the immature (c1, c2, c7,

185 c5, c6, and c10) clusters using pseudobulk analysis revealed 234 differentially expressed genes
186 with a p_{adj} threshold < 0.005 and log_2 fold change greater than 0.5, with 148 genes exhibiting
187 decreased expression in B6.SAP$^{-/-}$ γδ T cells, and 86 genes exhibiting increased expression (**Fig.**
188 **2B, Suppl. Table 3**). Consistent with the decreased frequencies of the c1/c2 clusters in B6.SAP$^{-/-}$
189 mice, a significant fraction of the differentially expressed genes that were down-regulated in
190 B6.SAP$^{-/-}$ mice reflected γδT17-associated genes (e.g., *Maf, Blk, Ccr2, Sox13, Etv5, etc.*) that were
191 present in the c2 and c1 clusters, as well as a number of c1/c2-enriched genes (e.g., *Cpa3, Tox2,*
192 *Pdcd1, Tmem121, Bex6*, and *Scin*) whose importance in γδ T cell development is unclear (**Fig. 2B-**
193 **C, Suppl. Table 2**). This was not solely due to the decreased frequency of the c2 and c1 clusters
194 in B6.SAP$^{-/-}$ mice, as a closer analysis revealed a decreased number of transcripts for many
195 signature genes (e.g., *Blk*, *Etv5*, *Ccr2*) prevalent in the c2 cluster and to a lesser extent the c7
196 cluster **(Suppl. Fig. 4**). In contrast, a large number of genes whose expression was significantly
197 increased in B6.SAP$^{-/-}$ mice were those whose expression was mostly confined to the c6 cluster
198 (e.g., *Cd4, Cd8b1, Ptcra, Rag2*) or whose expression was highest in c6 (e.g., *Tcf7, Thy1*)(**Fig. 2B-**
199 **C, Suppl. Fig. 4)**. Together, these data identified the *Gzma*$^+$*Etv5*$^+$*Sox13*$^+$*Blk*$^+$*Tox2*$^+$ c2 and
200 *Cd4*$^+$*Cd8b1*$^+$*Ptcra*$^+$*Rag2*$^+$ c6 clusters as SAP-dependent developmental checkpoints.

201 Next, we asked whether these SAP-dependent alterations in γδ T cell development were
202 associated with any changes in the TCR repertoire. A comparison of all γδ TCR clonotypes
203 between E17 B6 and B6.SAP$^{-/-}$ γδ T cells revealed no significant changes in overall clonotype
204 frequency (**Fig. 2D**). However, a closer examination of TCR repertoire revealed significant
205 changes in the distribution of specific TCR clonotypes. For example, within the TRGV4 repertoire,
206 which represents the dominant TCR among immature clusters at E17, we observed a significant
207 decrease in TRGV4/TRDV5 clonotypes in the c2 cluster and a concomitant increase of these

208 clonotypes in the c6 cluster (**Fig. 2E**). Among the TRGV4 clonotypes, this appeared to be specific
209 to the TRDV5 clonotypes, as we observed no significant differences c2 and c6 frequencies among
210 TRGV4/TRDV2-2 and TRDV7 clonotypes (**Fig. 2E**). We did note, however, a significant increase
211 in the TRGV4/TRDV7 clonotypes in the *Il2ra*$^{+}$ c5 cluster (**Fig. 2E**). Within the TRGV1 repertoire,
212 we noted a significant increase in TRGV1/TRDV4 clonotypes within the c6 cluster (**Fig. 2E**).
213 Together, these data suggested that SAP operated at an early stage of γδ T cell development during
214 or soon after the down-regulation of *Il2ra,* and that it positively regulated entry into the γδT17
215 pathway at the c5/c7 to c2 transition, while at the same time inhibiting entry into the CD4^{+}CD8^{+}
216 αβ T cell-like c6 cluster. The net result of these changes appeared to be that specific TCR
217 clonotypes such as TRGV4/TRDV5 were diverted from the γδT17 pathway into the αβ T cell-like
218 pathway.
219
220 *SAP deficiency is associated with increased numbers of immature CD4^{+}CD8^{+}RORγt^{+} thymic γδ*
221 *T cells*
222 Next, we independently evaluated these observations using flow cytometry. This analysis
223 revealed that while SAP deficiency did not affect the overall number of E17 γδ T cells (**Suppl.**
224 **Fig. 5**), it did result in a significant decrease of immature CD24^{pos}BLK^{pos}MAF^{pos}RORγt^{pos} γδ T
225 cells in E17 B6.SAP$^{-/-}$ thymus (**Fig. 3A-B**). We found that this decrease was most pronounced in
226 the CD44^{pos} population after downregulation of CD25 (**Fig 3A, Suppl. Fig. 5**) and that this
227 population exhibited a high level of PLZF expression, suggesting it corresponded to the
228 CD44^{+}*Blk*$^{+}$*Maf*$^{+}$*Zbtb16*$^{+}$*Rorc*$^{+}$ c1 cluster (**Suppl. Fig. 5**). In addition, UMAP analysis of E17 Vγ4
229 T cells flow cytometric data revealed the presence of a SAP-dependent
230 CD24^{pos}BLK^{pos}PLZF^{pos}RORγt^{neg} population in B6.SAP$^{-/-}$ thymus **(Suppl. Fig. 5**) consistent with

231 the phenotype of the c2 cluster which expressed lower levels of *Rorc*. In contrast, we found no
232 evidence of a SAP-dependent decrease in the CD25^{pos} population frequency, consistent with the
233 notion that SAP exerts its effect during or after this stage of development (**Fig. 3A**). We also noted
234 that in addition to its effect on the numbers of immature thymic γδT17, SAP deficiency resulted
235 in the reduced expression levels of some of these markers, most notably BLK (**Fig. 3C**), a finding
236 that was consistent with the decreased number of *Blk* transcripts observed in Fig. 2. Interestingly,
237 as PLZF induction is often associated with SLAM/SAP signaling, we noted that SAP did not affect
238 overall PLZF expression levels in E17 thymic γδ T cells (**Suppl. Fig. 5**).

239 In contrast to the decreased numbers of CD24^{pos}BLK^{pos}MAF^{pos}PLZF^{pos} RORγt^{pos} γδ T
240 cells, we observed a significant increase in the frequency and number of
241 CD24^{pos}BLK^{neg}MAF^{neg}PLZF^{neg}RORγt^{pos} γδ T cells (**Figs. 3A-B**), whose phenotype was consistent
242 with the αβ T cell-like c6 cluster in Fig. 2. Consistent with our finding that the c6 cluster was
243 enriched in CD4 and CD8, we found that the frequency and number of CD4 and CD8-expressing
244 CD24^{pos} TCRδ^{pos}TCRβ^{neg} BLK^{neg}MAF^{neg}RORγt^{pos} thymic γδ T cells was significantly increased
245 in B6.SAP$^{-/-}$ mice (**Fig. 3D**). Together, these analyses confirmed our single-cell CITEseq analysis,
246 and suggested that SAP regulated both the throughput of immature γδ T cells in the γδT17 cell
247 pathway as well as the αβ T cell-like pathway. More specifically, the data suggested that SAP
248 promoted progression to the CD24^{pos} BLK^{pos}MAF^{pos}PLZF^{pos}RORγt^{low} c2 cluster that is enriched
249 in a number of genes (e.g., *Sox13, Etv5, Blk, Maf)* known to regulate γδT17 development, but that
250 it inhibited entry into the CD24^{pos}44^{neg}BLK^{neg}MAF^{neg}RORγt^{pos} αβ−T cell-like pathway (c6
251 cluster).
252

253 *Identification of SAP-dependent developmental checkpoints during neonatal and adult thymus γδ*
254 *T cell developmental programming.*

255 The neonatal period is a time of rapid expansion of numerous γδ T cell subsets in the
256 thymus including Vγ4 γδT17 and γδNKT. Therefore, we conducted a comparison between B6 and
257 B6.SAP$^{-/-}$ neonatal as well as adult thymic γδ T cells to both identify novel SAP-dependent
258 developmental checkpoints and to track the outcome of the SAP-dependent alterations in γδ T cell
259 development observed in E17 thymus. Neonate datasets revealed a similar branched clustering
260 pattern as in E17 with some notable differences. Similar to E17, we observed immature
261 CD24^{pos}73^{low}SLAMF1^{pos}SLAMF6^{pos} clusters (c0, c1, c2, c3, c9, c12, c14),
262 CD24^{pos}73$^{low/pos}$SLAMF1^{pos}SLAMF6^{pos} (c4, c5, c10, c15) *S1pr1*-enriched "naïve" clusters,
263 mature CD24^{neg}73^{low}SLAMF1^{pos}SLAMF6^{neg} (c6, c7) γδT17 clusters, and a mature
264 CD24^{neg}73^{pos}SLAMF1^{neg}SLAMF6$^{low/pos}$*Slamf7*^{high} (c8) γδT1 cluster (**Fig. 4A-B**, **Suppl. Fig. 6)**. In
265 general, we noted good correlation with cluster-specific gene expression between the E17 and D9
266 (Day 9) datasets. A notable exception was a striking decrease in *Zbtb16* expression among all
267 immature neonatal γδ T cells, which is consistent with previous reports[10, 34] (**Suppl. Fig. 6, Suppl.**
268 **Table 3**).

269 In contrast to the E17 dataset, the neonatal thymic γδ T cell dataset contained a
270 CD24^{neg}73^{pos}SLAMF1^{neg}SLAMF6^{high}*Slamf7*^{neg} (c13) γδT2 cluster enriched in *Il4, Il13, Zbtb16,*
271 *Cd40lig*, and *Nos1* (**Suppl. Fig. 6, Suppl. Table 1),** suggesting it represented IL-4-producing
272 γδNKT cells. Indeed, examination of the γδT2 (c13) and γδT1 (c8) cluster TCR repertoires
273 revealed a significant enrichment of canonical TRGV1 and TRAV15N-1 or TRAV15-1/DV6-1
274 sequences characteristic of γδNKT cells (**Fig. 4C, Fig. 5**)[21]. Analysis of the differentially
275 expressed genes in the γδT1 (c8) and γδT2 (c13) clusters revealed that *Zbtb16*, *Icos,* and *Slamf6*

276 were markers of γδT2 cells while *Tbx21*, *Klrb1c* (NK1.1), and *Slamf7* were markers of γδT1 cells
277 in neonatal thymus (**Suppl. Fig. 6**). Flow cytometric analysis confirmed that PLZF^{hi} γδT2
278 Vγ1Vδ6.3 cells co-express SLAMF6 and ICOS while Tbet^{hi} γδT1 Vγ1Vδ6.3 cells are NK1.1^{+} and
279 are either SLAMF6^{-}SLAMF7^{+} or SLAMF6^{+}SLAMF7^{+} **(Suppl. Fig. 7)**.

280 A comparison of B6 and B6.SAP$^{-/-}$ neonatal γδ T cells revealed multiple SAP-dependent
281 changes in clustering. Among the immature γδ T cells, we observed a decreased frequency of the
282 immature CD24^{high}73^{neg}SLAMF1^{pos}SLAMF6^{pos} c1 cluster (**Fig. 4D**) that was enriched in *Blk, Etv5,*
283 *Sox13, Rorc,* and *Maf* (**Suppl. Fig. 6**), suggesting it was analogous to the SAP-dependent c2
284 cluster in E17 γδ T cells. Similar to our observations in E17 γδ T cells, flow cytometric analysis
285 confirmed both a decrease in BLK^{pos}RORγt^{pos} and BLK^{pos}RORγt^{neg} γδ T cell populations, as well
286 as a decreased level of BLK expression (**Fig. 4E-F**). In addition, we observed an increased
287 frequency of immature CD24^{high}73^{neg}SLAMF1^{pos}SLAMF6^{pos} cluster with characteristics of αβ T
288 cells (c14) in B6.SAP$^{-/-}$ D9 thymic γδ T cells **(Fig. 4D, Suppl. Fig. 6**). While this increase did not
289 reach the level of significance, presumably due to the very low number of c14 cells in the dataset,
290 flow cytometric analysis revealed a significant increase in immature CD24^{pos}73^{neg}BLK^{neg}RORγt^{pos}
291 γδ T cells, a phenotype consistent with γδ T cells that have been diverted to the αβ developmental
292 pathway (**Fig. 4E**). Last, we observed an increased frequency of immature CD24^{pos}73$^{low/pos}$
293 SLAMF1^{pos}SLAMF6^{pos} *S1pr1*-enriched c4 and c5 clusters, but not the closely related *Cd200*-
294 enriched c10 cluster (**Fig. 4D).** While we did confirm an increased number CD200^{neg}S1pr1^{pos} γδ
295 T cells in neonatal thymus by flow cytometry, this increase was relatively small and its significance
296 is unclear **(Suppl. Fig. 7).** Independent confirmation of these SAP-dependent changes in neonatal
297 γδ T cell gene expression was obtained by conducting bulk RNAseq analysis of FACSs-sorted
298 CD24^{high} neonatal thymic γδ T cells from B6 and B6.SAP$^{-/-}$ mice (**Suppl. Table 4**).

299 Among the mature neonatal γδ T cells, we observed a decreased frequency of the
300 CD24^{low}73^{neg}SLAMF1^{pos}F6^{low} γδT17 c6 cluster which was consistent with our previous
301 observation of decreased IL-17 production in B6.SAP$^{-/-}$ neonatal γδ T cells[18]. Interestingly, we
302 observed a striking loss of the CD24^{low}73^{high}SLAMF1^{low}F6^{high}F7^{neg} γδT2 c13 cluster in B6.SAP$^{-/-}$
303 mice, as well as a decreased frequency of the mature CD24^{low}73^{high}SLAMF1^{low}F6^{low}F7^{high} γδT1
304 c8 cluster (**Fig. 4A - D**). These findings were consistent with a SAP-dependent loss of both the IL-
305 4- and IFN-γ-producing γδNKT as well as non-γδNKT γδT1 cells (discussed further below).
306 Unfortunately, while we were able to define mature SAP-dependent γδNKT subsets, we found no
307 evidence of immature γδNKT cells in our dataset, suggesting that they develop during a brief
308 developmental window between E17 and D9 after birth.

309 A comparison of B6 adult thymic γδ T cells between B6 and B6.SAP$^{-/-}$ mice recapitulated
310 many of our observations of the neonatal thymus, although to a somewhat lesser degree. For
311 example, we observed a small but significant decrease in the frequency of the CD24^{high}CD73^{low}
312 adult thymic c1 and c2 clusters in B6.SAP$^{-/-}$ mice that was coupled with an increased frequency of
313 the CD24^{pos}CD73$^{+/-}$ c0 cluster **(Suppl. Fig. 8)**. Like the SAP-dependent E17 c2 and D9 c1 clusters,
314 the adult thymus c1 and c2 clusters were enriched in γδT17-associated *Blk, Etv5, Sox13*, *Maf,* and
315 *Rorc* (mostly in c2) indicating that SAP regulates this γδ T cell thymic developmental checkpoint
316 at all ages. Likewise, the adult thymus c0 cluster that was increased in B6.SAP$^{-/-}$ mice was enriched
317 in *Ms4a4b, Ms4a6b, Dgka, Klf2,* and *S1pr1* similar to the neonatal c4 and c5 clusters whose
318 frequencies were increased in B6.SAP$^{-/-}$ γδ T cells. Just as we observed in neonatal thymic γδ T
319 cells, we noted a near complete loss of mature γδNKT cells (*Zbtb16, Icos*, and *Il4*-enriched γδT2
320 c8 cells and *Tbx21, Slamf7*, and *Il2rb*-enriched γδT1 c11 cells) as well as a decreased frequency
321 of mature non-γδNKT γδT1 c10 cluster cells in B6.SAP$^{-/-}$ adult thymus (**Suppl. Fig. 8**). Unlike the

322 E17 and neonatal thymic datasets, however, the frequency of γδ T cells with an αβ T cell-like
323 signature in the adult thymic γδ T cell dataset was minimal. Collectively, these data supported the
324 presence of multiple SAP-dependent developmental checkpoints during neonatal and adult γδ T
325 cell development—a reduction in the $CD24^{pos}CD73^{neg}$ $SLAMF1^{+}SLAMF6^{+}$ cluster enriched in
326 γδT17 development-associated transcripts, an increased frequency of immature *S1pr1*-enriched γδ
327 T cells, and decreased frequencies of both γδNKT cells (γδT1 and γδT2) as well as non-γδNKT
328 γδT1 cells.
329
330 *SAP shapes the thymic γδ TCR repertoire*
331 Given our observation of altered γδ TCR clonotype distribution among E17 γδ T cells and
332 the substantial changes in clustering we observed in SAP-deficient mice, we were next interested
333 in determining the effect of SAP deficiency on the neonatal and adult γδ TCR repertoires. A
334 comparison of frequencies of the top 100 TCR clonotypes between B6 and B6.$SAP^{-/-}$ mice revealed
335 significant changes in the overall frequency of several TRGV1 and TRGV4 clonotypes (**Fig. 5A**).
336 Consistent with a SAP-dependent loss of γδNKT, we observed a profound loss of TRGV1
337 clonotypes utilizing the canonical TRAV15N-1 and TRAV15-1/TRDV6-1 γδNKT cell TCRs (**Fig.**
338 **5B**). Loss of these clonotypes was directly tied to the significant decrease of the γδT1 c8 and γδT2
339 c13 clusters, in which nearly all these clonotypes resided.
340 Within the B6 γδT2 c13 cluster the vast majority (~86%) of TCR sequences were highly
341 restricted canonical γδNKT cell clonotypes **(Suppl. Table 2**) and nearly all of these clonotypes
342 were also present in the γδT1 c8 cluster consistent with the ability of γδNKT cells to produce both
343 IFN-γ and IL-4. In contrast, while the B6 γδT1 c8 cluster contained a large proportion of canonical
344 γδNKT cell clonotypes (~46% of c8 TCRs), it also contained TCRs with a diverse pool of

345 clonotypes that utilized TRGV1 (~70% of c8 TCRs), TRGV4, TRGV5, TRGV6, and TRGV7 and
346 were present only in the c8 γδT1 cluster. Therefore, in neonates, the thymic γδT1 population is a
347 mixture of γδNKT and "non-γδNKT" γδT1 clonotypes, and each of these clonotype pools is
348 diminished in B6.SAP$^{-/-}$ mice. As noted above, these findings were largely reproduced in the adult
349 thymus where the γδNKT clonotypes associated with the c8 and c11 clusters were virtually absent
350 in B6.SAP$^{-/-}$ mice, and where the diverse pool of γδT1 c10 clonotypes was significantly diminished
351 (**Suppl. Table 2)**.

352 Interestingly, a closer examination of the neonatal thymic TRGV4 clonotypes revealed a
353 significant decrease in the frequencies of γδT17-associated clonotypes with a germline-encoded
354 TRDV5[46] (**Fig. 5B**), some of which were identical to those that were redistributed to the αβ T cell-
355 like c6 cluster in E17 γδ T cells **(Fig. 2E)**. When these clonotypes were mapped to their D9 clusters,
356 we noted a significant decrease in the frequency of TRGV4/TRDV5 clonotypes in the mature
357 γδT17 c6 cluster (**Fig 5C**). We note that while we observed a trend toward an increased frequency
358 of TRGV4/TRDV5 and TRGV4/TRDV2 clonotypes in the *S1pr1*$^{+}$ c4/c5 clusters, analysis of these
359 sequences revealed that they largely exhibited diverse CDR3 rather than the restricted CDR3
360 observed in the γδT17 c6 cluster (**Suppl. Table 2**). Taken together, these data indicate that the
361 TCR clonotypes of immature embryonic day 17 γδ T cells that were redirected to the αβ T cell
362 pathway in B6.SAP$^{-/-}$ mice, were underrepresented among the mature B6.SAP$^{-/-}$ neonatal γδ T
363 cells.

364

365 *Restricted TCR repertoire in innate-like γδT1 as well as γδT17 in the periphery.*

366 We previously demonstrated that SAP-deficiency results in a significant impairment in γδ
367 T cell function in the periphery[18]. Specifically, we observed that γδ T cell IL-17 production is

368 impaired in the lungs of young mice, but that this had largely corrected itself as the mouse reached
369 maturity. In contrast, we observed that both Vγ1 and Vγ4 IFN-γ production were significantly
370 impaired in B6.SAP$^{-/-}$ adult lung and spleen. To better understand how SAP-dependent alterations
371 in thymic development ultimately affected the peripheral γδ T cell compartment, we compared B6
372 and B6.SAP$^{-/-}$ lungs using single-cell RNAseq with V(D)J profiling.

373 Our initial annotation of the B6 lung γδ T cell transcriptome revealed the presence of 11
374 clusters of the lung γδ T cells that we annotated based on cluster-specific gene expression and
375 TRGV and TRDV usage (**Figure 6A**). Based on their expression of signature cytokines and
376 transcription factors, we identified 2 γδT17 clusters (c1 and c4), 4 γδT1 clusters (c2, c3, c7, and
377 c9), 1 γδTNKT-like cluster (c10) with very few cells, as well as a *Cd24*-enriched cluster (c5)(**Fig.
378 6B and 6C, Suppl. Table 5**). Consistent with previous observations, we noted that the c1 and c4
379 γδT17 clusters were enriched in *Slamf1* and that the c2/c3/c7/c9 γδT1 clusters were enriched in
380 *Slamf7* and *Slamf6* (**Fig. 6B**). Indeed, flow cytometric analysis revealed that SLAMF7 expression
381 was restricted to the innate-like lung CD44^{+}CD45RB^{+} γδT1 cell population, and that γδT1 cells
382 are SLAMF1^{-}F6^{+}F7^{+}, while the CD44^{+}CD45RB^{-} γδT17 subsets are SLAMF1^{+}F6^{-}F7^{-} (**Fig. 6D**).
383 Further annotation using V(D)J profiling revealed that the c1 cluster corresponded to Vγ4 γδT17
384 (primarily TRGV4/TRDV5 and TRGV4/TRDV2-2) while the c4 cluster corresponded to lung Vγ6
385 (TRGV6/TRDV4) (**Fig. 6E, Suppl. Table 6**). The c10 cluster was enriched in *Zbtb16*, *Il4*, and
386 *Icos* (**Fig. 6B-C**) as well as TRGV1/TRAV15N-1 and TRGV1/TRDV6 sequences (**Fig. 6E**, **Suppl.
387 Table 6**) consistent with γδNKT cells. We did note, however, that the TRAV15N-1 and TRDV6
388 sequences in the c10 cluster were, for the most part, non-canonical γδNKT cell clonotypes,
389 suggesting a degree of flexibility in the TRAV15N-1 and TRDV6 CDR3 sequences that can be
390 utilized by γδNKT cells.

391 Interestingly, while the γδT1 c2/c3/c7/c9 clusters contained primarily Vγ1 and Vγ4 T cells
392 as expected, we noted that Vγ4 γδT1 cells exhibited a striking preference in the usage of TRAV13-
393 4(DV7), and that TRGV4/TRDV7 pairings accounted for 80% of all Vγ4 clonotypes in the γδT1
394 clusters **(Fig. 6E, Suppl. Table 6**). Analysis of the γδT1 TRAV13-4/DV7 CDR3 sequences
395 revealed a high level of diversity that showed no evidence of clonal expansions (**Fig. 6F**). This
396 was in contrast to the highly restricted Vγ6 repertoire in the c4 γδT17 cluster, as well as the
397 restricted Vγ4 repertoire in the c2 γδT17 cluster that was dominated by semi-invariant TRDV5
398 and TRDV2-2 sequences (**Fig. 6F**). As no Vδ7-specific antibody was available, we independently
399 confirmed this observation using single-cell PCR to assess the lung Vγ4 CDR3δ sequences from
400 13 individual mice. These data demonstrated that, other than TRDV2-2 and TRDV5, TRDV7 is
401 the only other TCR delta chain used at an appreciable frequency by Vγ4 T cells in the B6 mouse
402 lung and that it exhibits significant diversity in its CDR3 (**Suppl. Fig. 9**). Vγ1 γδT1 cells, in
403 contrast, exhibited a more mild pairing preference where 44% of the γδT1 clonotypes utilized
404 TRAV15N-1, TRAV15-1/DV6-1, or TRAV15D-2/DV6D-2 and 13% utilized TRAV13-4/DV7
405 (**Suppl. Table 6**). Together these data formed a comprehensive map of B6 lung γδ T cell
406 transcriptomes and revealed that lung innate-like γδT1, like γδT17 and γδNKT, are all
407 characterized by preferential TCR γ- and δ-chain pairings. This was especially notable for Vγ4 and
408 our data suggested that Vγ4 γδT1 exhibited a distinct preference for the utilization of TRAV13-
409 4(DV7) chains with diverse CDR3.
410
411 *SAP regulates peripheral Vγ4/Vδ7 γδT1 cells and shapes the lung γδT17 repertoire.*
412 Next, we assessed the effect of SAP deficiency on the lung γδ TCR repertoire by comparing
413 B6 and B6.SAP$^{-/-}$ lung γδ T cells (**Fig. 7A**). Consistent with our previous observation that lung γδ

414 T cell IFN-γ production is decreased in SAP-deficient mice[18], we observed a decrease in the
415 frequency of the γδT1 c2, c3, and c7 clusters (**Fig. 7B**). Moreover, we observed a striking decrease
416 in the frequency of TRGV4/TRDV7-expressing cells in the lungs of B6.SAP$^{-/-}$ mice (**Figs. 7C-D,**
417 **Suppl. Table 6),** and we noted that we found no evidence of a compensatory increase in the
418 frequency of other TRDV-expressing lung Vγ4 γδT1 cells in the B6.SAP$^{-/-}$ lung. We independently
419 confirmed this SAP-dependent decrease in TRAV13-4/TRDV7 in both lung and spleen using
420 qPCR (**Suppl. Fig. 10**), and we demonstrated a significant decrease in the number of
421 CD44^{+}SLAMF7^{+} Vγ4 T cells in both the lungs and spleen of B6.SAP$^{-/-}$ mice (**Fig. 7E, Suppl. Fig.**
422 **10**). The decreased lung γδT1 did not appear to be due to a SAP-dependent decrease in homeostatic
423 proliferation, nor to increased apoptosis, since we observed no significant change in lung γδ T cell
424 BrdU incorporation or Annexin V staining in B6.SAP$^{-/-}$ mice (**Suppl. Fig. 10**).

425 In addition to the decrease in lung γδT1, we also noted a loss of the c10 γδT2 cluster
426 consistent with the enrichment in SAP-dependent γδNKT TCRs in this cluster, and we observed
427 an increased frequency of the Vγ4 γδT17 c1 cluster (**Fig. 7B**). Given our previous observation of
428 a SAP-dependent decrease in lung γδ T cell IL-17 production in young, but not adult mice[18], and
429 our findings here of SAP-dependent alterations in γδT17 clonotypes, we were interested in
430 determining whether the adult lung γδT17 repertoire was altered in SAP-deficient mice. Indeed, a
431 comparison of the lung Vγ4 c1 γδT17 CDR3 sequences between B6 and B6.SAP$^{-/-}$ mice revealed
432 significant alterations in the γδT17 c1 cluster TCR repertoire. Specifically, we noted a decreased
433 frequency of TRGV4 chains that exhibited a germline-encoded CDR3γ (CSYGYSS) and an
434 increased frequency of TRGV4 chains with a CDR3γ exhibiting evidence of N/P additions
435 (CSYG(X)YSS). These changes were associated with a significant shift in the usage of TRDV2-2
436 CDR3δ sequence usage (**Fig. 7F**) and an altered c1 TCR clonotype frequency in B6.SAP$^{-/-}$ mice

437 **(Fig. 7G**). Although the number of germline-encoded invariant TRGV4/TRDV5 clone (clonotype
438 1 in Fig. 6B) was diminished in B6.SAP$^{-/-}$ lung γδ T cells (**Fig. 7G, Suppl. Table 6**), the low
439 numbers of cells available for analysis precluded us from making strong conclusions regarding the
440 loss of any one particular clonotype. Taken together, these data suggest that Vγ4 γδT1
441 preferentially utilize the TRAV13-4(DV7) chain in the lung and that the SAP-dependent decrease
442 in peripheral γδ T cell IFN-γ production is not due to dysregulated cytokine production, but rather
443 due to a specific loss of innate-like γδT1 subsets. This finding, together with our finding that the
444 adult lung γδT17 TCR repertoire is altered in SAP-deficient mice suggests that SLAM/SAP
445 signaling plays a role in shaping the γδ TCR repertoire.

446 **Discussion**

447 A common denominator in most innate-like T cell developmental programming is a
448 dependence on the SLAM/SAP signaling pathway[11, 18, 19, 54]. In the γδ T cell lineage, SAP plays a
449 critical role in the development of IFN-γ and IL-4-producing γδNKT cells[21], as well as in γδT1
450 and γδT17[18], but exactly when during γδ T cell development SAP functions, and how it exerts
451 these effects is unknown. Here, we provide evidence that SAP mediates its effects on immature,
452 uncommitted thymic γδ T cells and that it works to simultaneously promote progression through
453 the γδT17 developmental pathway while inhibiting the diversion of γδ T cells into the αβ T cell
454 pathway. The redirection of γδ T cell clonotypes into the αβ T cell pathway at E17 is associated
455 with a decreased frequency of these mature clonotypes in neonatal thymus, and an altered γδT17
456 TCR repertoire in the periphery. Finally, we identify Vγ4/Vδ7 T cells as a novel, SAP-dependent
457 IFN-γ-producing Vγ4 γδT1 subset.

458 The developmental pathway(s) that gives rise to γδ T cell functional subsets remains unclear.
459 γδ T cells develop at the DN2/DN3 stage after receiving a sufficiently strong γδTCR-mediated
460 signal[55]. Within the continuum of signals that can drive γδ T cell development, it is the relatively
461 weaker TCR signals that promote γδT17 programming while the stronger TCR signals foster
462 γδNKT and γδT1 programming[4, 8, 11, 14, 56, 57]. Despite considerable effort, the precise thymic
463 developmental stages at which γδ T cell lineage diversification occurs remains unclear. Recent
464 studies examining this issue have demonstrated that effector programming can occur at a
465 $CD44^{neg}CD45RB^{neg}$ stage[4, 14], and that c-Maf-directed γδT17 programming occurs at a $CD45RB^{low}$
466 stage[36]. In addition, by altering TCR signal strength in a transgenic model, Chen et al., defined a
467 *Ccr9*-enriched cluster as a point of effector lineage diversification[10]. Our findings here suggest that
468 SAP influences γδT17 developmental programming during the immature uncommitted

469 CD24^{hi}CD73^{neg} stage, either during or soon after *Il2ra (*CD25) downregulation. The SAP-
470 dependent c2 cluster we define here was highly enriched in numerous genes (e.g., *Sox13*[40], *Blk*[35],
471 *Maf*[36], *Etv5*[39], *Sh2d1a*[18]) previously associated with γδT17 development as well as *Ccr9*, and the
472 cell surface phenotype of c2 γδ T cells is SLAMF1^{pos}SLAMF6^{pos}CD44$^{low/high}$CD45RB^{low}.
473 Altogether, these data suggest that the SAP-dependent c2 cluster is identical to these previously
474 defined developmental checkpoints. Given that these previous studies have demonstrated that this
475 developmental checkpoint is influenced by TCR signaling, it is interesting to note that SLAM/SAP
476 signaling has previously been demonstrated to foster semi-invariant NKT cell differentiation
477 through its ability to regulate TCR signal strength[58].

478 To that end, we noted that in addition to a decrease in the number of immature γδ T cells
479 expressing BLK, the expression level of BLK was decreased in B6.SAP$^{-/-}$ γδ T cells. BLK is a
480 member of the Src tyrosine kinase family whose members also include LCK and FYN. All three
481 of these kinases have been implicated in γδ T cell development[59] and BLK has been shown to
482 promote γδT17 development[35]. Thus, it's possible that decreased BLK expression could contribute
483 to the impaired γδT17 development observed in SAP-deficient mice. In addition, since SAP has
484 been shown to regulate conventional αβ T cell differentiation through its ability to interact with
485 FYN[60], it's possible that SAP interacts with one or all of these Src kinase family members to exert
486 its effects. Whether SAP works to regulate TCR signal strength during γδ T cell development, or
487 whether it exerts its effects through a TCR-independent mechanism is currently under
488 investigation.

489 Nevertheless, our finding that, in addition to regulating the frequency of the c2 cluster, SAP
490 inhibits the number of γδ T cells that enter the αβ T cell developmental pathway, is reminiscent of
491 previous work using transgenic TCR models demonstrating that a reduction of TCR signal strength

492 results in a redirection of γδ T cells to the αβ T cell lineage[53, 61] In addition, Fahl et al. recently
493 demonstrated that both entry into the γδ T cell lineage as well as γδ T cell effector programming
494 involved repression of TCF1 expression by TCR-driven increases in *Id3*[42]. Consistent with these
495 results, we found that *Tcf7* (encoding TCF1) transcript levels were highest in the αβ T cell-like c6
496 cluster, and we note that *Tcf7* transcripts levels were noticeably higher in the *Il2ra*-enriched post-
497 selection c5 cluster in B6.SAP$^{-/-}$ γδ T cells. *Id3* expression, however, did not appear to be altered
498 in SAP-deficient mice. Whether SAP-mediated signals could alter γδ T cell *Tcf7* expression
499 through a TCR-independent mechanism remains an open question. Indeed, recent evidence that
500 some DN1 thymocytes possess a SOX13^{hi} IL-17-like phenotype and that Vγ4 γδT17 arise from
501 DN1 precursors[12, 62] indicates the existence of such a TCR-independent developmental
502 programming stage. It may be possible, therefore that SLAM/SAP-mediated signals could regulate
503 the number and/or fitness of these DN1 precursors prior to the expression of TCR.

504 While our data indicate that SAP regulates the diversion of at least some TCR clonotypes
505 into the αβ TCR pathway, the fate of those cells is unclear. Certainly, the fact that the clonotypes
506 that were diverted to the αβ T cell pathway in E17 thymus are under-represented in the mature D9
507 thymus γδT17 clusters suggests that this diversion has significant consequences on the γδ T cell
508 receptor repertoire, but whether these diverted γδ T cells contribute to the αβ T cell compartment
509 is unclear. Recently, a population of hybrid αβ-γδ T cells was described in both mouse and
510 human[63] that responds to peptide/MHC stimulation like conventional αβ T cells, as well as to IL-
511 1 and IL-23 which induce both IFN-γ and IL-17 production[63]. In the mouse, at least some of these
512 cells are Vγ4/Vδ5, Vγ4/Vδ4, or Vγ4Vδ7 and are present in the embryonic thymus, raising the
513 possibility that γδ T cells diverted to the αβ T cell pathway in B6.SAP$^{-/-}$ mice contribute to this

514 αβ-γδ T cell population. While we have not observed a significant increase in the overall numbers
515 of αβ-γδ T cells in B6.SAP$^{-/-}$ thymus (not shown), a direct comparison of B6 and B6.SAP$^{-/-}$ αβ-
516 γδ TCRs may be necessary to see such an effect.

517 Our previous observations that SAP deletion did not completely abolish the development of
518 IL-17- and IFN-γ producing γδ T cells[18] suggested the possibility that SAP may be critical for the
519 development of additional γδ T cell clonotypes other than the Vγ1Vδ6.3 subset. Therefore, we
520 compared the SAP-dependent and SAP-independent γδTCR repertoires using paired TCR
521 clonotype analysis, which allowed us to track clonotype fate during development. Our findings not
522 only confirmed previous results demonstrating highly restricted γδT17[45, 46], and γδNKT[21] TCR
523 repertoires, they also revealed that the vast majority of Vγ4 γδT1 subsets in the periphery
524 preferentially utilize TRGV4/TRAV13-4(DV7) clonotypes, thereby further highlighting the strong
525 links between γδ T cell function and the utilization of specific TCRs[23]. The reason for this
526 preferential TRDV usage in Vγ4/Vδ7 γδT1 is unclear. While the TRAV13-4(DV7) CDR3
527 sequences were diverse and did not suggest evidence of clonal expansion, it may be possible that
528 TRDV-encoded sequence motifs could be required to interact with a ligand, similar to the way that
529 TRGV-encoded sequences mediate recognition of butyrophilins[64, 65].

530 Exactly when during development SAP exerts its effects on Vγ4/Vδ7 T cells is still
531 somewhat unclear. We found comparatively low numbers of TRGV4/TRDV7 γδ T cells in
532 embryonic, neonatal, or adult thymus, and those that were identified were generally found in the
533 immature clusters. The increased frequency in B6.SAP$^{-/-}$ E17 thymus of TRGV4/TRDV7 γδ T
534 cells in the *Il2ra*$^{+}$ c5 cluster coupled with their decreased frequency in the emigrating *S1pr1*$^{+}$ c4
535 cluster suggests a model where SAP promotes progression through the early stages of development
536 through thymic egress. SAP deficiency, therefore, could result in lower Vγ4/Vδ7 output. However,

537 this model is at odds with our finding that the frequency of *S1pr1*$^{+}$ clusters in neonatal thymus is
538 increased in B6.SAP$^{-/-}$, and that these clusters contained increased numbers of TRGV4/TRDV7 γδ
539 T cells. A possible explanation could be found in a previous report demonstrating that a Vγ4/Vδ7
540 subset increases in frequency in the periphery of B6 mice over time and undergoes extrathymic
541 expansion[66]. Our finding here that that the Vγ4/Vδ7 T cells represent a SAP-dependent innate-like
542 γδT1 subset raise the possibility that SAP regulates the homeostatic expansion of this subset.
543 subset after it leaves the thymus. The mechanism, however, through which SAP is regulating the
544 number of the Vγ4/Vδ7 subset remains unclear as we have so far observed no evidence of changes
545 in homeostatic proliferation or apoptosis of these cells in the lungs.

546 We previously demonstrated that the SAP-dependent dependent impairment in γδT17
547 function in the neonatal periphery largely corrects itself as mice mature[18]. This suggested the
548 possibility that SAP-dependent γδT17 clonotypes originating in the embryonic thymus were being
549 replaced over time by SAP-independent γδT17 clonotypes. Although our data certainly point to a
550 SAP-dependent decrease in a germline-encoded Vγ4/Vδ5 clonotype in neonatal thymus, the low
551 numbers of this clonotype in the lung makes it difficult to draw definitive conclusions in the
552 periphery. Still, we did observe a role for SAP in shaping the peripheral γδT17 repertoire, as we
553 noted we noted a decreased frequency of germline-encoded TRGV4 sequences (so-called
554 "GYSS"[67]) coupled with an increased frequency of TRGV4 sequences with more diverse CDR3
555 ("GXYSS") in the periphery. Although the potential significance of this change on γδ T cell
556 function is unclear, it does support a model in which SAP regulates γδT17 developmental
557 programming during embryonic thymic development, where the low expression of terminal
558 deoxynucleotide transferase results in a high frequency of germline-encoded V-J junctions.

559 In summary, our findings reveal the presence of multiple SAP-dependent developmental

560 checkpoint during the very early stages of γδ T cell development in the thymus, indicating a more
561 complex role for this signaling pathway in γδ T cell developmental programming than previously
562 appreciated. Indeed, our data indicate that SAP functions to regulate entry into the γδ and αβ T
563 cell developmental pathways, and we make the striking observation that nearly all Vγ4 γδT1 cells
564 in the periphery preferentially use Vδ7 chains and that it is a decrease in the Vγ4/Vδ7 subset that,
565 in part, underlies the SAP-dependent decrease in γδ T cell IFN-γ production. Whether SAP
566 regulates these phenotypes through regulation of TCR signal strength or additional pathways
567 remains an open question. Taken together, the data presented here suggest a key role for the
568 SLAM/SAP signaling pathway in generating and/or maintaining the innate-like phenotype in the
569 γδ T cell lineage.

570 **Methods**

571 *Mice*

572 C57BL/6J (B6) and B6.*Sh2d1a*$^{-/-}$ (SAP$^{-/-}$) mice were purchased from the Jackson
573 Laboratory (Bar Harbor, ME) and were housed and bred in a specific pathogen-free facility at the
574 animal facility of the University of Vermont. For experiments using E17 mice, timed-pregnant
575 matings were used. The presence of a vaginal plug indicated day 0 of pregnancy. The flow
576 cytometry experiments included 8-13 weeks old B6 and B6.SAP$^{-/-}$ mice (age and sex-matched).
577 All experimental procedures on animals were carried out with the approval of the University of
578 Vermont Institutional Animal Care and Use Committee.

579

580 *Tissue Processing*

581 Single-cell suspensions from the spleen and thymus were obtained by gently passing tissue
582 through nylon mesh. Red blood cells (RBCs) were lysed with Gey's solution. Single-cell
583 suspensions from the lungs were prepared as described (Benoit et al., 2015). Briefly, dissected
584 lungs were finely minced in a digestion buffer containing DMEM, 1 mg/ml collagenase type IV
585 (Gibco), and 0.2 mg/ml DNase (Sigma-Aldrich). After shaking at 200 rpm at 37˚C for 20 min, the
586 lung digests were triturated with a 16-gauge needle, followed by an additional 20 min shaking at
587 200 rpm at 37˚C. Following the final trituration, red blood cells (RBC) were lysed with Gey's
588 solution. Finally, the digested lung tissues were filtered through a 70-µm filter and washed in
589 PBS/2%FBS. Cells were counted either on a MACSQuant VYB or using a hemacytometer
590 following trypan blue staining.

591 *Flow Cytometry*

592 Cells were incubated with LIVE/DEAD™ Fixable Blue Dead Cell stain (Thermo Fisher
593 Scientific, Grand Island, NY) for 30 min at 4^0C in PBS, after which they were resuspended in Fc-
594 Block (BioLegend) containing PBS/2% FCS/0.1% sodium azide buffer. After a 5-10 min
595 incubation on ice, antibodies specific for cell surface markers were added, incubated for 30 min
596 on ice, and washed in PBS/2% FCS/0.1% sodium azide buffer. Brilliant Violet Staining buffer
597 (BD Biosciences) was used in experiments contain more than one Brilliant Violet, Brilliant UV,
598 or SuperBright-conjugated Ab. Cells were fixed in PBS/1% PFA buffer and stored at 4^0 C prior to
599 data collection.

600 For nuclear staining, cells were permeabilized with Foxp3 transcription factor
601 fixation/permeabilization buffer (ThermoFisher) following surface staining. Cells were incubated
602 overnight at 4˚C, washed, and incubated with 25 micrograms/ml total rat IgG before adding Abs
603 against transcription factors. After staining, cells were washed and resuspended in PBS/2%
604 FCS/0.1% sodium azide buffer. For intracellular cytokine staining, cells were permeabilized with
605 PBS/1% FCS/0.1% sodium azide/0.1% saponin following surface staining and fixation. To reduce
606 unspecific binding, 25 μg/ml total rat IgG was added prior to cytokine staining with fluorescent-
607 labeled antibodies.

608 Flow cytometry data were collected on a Cytek® Aurora (Cytek Biosciences) spectral
609 cytometer, and data analysis was performed using FlowJo Software (Tree Star). In some cases,
610 visualization of flow cytometry data was conducted by concatenation of individual .fcs files,
611 followed by dimensionality reduction and clustering using UMAP and FlowSOM[68] in FlowJo.
612 Antibodies used in these experiments are anti-CD4 (RM4-5), anti-CD11b (M1/70), anti-CD11c
613 (N418), anti-CD19 (1D3), anti-CD24 (M1/69), anti-CD25 (PC61), anti-CD27 (LG.3A10), anti-

614 CD44 (IM7), anti-CD45RB (C363-16A) , anti-CD73 (TY/11.8), anti-CD150 (TC15-12F12.2),
615 anti-CD196 (29-2L17), anti-CD319 (4G2), anti-cMAF (sym0F1), anti-IFNγ (XMG1.2), anti-
616 IL17a (TC11-18H10.1), anti-IL4 (11B11), anti-PLZF (9E12), anti-T-bet (4B10), anti-TCRβ (H57-
617 597), anti-Vγ5 (536), and anti-Vd6.3 (C504.17c) from BioLegend; and anti-RORγt (Q31-378),
618 anti-TCRδ (GL3), anti-Vγ1 (2.11) from BD biosciences; and anti-CD8a (53-6.7), anti-CD45 (30-
619 F11), anti-CD200 (OX90), anti-CD278 (7E17G9), anti-Ki-67 (SolA15), anti-Ly108(13G3-19D),
620 anti-Vγ4 (UC3-10A6) from eBiosciences; anti-S1P1 (713412) from R&D systems; anti-Blk
621 (polyclonal) from Cell Signaling Technology; and anti-17D1
622
623 *In vivo proliferation and apoptosis*
624 For *in vivo* proliferation analysis, each mouse was intraperitoneally injected with 1 mg of
625 5-bromo-deoxyuridine (BrdU) (Sigma-Aldrich) each day for 3 days. Lung cell suspensions were
626 prepared as above, stained with surface markers, after which they staining with anti-BrdU antibody
627 according to the manufacturer's instructions (BrdU Flow Kit; BD Biosciences). For apoptotic cell
628 detection, annexin V staining was performed. Briefly, surface staining was followed by dead cell
629 staining with Fixable Viability Dye eFluor™ 780 dye. The cells were washed and resuspended in
630 an annexin-binding buffer (10 mM HEPES, 140 mM NaCl, and 2.5 mM CaCl2, pH 7.4). Finally,
631 1 µl of Annexin V Conjugate (Thermo Fisher Scientific, Grand Island, NY) was added to each
632 tube, and cells were incubated for 15 minutes at room temperature (RT) prior to data collection.
633
634 *Bulk RNA Sequencing and data analysis*
635 For the bulk RNA sequencing, thymocytes from 10-day old B6 (n=4 male, n=2 female)
636 and B6.SAP$^{-/-}$ (n=5 male, n=1 female) mice were prepared by depleting CD4+ cells from

637 thymocytes using the EasySepTM Mouse CD4 Positive Selection Kit II (STEMCELL
638 Technologies). Cells were then incubated with Fixable Viability Dye eFluor™ 780 (Thermo Fisher
639 Scientific, Grand Island, NY) for 30 min at 4^0C in PBS, after which they were resuspended in Fc-
640 Block (BioLegend) containing PBS/2% FCS. After washing, cells were stained with antibodies
641 against CD11b (M1/70), CD19 (1D3), CD24 (M1/67), CD45 (30-F11), TCRβ (H57-597), and
642 TCRδ (GL3) for 30 min at 4^0C. Following surface staining, $CD24^{hi}$TCRδ+ cells were sorted from
643 a $CD11b^-CD19^-$TCRb- population of live $CD45^+$ lymphocytes. Immature ($CD24^{high}$) thymocytes
644 from both B6 and B6.$SAP^{-/-}$ mice were sorted directly into 350 microliters of RLT lysis buffer
645 (Qiagen). RNA was extracted using the RNeasy Micro kit (Qiagen) according to manufacturer
646 instructions. After RNA quantification and quality assessment, cDNA libraries were prepared
647 using SMARTer Stranded Total RNA-Seq Kit v3 - Pico Input Mammalian (Takara, Japan)
648 according to the manufacturer's protocol. Following library clean-up and quantification, the
649 libraries were sequenced (single-end 75 bp) on an Illumina HiSeq1500.

650 The Fastq files were checked for data quality using FastQC and MultiQC[69] bioinformatics
651 tools. Cutadapt[70] was used to filter out low-quality sequences and to remove adapter sequences
652 from all reads. The expression of transcripts was quantified using the mapping-based mode of
653 Salmon[71], which quasi-mapped RNA-seq reads to an index created from a mouse reference
654 transcriptome (GRCm39). The transcript abundance estimates were imported using tximport[72] and
655 differential gene expression (DE) analysis was performed using DEseq2[73] employing the Wald
656 test of the negative binomial model coefficients to determine statistical significance. The results
657 were analyzed based on Log_2 fold change ($Log_2FC \geq 0.5$ or ≤ -0.5) and adjusted P-value (padj
658 ≤ 0.0001) to determine whether a gene was differentially expressed.

659

660 *Cell sorting and library preparation for CITE-seq and V(D)J enrichment*

661 For thymus single-cell transcriptome analysis, we used embryonic day 17 (E17) B6 (n=4)
662 and B6.*Sh2d1a*$^{-/-}$ (SAP$^{-/-}$) (n=4) mice, nine day-old (D9) B6 (n=3) and B6.SAP$^{-/-}$ (n=3) mice, and
663 six-week-old B6 (n=3 male) and B6.SAP$^{-/-}$ (n=2 male, n=1 female) mice. For single-cell analysis
664 of adult lung γδ T cells, we used 13 week old B6 and B6.SAP$^{-/-}$ littermates (pooled cells from 2
665 males and one female mouse in each group).

666 Analysis of gene expression, surface protein expression, and TCR V(D)J repertoire was
667 performed using the 10X Genomics Chromium Next GEM Single Cell 5' V(D)J with feature
668 barcoding kit (version 1.1). To sort cells for scRNAseq, thymocytes were stained with anti-TCRδ-
669 PE (GL3) antibody and enriched using anti-PE MicroBeads kit (Miltenyi Biotec). The exception
670 was E17 thymus which did not undergo TCRδ enrichment. Following live/dead staining with
671 Fixable Viability Dye eFluor™ 780 (Thermo Fisher Scientific, Grand Island, NY) for 30 min at
672 4° C in PBS, cells were resuspended in Fc-Block (BioLegend) containing PBS/2% FCS. Cells were
673 then simultaneously stained with oligonucleotide-conjugated antibodies targeting CD24, CD44,
674 CD45RB, CD73, SLAMF1, SLAMF6, Vγ1, and Vγ4 (TotalSeqC-BioLegend), oligonucleotide-
675 conjugated hashtag antibodies (TotalSeqC-BioLegend), and fluorophore-conjugated antibodies for
676 cell sorting which included the anti-CD11b (M1/70), anti-CD11c (N418), anti-CD19 (1D3), anti-
677 CD45.2 (104) and anti-TCRβ (H57-597) antibodies. Following surface staining of the enriched
678 population, TCRδ^{+} cells were sorted from a CD11b^{-}CD11c^{-}CD19^{-}TCRβ^{-} population of CD45.2^{+}
679 live lymphocytes.

680 Libraries were prepared according to the manufacturer's instructions with modifications to
681 the V(D)J enrichment procedure. Equal numbers of live GL3^{+} γδ T cells from B6 and B6.SAP$^{-/-}$
682 mice were pooled and captured (between 5000 – 7000 cells) using a 10x Chromium controller.

683 Following cDNA preparation, the gene expression and CSP libraries were created according to the
684 manufacturer's instructions. To obtain TCR gamma and delta chain sequences, we replaced kit-
685 provided enrichment primers with custom mouse γ and δ chain-specific primers and modified the
686 number of PCR cycles used from manufacturer recommended cycling conditions. In the first
687 enrichment step, an equal amount of cDNA was used as a template for PCR amplification of γ and
688 δ chains separately using a total of 12 and 10 PCR cycles, respectively. The primers used for the
689 first γ-chain enrichment are: Forward Primer 5'-AATGAT ACGGCGA CCACCG AG
690 ATCTACACTCTT TCCCTACAC GACGCTC-3' (2 μM) and Reverse Outer Primers 5'-GGAA
691 AGAACTT TTCAAGGAS ACAAAG-3' (1 μM), 5'-CCCTTATG ACTTCAGG AAAGAA
692 CTTT-3' (0.5 μM) . The primers used for the first δ-chain enrichment are: Forward Primer 5'-
693 AATGAT ACGGCGACCACCG AGATCTACACTC TTTCCCTAC ACGACGCTC-3' (2 μM)
694 and Reverse Outer Primer 5'-CCACAATC TTCTTGGATG ATCTGAG-3' (0.5 μM). Following
695 PCR product purification, the γ-chain and δ-chain amplicons went through the second round of
696 enrichment separately using a total of 12 and 10 PCR cycles, respectively. The primers used for
697 the second γ-chain enrichment are: Forward Primer 5'-AATGA TACGGCGACCA
698 CCGAGATCT-3' (0.5 μM) and Reverse Inner Primers 5'-ACAAA GGTATGTCCCA
699 GTCTTATGGA-3' (0.5 μM), 5'-GGAGACA AAGGTAGGT CCCAGC-3' (0.5 μM). The
700 primers used for the second δ-chain enrichment are: Forward Primer 5'-AATGATA
701 CGGCGACCACC GAGATCT-3' (0.5 μM) and Reverse Inner Primer 5'-GTCACCTC
702 TTTAGGGTAG AAATCTT-3'. Following PCR product cleanup, the second round PCR products
703 (γ-chain and δ-chain amplicons) were quantified and combined in equal quantity making the final
704 TCR V(D)J library. Finally, all three libraries (gene expression, cell surface protein expression,

705 and TCR V(D)J) were sequenced (paired-end 26 x 91 bp) on an Illumina HiSeq 1500 sequencer
706 or a NextSeq 2000.
707
708 *CITE-seq quality control, filtering and demultiplexing*
709 Raw sequence reads from the gene expression and CSP libraries were processed using the
710 Cell Ranger software (v4.0.0)[74]. Reads were mapped to the GRCm38 (mm10) mouse reference
711 genome. To exclude the possibility of TCR transcripts playing a role in UMAP clustering, all TCR
712 genes were omitted from the analysis using the "cellranger reanalyze" argument of Cell Ranger
713 software.
714 Quality control, filtering, UMAP projection, and clustering analysis were conducted using
715 Seurat (v4.3.0.1)[75] R package. Briefly, cells with a low number (≤2000 for E17 thymus dataset,
716 ≤1200 for D9 thymus dataset and ≤750 for lung dataset) of unique genes (nFeature_RNA), a
717 frequency of mitochondrial reads > 4% and a frequency of ribosomal protein < than ~12% were
718 eliminated from further analysis. To reduce cell cycle-related and stress-related heterogeneity in
719 the normalized data, selected cell cycle genes and stress-induced genes [76] were regressed out
720 during the data normalization step. Note that in some instances, contaminating clusters expressing
721 macrophage specific marker genes were manually removed using Seurat "CellSelector ()"
722 argument. We used the Seurat function "HTODemux()" to demultiplex single cells back to their
723 sample of origin [77].
724
725 *CITE-Seq and V(D)J enrichment data analysis*
726 The demultiplexed datasets were further analyzed for gene expression, cell surface protein
727 expression following the multimodal analysis pipeline of Seurat[75]. For each dataset, we performed

728 normalization and variance stabilization of the gene expression data using the scTransform[78].
729 Following identification of top significant principal components (PCs) using the principal
730 component analysis (PCA), we performed a graph-based (UMAP) semi-supervised clustering of
731 cells with similar gene expression patterns using specific number of top PCs (E17 = 25, D9 = 30,
732 W6 = 27, lung = 28) and resolution values (E17 = 1.2, D9 = 1.6, W6 = 0.65, lung =1.2) for each
733 dataset. The cell surface protein expression data (Centered Log Ratio (CLR) normalized) from
734 CSP libraries as well as the gene expression data were then visualized on the clustered cells using
735 the R package scCustomize[79]. The differentially expressed features of each cluster (cluster
736 biomarkers) were identified using FindAllMarkers() function using the Wilcoxon Rank Sum test.
737 For identifying differentially expressed genes (DEGs) between B6 and B6.SAP$^{-/-}$ samples, we
738 performed a pseudobulk DE (differential expression) analysis of aggregated read counts using the
739 DEseq2 package, which accounts for biological replicates making it a better approach than other
740 specialized single-cell DE analysis methods[80]. Briefly, for cells of a given sample type, we
741 aggregated RNAseq reads across biological replicates identified by individual hashtags. Then
742 transformed the genes-by-cell matrix to a genes-by-replicates matrix and performed DE analysis
743 using the DESeq2[73] package employing the Wald test of the negative binomial model coefficients
744 to determine statistical significance. Finally, the trajectory and pseudotime inference analysis was
745 performed using the partition-based graph abstraction (PAGA)[81] analysis, which is a part of the
746 Scanpy[82] python package.

747 For the analysis of V(D)J library sequences, Cell Ranger v6.1.2 ("cellranger vdj"
748 argument) was used to map the TCR V(D)J) reads to a custom-made reference containing
749 sequences from the IMGT database[83]. The Cell Ranger V(D)J output was then processed with
750 custom bashscripts. Briefly, the TRGV and TRAV/TRDV contigs identified by Cell Ranger V(D)J

751 were demultiplexed to individual barcodes after which the dominant TRGV and TRAV/DV
752 transcripts were selected per cell. Finally, the V(D)J information of each cell was integrated with
753 scCITE-seq data and visualized using a combination of Seurat and custom-made R scripts. We
754 note that since about half of Vγ1, Vγ4, and Vγ7 T cells contain functionally rearranged TRGV2
755 chains, but only a small percentage express Vγ2 on the cell surface[84], the methods used here cannot
756 adequately assess the true TRGV2 repertoire. Therefore, we report it here for accuracy but have
757 omitted TRGV2 from our analysis.
758
759 *Quantitative PCR*
760 Lung qPCR samples were prepared by positively selecting leukocytes using CD45 MicroBeads
761 (Miltenyi Biotec). Spleen qPCR samples were prepared by depletion of CD19+ TCRβ+ cells using
762 biotinylated antibodies and Streptavidin MicroBeads (Miltenyi Biotec) according to the
763 manufacturer's instructions. Total RNA was extracted from approximately 5-10 million cells from
764 each organ using the RNeasy Mini Kit (QIAGEN). SuperScript® IV Reverse Transcriptase
765 (Thermo Fisher Scientific, Grand Island, NY) was used to generate cDNA using 400 ng of RNA
766 and oligodT primer according to the manufacturer's instructions. qPCR was performed using 1µl
767 of cDNA template in iTaq Universal SYBR Green Supermix (Bio-Rad) containing TCR delta
768 chain specific primer pairs. The qPCR reaction was run on a Bio-Rad CFX96 qPCR machine using
769 the following cycling conditions: 95^0C for 30 sec; 40 cycles of [95^0C for 5 sec; 60^0C for 30 sec;
770 72^0C for 30 sec]. The β2M and TRDC genes were used as endogenous housekeeping controls.
771 Primers used were as follows: mb2mforward, 5'- CATGGCTCG CTCGGTGACC-3',
772 mb2mreverse, 5'-AATGTGAGGC GGGTGGAACTG-3', TRDCforward, 5'- CTCCGGCCA
773 AACCATCTGTT-3', mouseDV2, 5'-CCAAGAAG CATACAAGCAGT ATAATG-3',

774 mouseDV5, 5'- CCCATGA TGCAGATTT TGTTCAAGG-3', mouseDV7, 5'- GGAAG
775 MCTCGTCAGC CTGTTGT-3', mouseDCrev, 5'- CCACAATCTT CTTGGAT GATCTGAG-3'.
776 Some primer sequences were adopted from Wei. et. al. (2015)[45].
777
778 *Vγ4 single cell sorting and TCR Sequencing*
779 The plate-based based γδ TCR repertoire analysis of single-cell sorted Vγ4 cells involved
780 adult lungs from 8-10 weeks old B6 male (n=7) and female mice (n=6). Lung Vγ4 TCR sequences
781 were obtained using a protocol modified from Wei *et al.*, (2015)[45]. Briefly, lung cell suspensions
782 were prepared as described above. After washing, cells were resuspended in Fc-Block
783 (BioLegend) containing PBS/2% FCS buffer, and stained with anti-CD11b (M1/70), anti-CD11c
784 (N418), anti-CD19 (1D3), anti-CD45 (30-F11), anti-TCRδ (GL3) and anti-Vγ4 (UC3-10A6) from
785 for 30 min at 4^0C in PBS. Fixable Viability Dye eFluor™ 780 (Thermo Fisher Scientific, Grand
786 Island, NY) was used to identify dead cells. Single-cell sorting of lung $V\gamma4^+TCR\delta^+$ from a $CD11b^-$
787 $CD11c^-CD19^-TCR\beta^-$ population of $CD45^+$ live lymphocytes were performed using a FACS Aria
788 III cell sorter (BD Bioscience). Cells were sorted directly into 12.5 µl (per well) of OneStep RT-
789 PCR Buffer mix (QIAGEN) in a 96-well PCR plate (one cell/well).
790 TCR sequences were then amplified and barcoded according to (Wei *et al.*, 2015). Briefly,
791 the first two nested PCR reactions involved primer-specific amplification of gamma and delta TCR
792 sequences. In both the first and second PCR reactions, the final concentration of each V-region
793 primer is 0.36µM, and each C-region primer is 0.6µM. The first RT-PCR step was performed using
794 the following cycling conditions: 50^0C for 30 min; 95^0C for 5 min; 25 cycles of [94^0C for 30 sec;
795 62^0C for 1min; 72^0C for1 min]; 72^0C for 7 min; 4^0C. Next, 1 µl of the first round PCR product was
796 used as a template for the second nested PCR reaction using HotStartTaq Master Mix Kit

797 (QIAGEN). The cycling conditions for the second PCR reaction were 95^0C for 5 min; 25 cycles
798 of [94^0C for 30 sec; 64^0C for 1min; 72^0C for1 min]; 72^0C for 7 min; 4^0C. In the third PCR reaction,
799 1 µl of second round PCR product as the template in a new 14 µl reaction using HotStartTaq Master
800 Mix Kit (QIAGEN). Each well was barcoded. The final concentration of 5' and 3' barcoding
801 primers was 0.05µM each and paired-end primers were 0.5µM each. The cycling conditions for
802 the third PCR reaction were 95^0C for 5 min; 36 cycles of [94^0C for 30 sec; 62^0C for 1min; 72^0C
803 for1 min]; 72^0C for 7 min; 4^0C. The γ and δ chain products were run on 1.2% agarose gel separately
804 and purified using the Qiagen QIAquick Gel Extraction Kit according to kit instructions. The final
805 products were then analyzed using the 2100 Bioanalyzer (Agilent Technologies). Finally, the γ
806 and δ TCR products were mixed in equal concentration and sequenced on the Illumina MiSeq
807 platform using the Illumina MiSeq Reagent Kit v2 (500-cycles).

808 The paired-end TCR sequencing reads were analyzed using a custom software pipeline
809 capable of de-multiplexing barcoded sequences to individual cells. The resulting de-multiplexed
810 reads were then analyzed by MiGMAP software, which identifies CDR3 sequences using the
811 IgBlast 1.4.0 (NCBI) V(D)J mapping tool[85, 86]. The single-cell TCR V(D)J profiling data were then
812 visualized using custom R scripts.

813

814 *Statistical analysis*

815 Prism (GraphPad Software, San Diego, CA) was used for the statistical analysis of data.
816 Unpaired Student t-tests, one-way ANOVA, or two-way ANOVA were used where appropriate.
817 Tests were considered significant when p-values were less than 0.05. Error bars represent standard
818 deviation (SD) unless otherwise indicated.

Acknowledgements

We thank Marlana Winschel, Cameron Moquin, and Erin Mathieu for help in tissue preparation and flow cytometry. We acknowledge Roxana del Rio Guerra for help in cell sorting. All flow cytometry data were collected at the Harry Hood Bassett Flow Cytometry and Cell Sorting Facility (Larner College of Medicine, University of Vermont) and was supported by NIH grant (S10OD026843). We thank Jessica Hoffman, Kris Finstaad, and the Vermont Integrated Genome Resource (Larner College of Medicine, University of Vermont) for help in scRNAseq, Julie Dragon and Korin Eckstrom for help in bioinformatics analysis. We thank Fred Kolling at the Genomics Shared Resource (Dartmouth Geisel School of Medicine) for help in sequencing. We also thank Willi Born and Rebecca O'Brien for the 17D1 hybridoma. This work benefitted from data assembled by the ImmGen consortium, and was supported by NIH grants R21AIO66465 and R03AI153902, S10OD026843 (JEB) and an AAI Careers in Immunology Fellowship (SKM, JEB).

831 **Author contributions**

832 S.K.M. and J.E.B. conceived and designed the project; S.K.M., J.E.B., E.A., K.J.H., B.M.H., R.S.,
833 and O.D. performed experiments and analyzed data; K.J.H., D.G., J.T.R., and N.S. aided with the
834 single-cell TCR sequencing; D.M. assisted with bulk RNA sequencing; S.K.M. and J.E.B.
835 performed the bioinformatics analysis of bulk RNA-seq and single-cell CITEseq (with immune
836 profiling) data; J.E.B. supervised the project; S.K.M. and J.E.B. prepared the manuscript.

837

838 **Competing interests**

839 All authors declare no competing interests.

840

841 **Materials and Correspondence**

842 Correspondence and requests for materials should be addressed to J.E.B. (email:
843 jonathan.boyson@med.uvm.edu)

844 **References**

845 1. Grigoriadou K, Boucontet L, Pereira P. Most IL-4-producing gamma delta thymocytes of
846 adult mice originate from fetal precursors. *J Immunol* **171**, 2413-2420 (2003).
847
848 2. Haas JD*, et al.* Development of interleukin-17-producing gammadelta T cells is restricted
849 to a functional embryonic wave. *Immunity* **37**, 48-59 (2012).
850
851 3. Ribot JC*, et al.* CD27 is a thymic determinant of the balance between interferon-gamma-
852 and interleukin 17-producing gammadelta T cell subsets. *Nat Immunol* **10**, 427-436
853 (2009).
854
855 4. Sumaria N, Grandjean CL, Silva-Santos B, Pennington DJ. Strong TCRgammadelta
856 Signaling Prohibits Thymic Development of IL-17A-Secreting gammadelta T Cells. *Cell*
857 *Rep* **19**, 2469-2476 (2017).
858
859 5. Chien YH, Zeng X, Prinz I. The natural and the inducible: interleukin (IL)-17-producing
860 gammadelta T cells. *Trends Immunol* **34**, 151-154 (2013).
861
862 6. Ribot JC, Lopes N, Silva-Santos B. γδ T cells in tissue physiology and surveillance.
863 *Nature reviews Immunology* **21**, (2021).
864
865 7. Turchinovich G, Hayday AC. Skint-1 identifies a common molecular mechanism for the
866 development of interferon-gamma-secreting versus interleukin-17-secreting gammadelta
867 T cells. *Immunity* **35**, 59-68 (2011).
868
869 8. Jensen KD*, et al.* Thymic selection determines gammadelta T cell effector fate: antigen-
870 naive cells make interleukin-17 and antigen-experienced cells make interferon gamma.
871 *Immunity* **29**, 90-100 (2008).
872
873 9. Munoz-Ruiz M*, et al.* TCR signal strength controls thymic differentiation of discrete
874 proinflammatory gammadelta T cell subsets. *Nat Immunol*, (2016).
875
876 10. Chen ELY, Lee CR, Thompson PK, Wiest DL, Anderson MK, Zuniga-Pflucker JC.
877 Ontogenic timing, T cell receptor signal strength, and Notch signaling direct gammadelta
878 T cell functional differentiation in vivo. *Cell Rep* **35**, 109227 (2021).
879
880 11. Kreslavsky T*, et al.* TCR-inducible PLZF transcription factor required for innate
881 phenotype of a subset of gammadelta T cells with restricted TCR diversity. *Proc Natl*
882 *Acad Sci U S A* **106**, 12453-12458 (2009).
883
884 12. Spidale NA*, et al.* Interleukin-17 Producing gammadelta T Cells Originate from
885 SOX13(+) Progenitors that Are Independent of gammadeltaTCR Signaling. *Immunity*,
886 (2018).
887

13. Laird SM, Tuckerman EM, Cork BA, Linjawi S, Blakemore AI, Li TC. A review of immune cells and molecules in women with recurrent miscarriage. *Hum Reprod Update* **9**, 163-174 (2003).

14. Sumaria N, Martin S, Pennington Daniel J. Constrained TCRγδ-associated Syk activity engages PI3K to facilitate thymic development of IL-17A–secreting γδ T cells. *Science Signaling* **14**, eabc5884 (2021).

15. Muro R, Nitta T, Nakano K, Okamura T, Takayanagi H, Suzuki H. gammadeltaTCR recruits the Syk/PI3K axis to drive proinflammatory differentiation program. *J Clin Invest* **128**, 415-426 (2018).

16. Cannons JL, Tangye SG, Schwartzberg PL. SLAM family receptors and SAP adaptors in immunity. *Annu Rev Immunol* **29**, 665-705 (2011).

17. Nichols KE*, et al.* Regulation of NKT cell development by SAP, the protein defective in XLP. *Nat Med* **11**, 340-345 (2005).

18. Dienz O*, et al.* Critical Role for SLAM/SAP Signaling in the Thymic Developmental Programming of IL-17- and IFN-gamma-Producing gammadelta T Cells. *J Immunol*, (2020).

19. Legoux F, Gilet J, Procopio E, Echasserieau K, Bernardeau K, Lantz O. Molecular mechanisms of lineage decisions in metabolite-specific T cells. *Nat Immunol* **20**, 1244-1255 (2019).

20. Koay HF*, et al.* A divergent transcriptional landscape underpins the development and functional branching of MAIT cells. *Sci Immunol* **4**, (2019).

21. Azuara V, Levraud JP, Lembezat MP, Pereira P. A novel subset of adult gamma delta thymocytes that secretes a distinct pattern of cytokines and expresses a very restricted T cell receptor repertoire. *Eur J Immunol* **27**, 544-553 (1997).

22. Havran WL, Allison JP. Developmentally ordered appearance of thymocytes expressing different T-cell antigen receptors. *Nature* **335**, 443-445 (1988).

23. O'Brien RL, Born WK. gammadelta T cell subsets: a link between TCR and function? *Semin Immunol* **22**, 193-198 (2010).

24. Stoeckius M*, et al.* Simultaneous epitope and transcriptome measurement in single cells. *Nature methods* **14**, 865-868 (2017).

25. Coffey F*, et al.* The TCR ligand-inducible expression of CD73 marks gammadelta lineage commitment and a metastable intermediate in effector specification. *J Exp Med* **211**, 329-343 (2014).

934 26. In TSH, *et al.* HEB is required for the specification of fetal IL-17-producing gammadelta
935 T cells. *Nat Commun* **8**, 2004 (2017).
936
937 27. Satija R, Farrell JA, Gennert D, Schier AF, Regev A. Spatial reconstruction of single-cell
938 gene expression data. *Nat Biotechnol* **33**, 495-502 (2015).
939
940 28. Havran WL, Chien YH, Allison JP. Recognition of self antigens by skin-derived T cells
941 with invariant gamma delta antigen receptors. *Science* **252**, 1430-1432 (1991).
942
943 29. Itohara S, *et al.* Homing of a gamma delta thymocyte subset with homogeneous T-cell
944 receptors to mucosal epithelia. *Nature* **343**, 754-757 (1990).
945
946 30. Wencker M, *et al.* Innate-like T cells straddle innate and adaptive immunity by altering
947 antigen-receptor responsiveness. *Nat Immunol* **15**, 80-87 (2014).
948
949 31. Buus TB, Odum N, Geisler C, Lauritsen JPH. Three distinct developmental pathways for
950 adaptive and two IFN-gamma-producing gammadelta T subsets in adult thymus. *Nat*
951 *Commun* **8**, 1911 (2017).
952
953 32. Xu H, *et al.* MS4a4B, a CD20 homologue in T cells, inhibits T cell propagation by
954 modulation of cell cycle. *PloS one* **5**, e13780 (2010).
955
956 33. Howie D, *et al.* MS4A4B is a GITR-associated membrane adapter, expressed by
957 regulatory T cells, which modulates T cell activation. *J Immunol* **183**, 4197-4204 (2009).
958
959 34. Sagar, *et al.* Deciphering the regulatory landscape of fetal and adult gammadelta T-cell
960 development at single-cell resolution. *EMBO J* **39**, e104159 (2020).
961
962 35. Laird RM, Laky K, Hayes SM. Unexpected role for the B cell-specific Src family kinase
963 B lymphoid kinase in the development of IL-17-producing gammadelta T cells. *J*
964 *Immunol* **185**, 6518-6527 (2010).
965
966 36. Zuberbuehler MK, *et al.* The transcription factor c-Maf is essential for the commitment
967 of IL-17-producing gammadelta T cells. *Nat Immunol* **20**, 73-85 (2019).
968
969 37. Narayan K, *et al.* Intrathymic programming of effector fates in three molecularly distinct
970 gammadelta T cell subtypes. *Nat Immunol* **13**, 511-518 (2012).
971
972 38. Lu Y, Cao X, Zhang X, Kovalovsky D. PLZF Controls the Development of Fetal-
973 Derived IL-17+Vgamma6+ gammadelta T Cells. *J Immunol* **195**, 4273-4281 (2015).
974
975 39. Jojic V, *et al.* Identification of transcriptional regulators in the mouse immune system.
976 *Nat Immunol* **14**, 633-643 (2013).
977
978 40. Malhotra N, *et al.* A network of high-mobility group box transcription factors programs
979 innate interleukin-17 production. *Immunity* **38**, 681-693 (2013).

980
981 41. He Q, *et al.* TOX deficiency facilitates the differentiation of IL-17A-producing
982 gammadelta T cells to drive autoimmune hepatitis. *Cellular & molecular immunology* **19**,
983 1102-1116 (2022).
984
985 42. Fahl SP, *et al.* The E protein-TCF1 axis controls gammadelta T cell development and
986 effector fate. *Cell Rep* **34**, 108716 (2021).
987
988 43. DiToro D, *et al.* Insulin-Like Growth Factors Are Key Regulators of T Helper 17
989 Regulatory T Cell Balance in Autoimmunity. *Immunity* **52**, 650-667 e610 (2020).
990
991 44. Roberts NA, *et al.* Rank signaling links the development of invariant gammadelta T cell
992 progenitors and Aire(+) medullary epithelium. *Immunity* **36**, 427-437 (2012).
993
994 45. Wei YL, *et al.* A Highly Focused Antigen Receptor Repertoire Characterizes gammadelta
995 T Cells That are Poised to Make IL-17 Rapidly in Naive Animals. *Frontiers in*
996 *immunology* **6**, 118 (2015).
997
998 46. Kashani E, *et al.* A clonotypic Vgamma4Jgamma1/Vdelta5Ddelta2Jdelta1 innate
999 gammadelta T-cell population restricted to the CCR6(+)CD27(-) subset. *Nat Commun* **6**,
1000 6477 (2015).
1001
1002 47. Sim GK, Augustin A. Dominantly inherited expression of BID, an invariant undiversified
1003 T cell receptor delta chain. *Cell* **61**, 397-405 (1990).
1004
1005 48. Scaramuzzino S, *et al.* Single-cell transcriptomics uncovers an instructive T-cell receptor
1006 role in adult gammadelta T-cell lineage commitment. *EMBO J* **41**, e110023 (2022).
1007
1008 49. Prinz I, Sansoni A, Kissenpfennig A, Ardouin L, Malissen M, Malissen B. Visualization
1009 of the earliest steps of gammadelta T cell development in the adult thymus. *Nat Immunol*
1010 **7**, 995-1003 (2006).
1011
1012 50. Mingueneau M, *et al.* The transcriptional landscape of alphabeta T cell differentiation.
1013 *Nat Immunol* **14**, 619-632 (2013).
1014
1015 51. Passoni L, *et al.* Intrathymic delta selection events in gammadelta cell development.
1016 *Immunity* **7**, 83-95 (1997).
1017
1018 52. Kang J, Coles M, Cado D, Raulet DH. The developmental fate of T cells is critically
1019 influenced by TCRgammadelta expression. *Immunity* **8**, 427-438 (1998).
1020
1021 53. Haks MC, *et al.* Attenuation of gammadeltaTCR signaling efficiently diverts thymocytes
1022 to the alphabeta lineage. *Immunity* **22**, 595-606 (2005).
1023
1024 54. Griewank K, *et al.* Homotypic interactions mediated by Slamf1 and Slamf6 receptors
1025 control NKT cell lineage development. *Immunity* **27**, 751-762 (2007).

1026
1027 55. Kreslavsky T, Garbe AI, Krueger A, von Boehmer H. T cell receptor-instructed alphabeta
1028 versus gammadelta lineage commitment revealed by single-cell analysis. *J Exp Med* **205**,
1029 1173-1186 (2008).
1030
1031 56. Fahl SP*, et al.* Role of a selecting ligand in shaping the murine gammadelta-TCR
1032 repertoire. *Proc Natl Acad Sci U S A* **115**, 1889-1894 (2018).
1033
1034 57. Verykokakis M, Boos MD, Bendelac A, Adams EJ, Pereira P, Kee BL. Inhibitor of DNA
1035 binding 3 limits development of murine slam-associated adaptor protein-dependent
1036 "innate" gammadelta T cells. *PloS one* **5**, e9303 (2010).
1037
1038 58. Lu Y*, et al.* SLAM receptors foster iNKT cell development by reducing TCR signal
1039 strength after positive selection. *Nat Immunol*, (2019).
1040
1041 59. Laird RM, Hayes SM. Roles of the Src tyrosine kinases Lck and Fyn in regulating
1042 gammadeltaTCR signal strength. *PloS one* **5**, e8899 (2010).
1043
1044 60. Davidson D*, et al.* Genetic evidence linking SAP, the X-linked lymphoproliferative gene
1045 product, to Src-related kinase FynT in T(H)2 cytokine regulation. *Immunity* **21**, 707-717
1046 (2004).
1047
1048 61. Hayes SM, Li L, Love PE. TCR signal strength influences alphabeta/gammadelta lineage
1049 fate. *Immunity* **22**, 583-593 (2005).
1050
1051 62. Oh S*, et al.* Distinct subpopulations of DN1 thymocytes exhibit preferential gammadelta
1052 T lineage potential. *Frontiers in immunology* **14**, 1106652 (2023).
1053
1054 63. Edwards SC*, et al.* A population of proinflammatory T cells coexpresses alphabeta and
1055 gammadelta T cell receptors in mice and humans. *J Exp Med* **217**, (2020).
1056
1057 64. Rigau M*, et al.* Butyrophilin 2A1 is essential for phosphoantigen reactivity by
1058 gammadelta T cells. *Science* **367**, (2020).
1059
1060 65. Melandri D*, et al.* The gammadeltaTCR combines innate immunity with adaptive
1061 immunity by utilizing spatially distinct regions for agonist selection and antigen
1062 responsiveness. *Nat Immunol* **19**, 1352-1365 (2018).
1063
1064 66. Sperling AI, Decker DC, DiPaolo RJ, Stern DA, Shum A, Bluestone JA. Selective
1065 expansion of Vgamma2-Vdelta7 TCR gammadelta cells in C57BL/6 mice is postnatal
1066 and extrathymic. *J Immunol* **159**, 86-91 (1997).
1067
1068 67. Sim GK, Augustin A. Extrathymic positive selection of gamma delta T cells. V gamma
1069 4J gamma 1 rearrangements with "GxYS" junctions. *J Immunol* **146**, 2439-2445 (1991).
1070

1071 68. Van Gassen S, *et al.* FlowSOM: Using self-organizing maps for visualization and
1072 interpretation of cytometry data. *Cytometry Part A : the journal of the International*
1073 *Society for Analytical Cytology* **87**, 636-645 (2015).
1074
1075 69. Ewels P, Magnusson M, Lundin S, Käller M. MultiQC: summarize analysis results for
1076 multiple tools and samples in a single report. *Bioinformatics (Oxford, England)* **32**,
1077 (2016).
1078
1079 70. Martin M. Cutadapt removes adapter sequences from high-throughput sequencing reads.
1080 *2011* **17**, 3 (2011).
1081
1082 71. Patro R, Duggal G, Love MI, Irizarry RA, Kingsford C. Salmon provides fast and bias-
1083 aware quantification of transcript expression. *Nature methods* **14**, 417-419 (2017).
1084
1085 72. Soneson C, Love MI, Robinson MD. Differential analyses for RNA-seq: transcript-level
1086 estimates improve gene-level inferences. *F1000Research* **4**, (2015).
1087
1088 73. Love MI, Huber W, Anders S. Moderated estimation of fold change and dispersion for
1089 RNA-seq data with DESeq2. *Genome biology* **15**, 550 (2014).
1090
1091 74. Zheng GXY, *et al.* Massively parallel digital transcriptional profiling of single cells.
1092 *Nature Communications* **8**, 1-12 (2017).
1093
1094 75. Hao Y, *et al.* Integrated analysis of multimodal single-cell data. *Cell* **184**, 3573-3587
1095 e3529 (2021).
1096
1097 76. Denisenko E, *et al.* Systematic assessment of tissue dissociation and storage biases in
1098 single-cell and single-nucleus RNA-seq workflows. *Genome biology* **21**, 130 (2020).
1099
1100 77. Stoeckius M, *et al.* Cell Hashing with barcoded antibodies enables multiplexing and
1101 doublet detection for single cell genomics. *Genome biology* **19**, 224 (2018).
1102
1103 78. Hafemeister C, Satija R. Normalization and variance stabilization of single-cell RNA-seq
1104 data using regularized negative binomial regression. *Genome biology* **20**, 296 (2019).
1105
1106 79. Marsh SE. scCustomize: Custom Visualizations & Functions for Streamlined Analyses of
1107 Single Cell Sequencing.) (2021).
1108
1109 80. Squair JW, *et al.* Confronting false discoveries in single-cell differential expression. *Nat*
1110 *Commun* **12**, 5692 (2021).
1111
1112 81. Wolf FA, *et al.* PAGA: graph abstraction reconciles clustering with trajectory inference
1113 through a topology preserving map of single cells. *Genome biology* **20**, 59 (2019).
1114
1115 82. Wolf FA, Angerer P, Theis FJ. SCANPY: large-scale single-cell gene expression data
1116 analysis. *Genome biology* **19**, 15 (2018).

83. Lefranc MP. IMGT, the International ImMunoGeneTics Information System. *Cold Spring Harb Protoc* **2011**, 595-603 (2011).

84. Pereira P, Boucontet L. Rates of recombination and chain pair biases greatly influence the primary gammadelta TCR repertoire in the thymus of adult mice. *J Immunol* **173**, 3261-3270 (2004).

85. M S*, et al.* VDJtools: Unifying Post-analysis of T Cell Receptor Repertoires. *PLoS computational biology* **11**, (2015).

86. J Y, N M, TL M, JM O. IgBLAST: an immunoglobulin variable domain sequence analysis tool. *Nucleic Acids Res* **41**, (2013).

1132 **Figure Legends**

1133 **Figure 1. SLAM family receptor expression marks transcriptionally distinct developmental**
1134 **stages among E17 γδ T cells. (A)** Schematic workflow depicting the methodology for single-cell
1135 RNA sequencing (scRNAseq) library preparation and subsequent data analysis pipeline employed
1136 in this study. **(B)** Uniform Manifold Approximation and Projection (UMAP) visualization
1137 displaying 11 distinct clusters of E17 B6 thymic γδ T cells, n = 4 individual mice. Clusters are
1138 annotated based on comprehensive protein and gene expression data. **(C)** Feature plots illustrating
1139 the cell surface protein expression profiles of CD24, CD73, CD44, CD45RB, SLAMF1, and
1140 SLAMF6 on B6 E17 thymic γδ T cells. Each data point represents a cell, color-coded to indicate
1141 varying protein expression levels (high: dark blue, low: yellow). **(D)** Feature plot illustrating the
1142 gene expression profiles of signature genes among individual B6 E17 thymic γδ T cells. Each data
1143 point represents a cell, color-coded based on gene expression levels (high: purple, low: yellow).
1144 **(E)** Dot plot demonstrating the scaled expression levels of selected genes in E17 B6 thymic γδ T
1145 cells. Normalized expression levels are depicted using a color scale ranging from low (yellow) to
1146 high (purple). Dot size corresponds to the fraction of cells within each cluster expressing the
1147 specific marker. **(F)** UMAP representation of E17 B6 thymic γδ T cells indicating the expression
1148 of selected TRGV (TCRγ; left) and TRDV (TCRδ; right) chain V-segment usage (in blue) across
1149 individual cells. **(G)** Violin plots illustrating the expression patterns of selected genes among E17
1150 B6 thymic γδ T cell clusters. **(H)** Visualization of single-cell trajectories using PAGA (partition-
1151 based graph abstraction) with single-cell embedding (left) showing connectivity between
1152 individual nodes (middle). Weighted edges represent statistical measures of interconnectivity. The
1153 diffusion pseudotime plot (right) delineates inferred pseudotime progression of cells along

1154 developmental trajectories using cluster 5 (C5) as the root, highlighting their developmental order
1155 (from purple to yellow).
1156
1157 **Figure. 2. Identification of SAP-dependent developmental checkpoints during E17 γδ T cell**
1158 **developmental programming. (A)** UMAP representation of B6 (left) and B6.SAP$^{-/-}$ (right) γδ T
1159 cells from E17 thymi (n = 4 mice per group) is shown at *left.* Clusters were annotated based on
1160 protein and gene expression data. The frequencies of B6 and B6.SAP$^{-/-}$ E17 γδ T cell clusters is
1161 shown at right. Bars represent the mean cluster frequency, error bars represent standard deviation,
1162 **$p \leq 0.01$, two-way ANOVA, Sidak multiple-comparisons test; n=4 mice/genotype. **(B)** Volcano
1163 plot of differentially expressed genes among immature CD24^{high}CD73^{neg} (clusters: C1, C2, C5, C6,
1164 C7, and C10) B6 and B6.SAP$^{-/-}$ γδ T cells using pseudobulk scRNAseq analysis. Genes exhibiting
1165 a $\log_2FC \geq 0.5$ or ≤ -0.5, and a $p_{adj} \leq 0.005$ in are shown in red. Only some selected genes are
1166 labelled for the sake of clarity. **(C)** Feature plots illustrating gene expression profiles of selected
1167 C2 and C6 cluster-specific genes among individual B6 and B6.SAP$^{-/-}$ E17 thymic γδ T cells. Each
1168 point represents a cell, color-coded by gene expression level (high: purple, low: yellow). **(D)** TCR
1169 clonotype bubble plot displaying the top 100 B6 and B6.SAP$^{-/-}$ TRGV4 clonotypes in E17 thymus.
1170 Bubbles represent unique TRGV4/TRDV clonotypes; size indicates frequency of clonotype among
1171 all Vγ4 T cells (n = 388 B6, 288 B6.SAP$^{-/-}$ cells), and colors denote specific TRDV chains utilized.
1172 Selected clonotypes are numbered and their respective CDR3γ and CDR3δ sequences displayed
1173 below. Data are **(E)** Altered TRGV/TRDV clonotype distribution between B6 and B6.SAP$^{-/-}$ E17
1174 thymic γδ T cells. Frequencies of selected clonotypes among different clusters of B6 and B6.SAP^{-}
1175 $^{/-}$ E17 γδ T cells is shown. Bars represent the mean clonotype frequency among the indicated

1176 TRGV/TRDV pairings shown, error bars represent standard deviation, *$p \leq 0.05$, ***$p \leq 0.001$,
1177 two-way ANOVA, Sidak multiple-comparisons test; n = 4 mice/genotype-age groups.
1178
1179 **Figure 3. Increased frequency and numbers of immature $CD4^+CD8^+$c-$MAF^-ROR\gamma t^+$ thymic**
1180 **γδ T cells in B6.$SAP^{-/-}$ E17 γδ T cells. (A)** Representative contour plots depicting $CD24^{pos}$ E17
1181 γδ T cells in B6 (top) and B6.$SAP^{-/-}$ (bottom) mice. Concatenated data from 2 B6 and 3 B6.$SAP^{-/-}$
1182 embryos are shown, and are representative of 2 independent experiments. Numbers in the plots
1183 represent the frequency as a percentage of $CD24^{pos}$ γδ T cells. **(B)** Cumulative frequency and
1184 number of immature $CD24^{pos}$ BLK- (left), c-MAF- (right), RORγt-expressing E17 thymic γδ T
1185 cells. The mean and standard deviation are indicated. Data are the cumulative data from 2
1186 independent experiments, n = 10 B6, 11 B6.$SAP^{-/-}$ pooled embryonic thymi, *$p \leq 0.05$, **$p \leq 0.01$,
1187 ***$p \leq 0.001$, ****$p \leq 0.0001$, two-way ANOVA, Sidak's multiple comparisons test. **(C)** Relative
1188 geometric mean of BLK, c-MAF, and RORγt expression in B6 and B6.$SAP^{-/-}$ E17 $CD24^+CD73^-$
1189 Vγ4 γδ T cells, *$p \leq 0.001$, ****$p \leq 0.0001$, two-way ANOVA, Sidak's multiple comparisons test.
1190 Data are representative of 2 independent experiments, 7-9 mice per group. **(D)** Cumulative
1191 frequency (left) and number (right) of immature CD4- and CD8- $MAF^{neg}ROR\gamma t^{pos}$ E17 thymic γδ
1192 T cells in B6 and B6.$SAP^{-/-}$ thymus. The mean and standard deviation are indicated. Data are the
1193 cumulative data from 2 independent experiments, n = 10 B6, 11 B6.$SAP^{-/-}$ pooled embryonic
1194 thymi, **$p \leq 0.01$, ***$p \leq 0.001$, ****$p \leq 0.0001$, two-way ANOVA, Sidak's multiple
1195 comparisons test.
1196
1197 **Figure 4. Identification of SAP-dependent developmental checkpoints during neonatal γδ T**
1198 **cell developmental programming. (A)** UMAP representation of B6 (left) and B6.$SAP^{-/-}$ (right)

1199 γδ T cells from D9 neonatal thymi (n = 3 mice per strain). Cluster annotation is based on
1200 comprehensive protein and gene expression data. **(B)** Feature plots displaying cell surface protein
1201 expression patterns of CD24, CD73, SLAMF1, and SLAMF6 on D9 B6 thymus γδ T cells. Data
1202 are color-coded based on protein expression level (high: dark blue, low: yellow). **(C)** UMAP
1203 representation of D9 B6 thymic γδ T cells exhibiting selected TRGV4 (left) and TRDV (right)
1204 chain V-segment usage (in blue) in individual cells. **(D)** Frequencies of B6 and B6.SAP$^{-/-}$ D9
1205 thymic γδ T cell clusters. Bars represent the mean cluster frequency, error bars represent standard
1206 deviation, *p ≤ 0.05, **p ≤ 0.01, two-way ANOVA, Sidak multiple-comparisons test, 3
1207 mice/strain. **(E)** Representative contour plots depicting BLK and RORγt expression in B6 and
1208 B6.SAP$^{-/-}$ CD24^{pos}CD73^{neg} D9 Vγ4 T cells are shown *above*. Cumulative frequencies of BLK and
1209 RORγt expression are shown *below*. The mean and standard deviation are indicated. Data are the
1210 cumulative data from 3 independent experiments, n = 13 B6, 16 B6.SAP$^{-/-}$ mice, ****p ≤ 0.0001,
1211 two-way ANOVA, Sidak's multiple comparisons test. **(F)** Decreased BLK expression in immature
1212 B6.SAP$^{-/-}$ γδ T cells. Data represent the mean expression of the indicated proteins in D6 neonate
1213 BLK^{pos}, RORγt^{pos}, or c-Maf^{pos} thymic γδ T cells, **p ≤ 0.01.
1214

1215 **Figure 5. SAP shapes the neonatal γδ TCR repertoire. (A)** TCR clonotype bubble plots
1216 depicting the top 100 B6 and B6.SAP$^{-/-}$ TCR clonotypes among D9 thymic γδ T cells. Each bubble
1217 represents a unique clonotype, is sized according to its frequency as a percentage of all γδ T cells
1218 n = 1429 B6, 1354 B6.SAP$^{-/-}$ cells), and is colored based on specific TRGV chains utilized. **(B)**
1219 TCR clonotype bubble plots depicting the top 100 B6 and B6.SAP$^{-/-}$ TRGV1 (*above*) and TRGV4
1220 (*below*) clonotypes among D9 γδ T cells. Bubble size indicates clonotype frequency as a
1221 percentage of TRGV1^{+} (n = 198 B6, 98 B6.SAP$^{-/-}$) or TRGV4^{+} (n = 646 B6, 669 B6.SAP$^{-/-}$) cells,

1222 and colors correspond to specific TRDV chains. Selected clonotypes are numbered and their
1223 corresponding CDR3γ and CDR3δ sequences are displayed below. **(C)** Distribution of selected
1224 TRGV/TRDV clonotypes among B6 and B6.SAP$^{-/-}$ D9 thymic γδ T cell clusters. Data
1225 representative of 3 mice/strain, *$p \leq 0.05$, ***$p \leq 0.001$, two-way ANOVA, Sidak multiple-
1226 comparisons test.
1227
1228 **Figure 6. Restricted TCR repertoire in innate-like γδT1 as well as γδT17 in the periphery.**
1229 **(A)** UMAP representation of B6 adult lung γδ T cells. Clusters are annotated based on gene
1230 expression and TCR profiling data. **(B)** Feature plot displaying gene expression profiles of selected
1231 genes among individual B6 lung γδ T cells, color-coded based on gene expression levels. **(C)** Dot
1232 plot indicating scaled expression levels of selected genes in B6 lung γδ T cells, with dot size
1233 representing the fraction of cells within each cluster expressing the marker. **(D)** SLAMF6 and
1234 SLAMF7 co-expression marks CD44^{+}CD45RB^{+} IFN-γ-producing cells in the periphery.
1235 Representative dot plots (left) of CD44 and CD45RB expression on lung Vγ1 (top) and Vγ4
1236 (bottom) γδ T cells. SLAMF7-expressing cells are highlighted in blue. Representative contour
1237 plots (right) of SLAMF1, SLAMF6, and SLAMF7 expression on IFN-γ^{+} and IL-17^{+} lung γδ T
1238 cells. **(E)** UMAP representation of B6 lung γδ T cells indicating selected TRG and TRD chain V-
1239 segment usage (blue). **(F)** Amino acid length distribution of lung CDR3δ clonotypes among
1240 immature C0/C5, γδT1 C2/C3/C7/C9, γδT17 C1, and γδT17 C4 clusters. The top 10 clonotypes in
1241 each group are color-coded, while all other clonotypes are shown in gray.
1242
1243 **Figure 7. Specific decrease in Vγ4/Vδ7 γδT1 cells in the lungs of SAP-deficient mice. (A)**
1244 UMAP representation of B6 (left) and B6.SAP$^{-/-}$ (right) lung γδ T cells, pooled from 3 mice per

1245 strain. **(B)** SAP-dependent variation in lung γδ T cell cluster frequencies. The frequency of each
1246 B6 and B6.SAP$^{-/-}$ cluster as a percentage of all lung γδ T cells is shown. (**C**) UMAP representation
1247 of selected TRG and TRD chain V-segment usage (blue) among B6 and B6.SAP$^{-/-}$ lung γδ T cells.
1248 **(D)** SAP-dependent decrease in lung γδT1 TRGV4/TRDV7. Normalized TRDV counts in B6 and
1249 B6.SAP$^{-/-}$ lung TRGV4^{+} γδT1 clusters (C2/C3/C7/C9). **(E)** SAP-dependent decrease in SLAMF7^{+}
1250 lung Vγ4 T cells. Representative contour plots of CD44 and SLAMF7 expression in B6 (left) and
1251 B6.SAP$^{-/-}$ (right) lung Vγ4 γδ T cells are shown at *left*. Relative frequencies and counts of
1252 CD44^{+}SLAMF7^{+} lung Vγ4 cells is shown at *right*. Data represent the cumulative data from five
1253 independent experiments, ****$p < 0.0001$ using unpaired t-test. **(F)** SAP-dependent skewing of
1254 the lung γδT17 TCR repertoire. Amino acid length distributions of B6 and B6.SAP$^{-/-}$ TRGV4^{+}
1255 CDR3γ (left) and TRDV2^{+} CDR3δ (right) sequences in the lung Vγ4 γδT17 C1 cluster. The top
1256 10 clonotypes are color-coded and all other clonotypes are shown in gray. Bars represent the
1257 frequency of γδ T cells in the c1 cluster. **(G)** TCR clonotype bubble plots depicting the top 50 lung
1258 TRGV4 clonotypes in the C1 γδT17 cluster. Bubble size indicates clonotype frequency as a
1259 percentage of C1 Vγ4 (n = 62 B6, 104 B6.SAP$^{-/-}$) T cells, and colors correspond to specific TRDV
1260 chains. Selected clonotypes are numbered and their corresponding CDR3γ and CDR3δ sequences
1261 are displayed below.

1262 **Supplementary Figure Legends**
1263
1264 **Supplemental Figure 1: Quality control for single cell CITE-seq. (A)** Representative gating
1265 scheme used for FACS sorting γδ cells from B6 (top) and B6.SAP$^{-/-}$ (bottom) thymus. **(B)** *Left,*
1266 Violin plots of B6 E17 thymic γδ T cells. nFeaure_RNA represents number of genes detected in
1267 each cell. nCount_RNA represents total number of molecules detected within a cell, percent.mt
1268 represents the frequency of mitochondrial genes expressed in each cell, and percent.ribo represents
1269 the frequency of ribosomal genes expressed in each cell. *Middle,* ridge plots demonstrating
1270 successful enrichment for selected hashtags in E17 thymus γδ T cells following demultiplexing.
1271 *Right,* UMAP representations showing distribution of demultiplexed γδ T cells among individual
1272 B6 E17 thymus samples. **(C)** Violin plots depicting distribution of cell surface protein oligo-
1273 conjugated antibody derived tags (ADTs) among different B6 E17 thymus γδ T cells clusters. **(D)**
1274 Violin plots depicting expression levels of selected genes among individual E17 B6 thymic γδ T
1275 cells clusters. **(E)** Representative dot plots of CD24 and SLAMF7 staining on neonatal thymus γδ
1276 T cells. The position of CD44^{+}CD45RB^{+} cells are shown in blue. Data are representative of two
1277 independent experiments, n = 10 mice.
1278
1279 **Supplemental Figure 2: TCR repertoire profiling of B6 E17 thymus γδ T cells. (A)** *Left,* TCR
1280 clonotype bubble plot depicting the top 100 TCR clonotypes among B6 E17 γδ T cells (n = 2502
1281 γδ T cells). Each bubble represents a unique TRGV/TRDV clonotype; the bubble size corresponds
1282 to the clonotype frequency, and colors correspond to specific TRGV chains utilized. The 4 most
1283 frequent clonotypes are numbered and their corresponding CDR3γ and CDR3δ sequences are
1284 displayed below. *Right*, UMAP representations depicting the location of the four most frequent
1285 clonotypes E17 thymic γδ T cell clusters. **(B)** Diversity of the E17 γδ TCR repertoire, represented

1286 by the Inverse Simpson index. **(C)** Amino acid length distributions of E17 thymic γδ T cell CDR3γ
1287 (top) and CDR3δ (bottom) in immature *Blk*$^{+}$, *Etv5*$^{+}$, *Maf*$^{+}$ C2 and C7 (left), immature RORγt^{high}
1288 C1 (middle), and mature RORγt^{high} c8 (right) clusters. The top 10 clonotypes are color-coded, all
1289 other clonotypes are shown in gray.
1290

1291 **Supplemental Figure 3: Identification of a BLK^{neg}MAF^{neg}RORγt^{pos} E17 γδ T cell population**
1292 **expressing CD4 and CD8. (A)** *Left,* Representative dot plot of CD24 and CD25 expression on
1293 E17 B6 thymic Vγ4 T cells. *Right,* Histograms depicting BLK, PLZF, and RORγt expression in
1294 the gated populations at left. The geometric mean fluorescence intensity of individual populations
1295 is shown. **(B)** Feature plots showing cell surface protein expression of Vγ1 (top) and Vγ4 (bottom)
1296 on B6 E17 thymus γδ T cells. Each point represents a cell, color-coded based on the protein
1297 expression level (high: dark blue, low: yellow). **(C)** *Top left*, UMAP representation of E17 B6 γδ
1298 T cell flow cytometry data with selected FlowSOM clusters indicated by color. All other cells are
1299 shown in gray. *Right,* Individual dot plots overlaid with the selected FlowSOM clusters from the
1300 UMAP plot. Data represent concatenated data from 5 B6 TCRβ^{neg}TCRδ^{pos} γδ T cells and are
1301 representative of 2 independent experiments. **(D)** Increasing BLK^{neg}RORγt^{pos} frequency as
1302 thymocytes progress to DN4 stage. Representative contour plots of E17 DN thymocytes with
1303 selected gates shown (*left*) and BLK and RORγt expression associated with each gated population
1304 (*right*). Numbers indicate the percentage of cells in the gated population. **(E)** Immature Vγ1Vδ1 T
1305 cells comprise the major IL17-producing Vγ1 T cell population in E17 thymus. *Left,* representative
1306 contour plot of Vγ1 and Vδ1 (17D1) expression among E17 thymic γδ T cells. *Middle,* Dot plot of
1307 CD24 and SSC expression on E17 thymic γδ T cells. The position of Vγ1^{+}Vδ1^{+} E17 T cells is

1308 shown in red. *Right,* Dot plots of IL-17 and IFN-γ expression in E17 thymic $V\gamma1^{+}17D1^{+}$ and
1309 $V\gamma1^{+}17D1^{-}$ cells after PMA/ionomycin stimulation.
1310
1311 **Supplemental Figure 4:** Violin plots showing expression levels of selected genes among
1312 individual B6 and B6.SAP$^{-/-}$ E17 thymic γδ T cell clusters. **(A)** Genes whose expression decreased
1313 in B6.SAP$^{-/-}$ immature γδ T cells. **(B)** Genes whose expression increased in B6.SAP$^{-/-}$ immature
1314 γδ T cells.
1315
1316 **Supplemental Figure 5: SAP-dependent regulation of immature BLK^{+}PLZF^{+}RORγt^{+} and**
1317 **BLK^{-}PLZF$^{+/-}$RORγt^{+} E17 thymic γδ T cells. (A)** Total number of E17 thymic γδ T cells in B6
1318 and B6.SAP$^{-/-}$ E17 thymus. **(B)** E17 thymic Vγ4 developmental checkpoints. *Left, U*MAP
1319 representation of E17 B6 and B6.SAP$^{-/-}$ Vγ4 T cell flow cytometry data with selected FlowSOM
1320 clusters indicated by color. All other cells are shown in gray. *Right,* Individual dot plots overlaid
1321 with the selected FlowSOM clusters from the UMAP plot. Data represent concatenated data from
1322 4 B6 and 4 B6.SAP$^{-/-}$ TCRβ^{neg}TCRδ^{pos} γδ T cells and are representative of 2 independent
1323 experiments. **(C)** Cumulative frequency and number of the indicated FlowSOM populations shown
1324 in (B), *$p \leq 0.05$, **$p \leq 0.01$, ***$p \leq 0.001$, unpaired t-test, corrected for multiple comparison
1325 using Holm-Sidak's test. **(D)** Decreased BLK, but not PLZF expression in B6.SAP$^{-/-}$ γδ T cells.
1326 *Above,* histograms of BLK and PLZF in immature E17 γδ T cells. B6 BLK (dark gray) and PLZF
1327 (red) histograms are overlaid on B6.SAP$^{-/-}$ (light gray) histograms for comparison. *Below,* control
1328 stains lacking BLK or PLZF. **(E)** Representative contour plots of immature CD25^{neg} E.17 Vγ4 T
1329 cells in B6 and B6.SAP$^{-/-}$ mice.
1330

1331 **Supplemental Figure 6: Transcriptional heterogeneity in neonatal thymic γδ T cells. (A)** Dot
1332 plot showing scaled expression level of selected genes in B6 D9 thymic γδ T cells. Level of
1333 normalized expression is shown using a color scale ranging from low (yellow) to high (purple).
1334 Dot size represents the fraction of cells within each cluster that express the marker. **(B)** Violin
1335 plots showing the specificity of the oligo-conjugated antibody derived tags (ADT) to cell surface
1336 proteins (CD24, CD73, SLAMF1, SLAMF6) among different B6 D9 thymus γδ T cell clusters.
1337 **(C)** Violin plots showing expression levels of selected genes among individual clusters in the B6
1338 D9 thymic γδ T cells. **(D)** Violin plots showing expression levels of *Zbtb16* gene (expressing
1339 PLZF) among individual clusters in the B6 E17 (top) and D9 (bottom) thymic γδ T cells.
1340

1341 **Supplemental Figure 7: Flow cytometric analysis of D9 thymic γδ T cells. (A)** SLAMF6 and
1342 SLAMF7 expression defines γδNKT cell subsets. *Left*, representative dot plot of PLZF and T-bet
1343 expression in B6 D9 thymic Vγ1Vδ6.3 γδNKT cells. Representative contour plots of ICOS and
1344 NK1.1 (*top right)* and SLAMF6 and SLAMF7 (*bottom right*) staining in PLZF^{hi}T-bet^{low} and
1345 PLZF^{low}T-bet^{high} subsets are shown at right. Data are representative of two independent
1346 experiments with a total of ten mice. **(B)** *Left,* representative dot plot of SLAMF6 and SLAMF7
1347 expression in B6 D9 thymic Vγ1Vδ6.3 γδNKT cells. *Right,* representative dot plots of intracellular
1348 IL4 and IFN-γ expression in SLAMF6^{hi}SLAMF7^{low}, SLAMF6^{high}SLAMF7^{hi}, and
1349 SLAMF6^{low}SLAMF7^{hi} γδNKT cell subsets. Numbers indicate percentage. Cumulative data of IL-
1350 4 and IFN-γ expression is shown below. Data are representative of two independent experiments
1351 with a total of ten mice. **(C)** Increased number of immature CD200^{-}S1P1^{+} γδ T cells in SAP-
1352 deficient neonatal thymus.
1353

1354 **Supplemental Figure 8: scRNA-seq with TCR repertoire profiling of B6 and B6.SAP$^{-/-}$ adult**
1355 **thymic γδ T cells. (A)** UMAP representation of B6 and B6.SAP$^{-/-}$ adult thymus (6 weeks old) γδ
1356 T cells, n = 3 mice per strain. **(B)** Feature plots illustrating the cell surface protein expression
1357 profiles of CD24, CD73, SLAMF1, and SLAMF6 on adult thymic γδ T cells. Each data point
1358 represents a cell, color-coded to indicate varying protein expression levels (high: dark blue, low:
1359 yellow). **(C)** Frequencies of B6 and B6.SAP$^{-/-}$ γδ T cell clusters. Bars represent the mean cluster
1360 frequency, error bars represent standard deviation, *$p \leq 0.05$, **$p \leq 0.01$, ****$p \leq 0.0001$, two-
1361 way ANOVA, Sidak multiple-comparisons test. **(D)** Dot plot showing scaled expression level of
1362 selected genes in B6 adult thymic γδ T cells. Level of normalized expression is shown using a
1363 color scale ranging from low (yellow) to high (purple). Dot size represents the fraction of cells
1364 within each cluster that express the marker. **(E)** Expression of selected TRG (left) and TRDs chain
1365 (right) V-segment usage (blue) by individual adult thymus γδ T cells in B6 and B6.SAP$^{-/-}$ mice.
1366

1367 **Supplemental Figure 9: Lung Vγ4 exhibit a high usage of TRDV7 chains with a diverse**
1368 **CDR3. (A)** TRDV usage among FACS-sorted lung Vγ4 γδ T cells from 7 male and 6 female mice.
1369 **(B)** *Left,* amino acid length distribution of top lung TRDV5^{+} CDR3δ clonotypes in the lung Vγ4
1370 γδ T cell population. *Right*, distribution of the most frequent clonotypes among individual B6 mice.
1371 **(C)** *Left,* amino acid length distribution of top lung TRDV2^{+} CDR3δ clonotypes in the lung Vγ4
1372 γδ T cell population. *Right*, distribution of the most frequent clonotypes among individual B6 mice.
1373 **(D)** *Left,* amino acid length distribution of top lung TRDV7^{+} CDR3δ clonotypes in the lung Vγ4
1374 γδ T cell population. *Right*, distribution of the most frequent clonotypes among individual B6 mice.
1375 **(E)** *Left,* amino acid length distribution of top lung TRGV4^{+} CDR3γ clonotypes in the lung Vγ4
1376 γδ T cell population. *Right*, distribution of the most frequent clonotypes among individual B6 mice.

1377 **Supplemental Figure 10: Significant and specific reduction in peripheral TRGV4/TRDV7^{+}**
1378 **γδT1 in B6.SAP$^{-/-}$ mice. (A)** The relative expression of the specified TRDV transcripts in adult
1379 lung and spleen CD45^{+} leukocytes (normalized to total TRDC transcript levels) in B6 and B6.SAP^{-}
1380 $^{/-}$ mice, **p < 0.01, ****p < 0.0001, two-way ANOVA followed by Sidak multiple-comparisons
1381 test. **(B)** SAP-dependent decrease in CD44^{+}SLAMF7^{+} spleen Vγ4 T cells. The relative percentage
1382 and count of CD44^{+}SLAMF7^{+} Vγ4 cells in B6 and B6.SAP$^{-/-}$ spleen subsets are shown. Data are
1383 representative of five independent experiments with 3-5 mice per strain per experiment, ****p,
1384 <0.0001, as determined by unpaired t tests. **(C)** No difference in lung Vγ4 homeostasis in B6.SAP^{-}
1385 $^{/-}$ mice. *Top left,* Representative contour plots showing the frequency of BrdU staining in B6 and
1386 B6.SAP$^{-/-}$ lung γδ T cells. Cumulative data from two independent experiments are shown at *top*
1387 *right*. *Bottom left,* representative contour plots depicting Annexin V and Live/Dead staining in B6
1388 and B6.SAP$^{-/-}$ lung γδ T cells. Cumulative results are shown at *bottom right,* and are representative
1389 of 3 independent experiments.

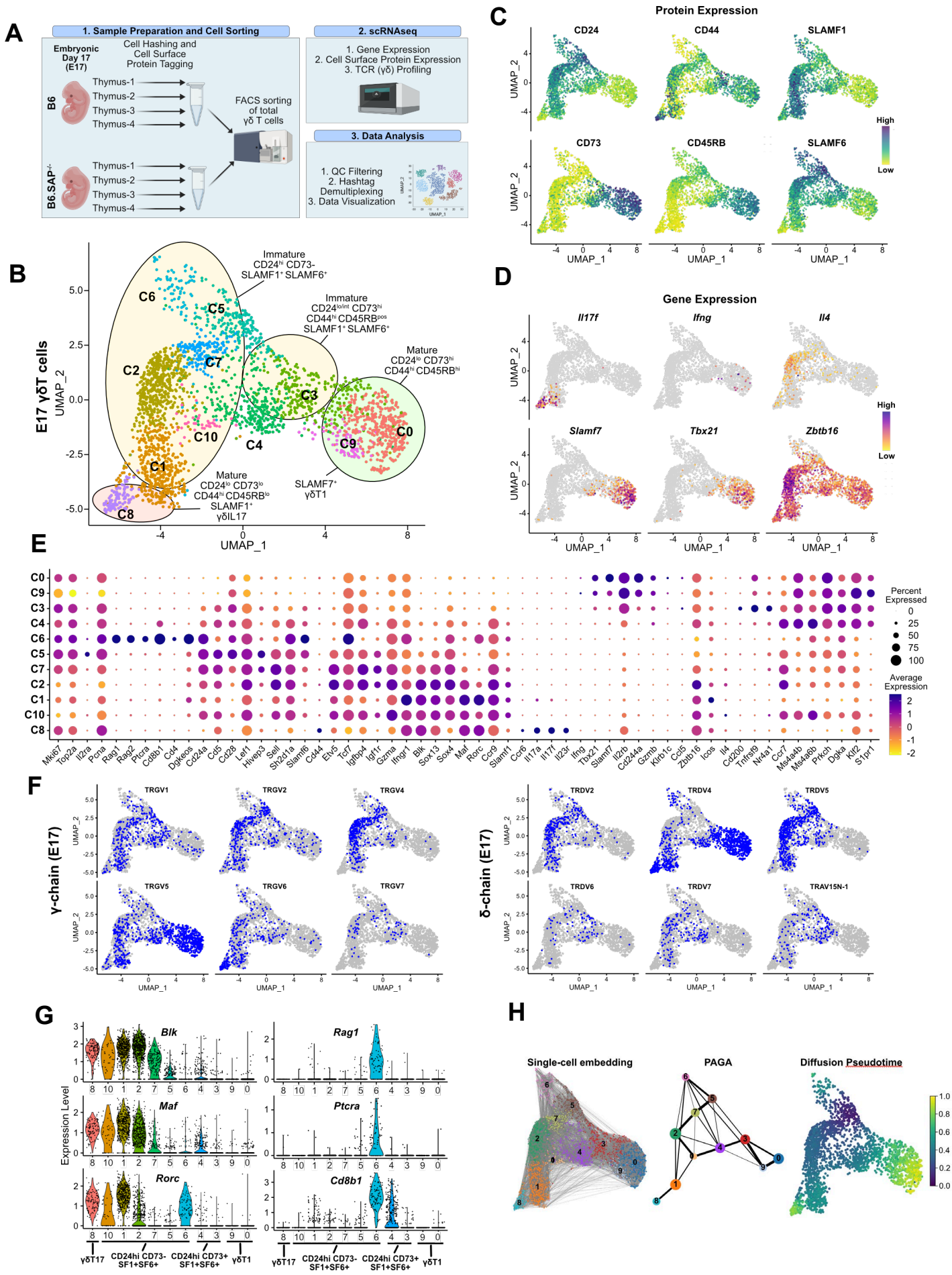
A
1. Sample Preparation and Cell Sorting
Embryonic Day 17 (E17)
Cell Hashing and Cell Surface Protein Tagging
B6
Thymus-1
Thymus-2
Thymus-3
Thymus-4
B6.SAP-/-
FACS sorting of total γδ T cells
2. scRNAseq
1. Gene Expression
2. Cell Surface Protein Expression
3. TCR (γδ) Profiling
3. Data Analysis
1. QC Filtering
2. Hashtag Demultiplexing
3. Data Visualization
B
E17 γδT cells
Immature CD24hi CD73- SLAMF1+ SLAMF6+
Immature CD24lo/int CD73hi CD44hi CD45RBpos SLAMF1+ SLAMF6+
Mature CD24lo CD73hi CD44hi CD45RBhi
Mature CD24lo CD73lo CD44hi CD45RBlo SLAMF1+ γδIL17
SLAMF7+ γδT1
C0
C1
C2
C3
C4
C5
C6
C7
C8
C9
C10
UMAP_1
UMAP_2
C
Protein Expression
CD24
CD44
SLAMF1
CD73
CD45RB
SLAMF6
High
Low
D
Gene Expression
Il17f
Ifng
Il4
Slamf7
Tbx21
Zbtb16
E
Percent Expressed
Average Expression
Mki67
Top2a
Il2ra
Pcna
Rag1
Rag2
Ptcra
Cd8b1
Cd4
Dgkeos
Cd24a
Cd5
Cd28
Lef1
Hlveps
Sell
Sh2d1a
Slamf6
Cd44
Etv5
Tcf7
Igfbp4
Igf1r
Gzma
Ifngr1
Blk
Sox13
Sox4
Maf
Rorc
Ccr9
Slamf1
Ccr6
Il17a
Il17f
Il23r
Ifng
Tbx21
Slamf7
Il2rb
Cd244a
Gzmb
Klrb1c
Cd5
Zbtb16
Icos
Il4
Cd200
Tnfrsf9
Nr4a1
Ccr7
Ms4a4b
Ms4a6b
Prkch
Dgka
Klf2
S1pr1
F
γ-chain (E17)
TRGV1
TRGV2
TRGV4
TRGV5
TRGV6
TRGV7
δ-chain (E17)
TRDV2
TRDV4
TRDV5
TRDV6
TRDV7
TRAV15N-1
G
Expression Level
Blk
Rag1
Maf
Ptcra
Rorc
Cd8b1
γδT17
CD24hi CD73- SF1+SF6+
CD24hi CD73+ SF1+SF6+
γδT1
H
Single-cell embedding
PAGA
Diffusion Pseudotime

Figure 1

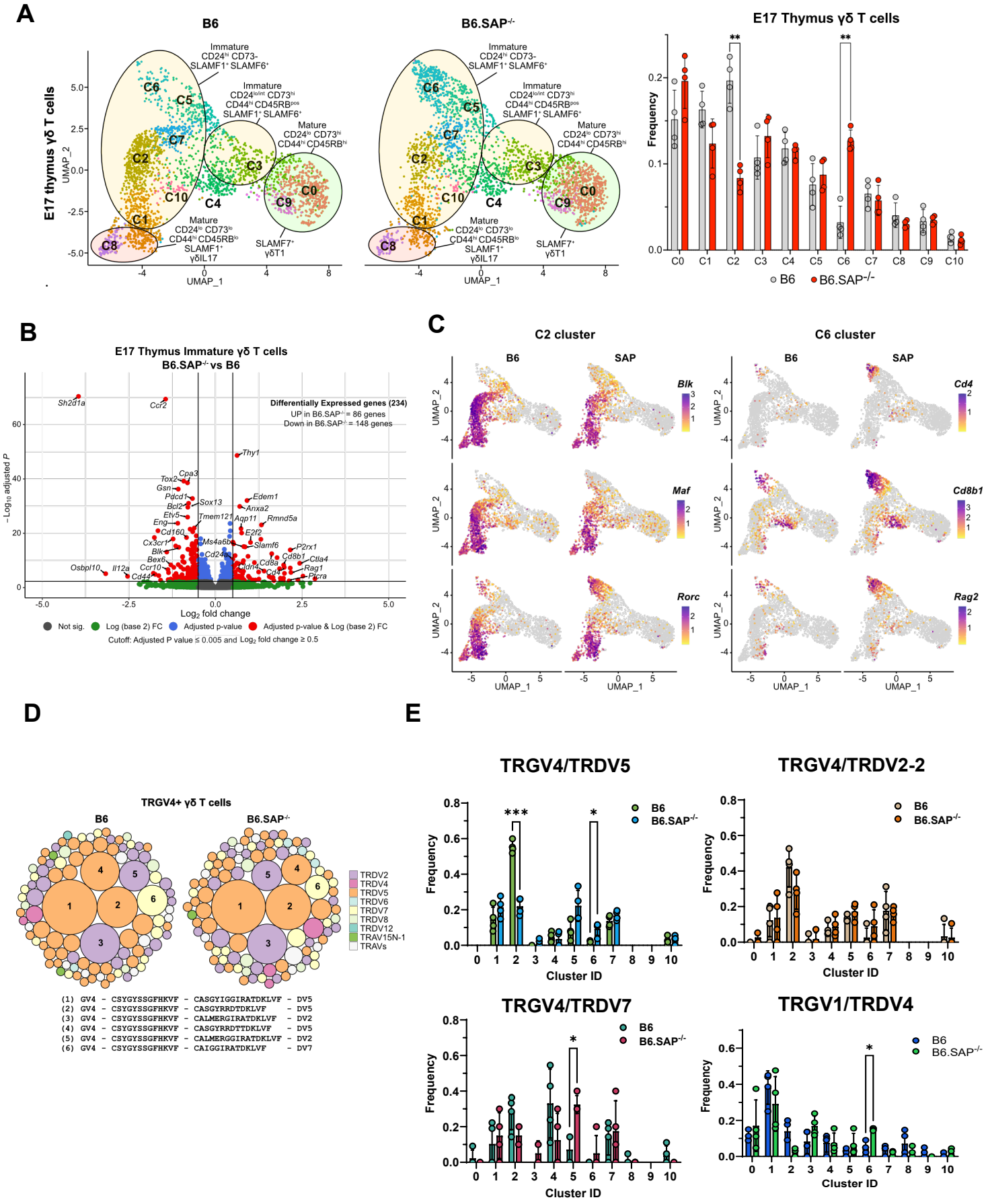
A
B6
B6.SAP-/-
E17 thymus γδ T cells
UMAP_1
UMAP_2
Immature CD24hi CD73- SLAMF1+ SLAMF6+
Immature CD24lo/int CD73hi CD44hi CD45RBpos SLAMF1+ SLAMF6+
Mature CD24lo CD73hi CD44hi CD45RBhi
Mature CD24lo CD73lo CD44hi CD45RBlo SLAMF1+ γδIL17
SLAMF7+ γδT1
E17 Thymus γδ T cells
Frequency
B6
B6.SAP-/-
B
E17 Thymus Immature γδ T cells
B6.SAP-/- vs B6
Differentially Expressed genes (234)
UP in B6.SAP-/- = 86 genes
Down in B6.SAP-/- = 148 genes
Log2 fold change
Not sig.
Log (base 2) FC
Adjusted p-value
Adjusted p-value & Log (base 2) FC
Cutoff: Adjusted P value ≤ 0.005 and Log2 fold change ≥ 0.5
C
C2 cluster
C6 cluster
B6
SAP
Blk
Maf
Rorc
Cd4
Cd8b1
Rag2
D
TRGV4+ γδ T cells
B6
B6.SAP-/-
TRDV2
TRDV4
TRDV5
TRDV6
TRDV7
TRDV8
TRDV12
TRAV15N-1
TRAVs
(1) GV4 - CSYGYSSGFHKVF - CASGYIGGIRATDKLVF - DV5
(2) GV4 - CSYGYSSGFHKVF - CASGYRRDTDKLVF - DV5
(3) GV4 - CSYGYSSGFHKVF - CALMERGIRATDKLVF - DV2
(4) GV4 - CSYGYSSGFHKVF - CASGYRRDTTDKLVF - DV5
(5) GV4 - CSYGYSSGFHKVF - CALMERGGIRATDKLVF - DV2
(6) GV4 - CSYGYSSGFHKVF - CAIGGIRATDKLVF - DV7
E
TRGV4/TRDV5
TRGV4/TRDV2-2
TRGV4/TRDV7
TRGV1/TRDV4
Frequency
Cluster ID
B6
B6.SAP-/-

Figure 2

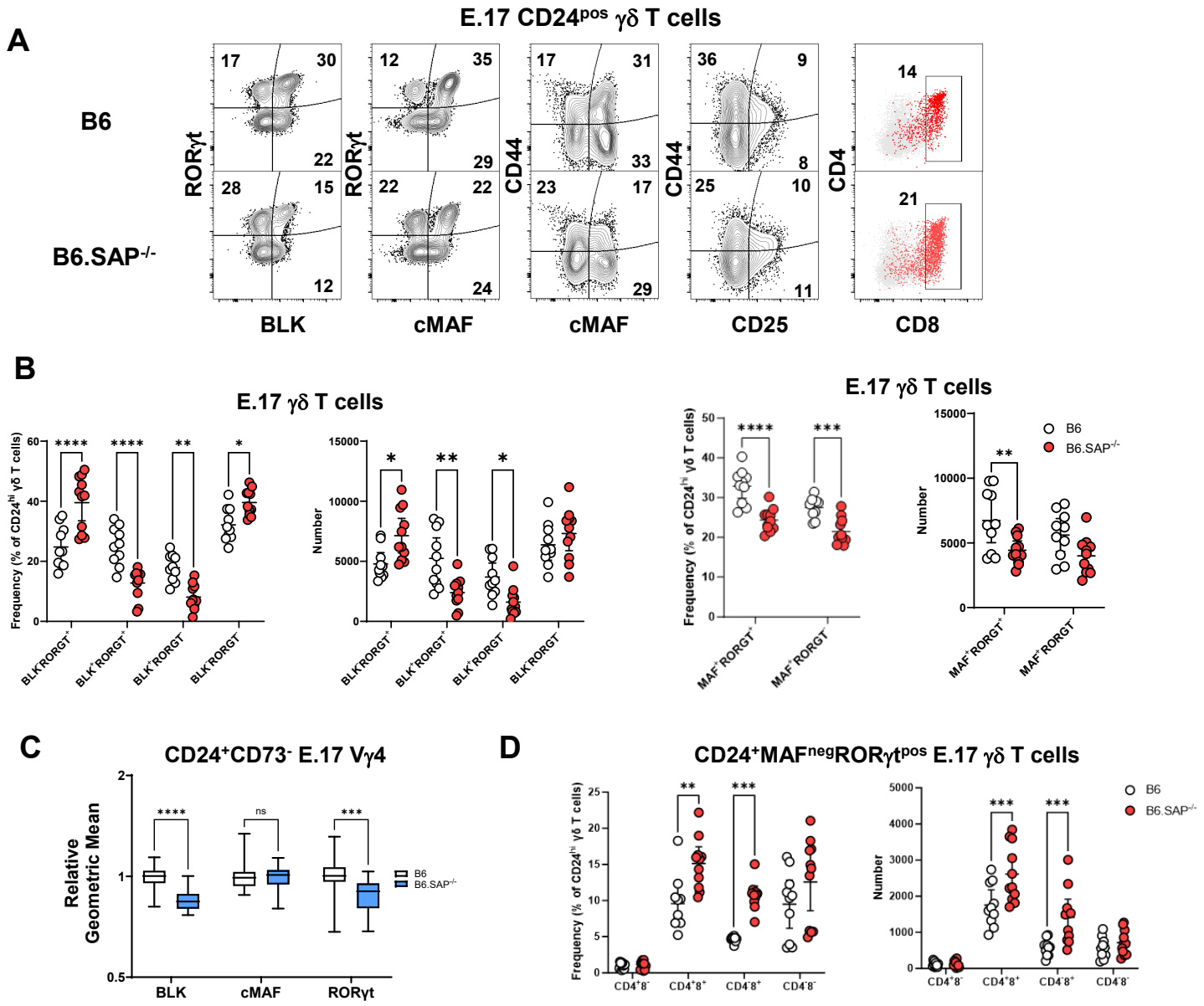
A
E.17 CD24pos γδ T cells
B6
B6.SAP-/-
RORγt
CD44
CD4
BLK
cMAF
CD25
CD8
B
E.17 γδ T cells
Frequency (% of CD24hi γδ T cells)
Number
BLK+RORGT+
BLK+RORGT-
BLK-RORGT+
BLK-RORGT-
MAF+RORGT+
MAF+RORGT-
B6
B6.SAP-/-
C
CD24+CD73- E.17 Vγ4
Relative Geometric Mean
ns
D
CD24+MAFnegRORγtpos E.17 γδ T cells
CD4+8-
CD4+8+
CD4-8+
CD4-8-

Figure 3

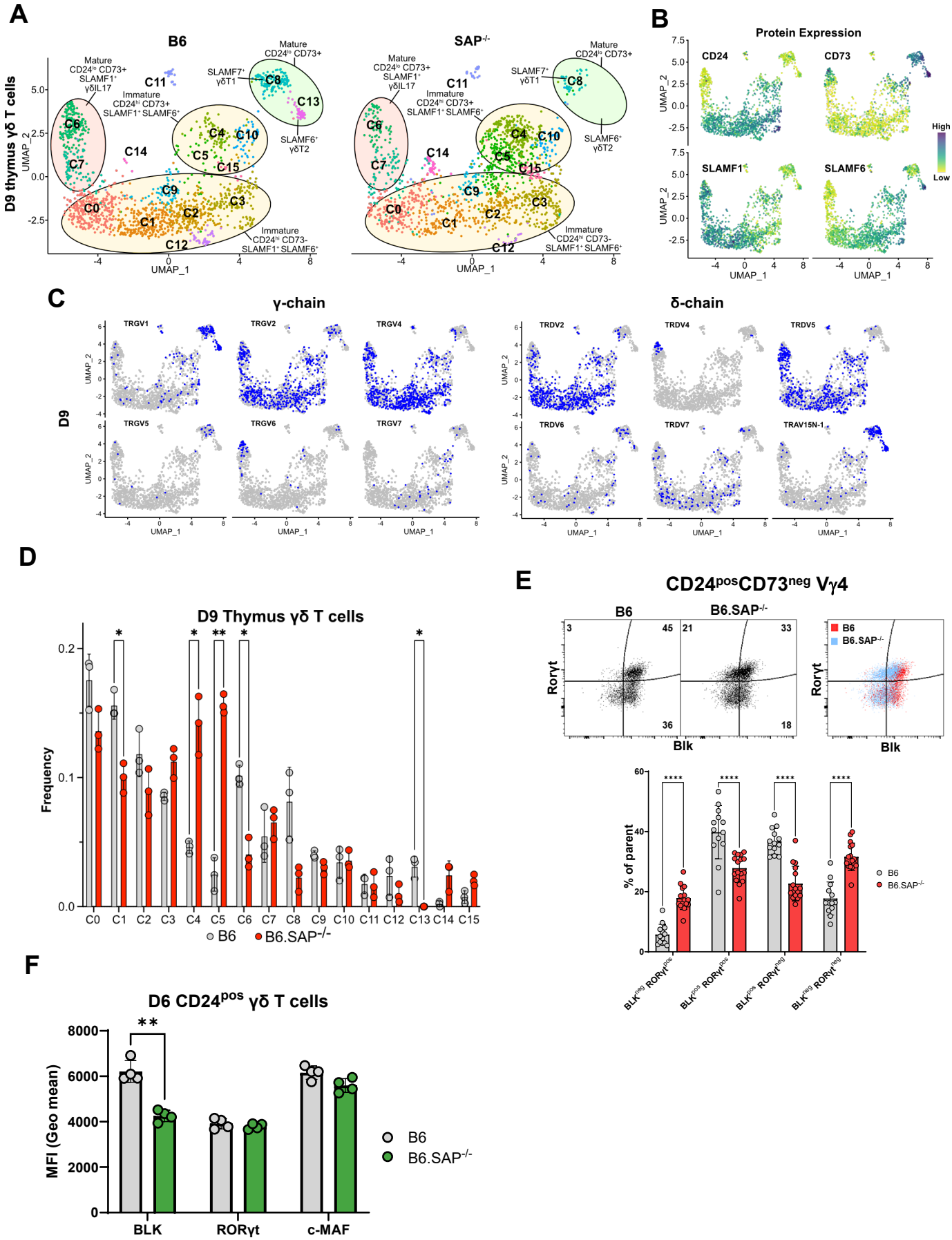
A
B6
SAP-/-
D9 thymus γδ T cells
Mature CD24lo CD73+ SLAMF1+ γδIL17
Immature CD24hi CD73+ SLAMF1+ SLAMF6+
Mature CD24lo CD73+
SLAMF7+ γδT1
SLAMF6+ γδT2
Immature CD24hi CD73- SLAMF1+ SLAMF6+
UMAP_1
UMAP_2
B
Protein Expression
CD24
CD73
SLAMF1
SLAMF6
High
Low
C
γ-chain
δ-chain
D9
TRGV1
TRGV2
TRGV4
TRGV5
TRGV6
TRGV7
TRDV2
TRDV4
TRDV5
TRDV6
TRDV7
TRAV15N-1
D
D9 Thymus γδ T cells
Frequency
B6
B6.SAP-/-
E
CD24posCD73neg Vγ4
B6
B6.SAP-/-
Roryt
Blk
% of parent
BLKneg RORγtpos
BLKpos RORγtpos
BLKpos RORγtneg
BLKneg RORγtneg
F
D6 CD24pos γδ T cells
MFI (Geo mean)
BLK
RORγt
c-MAF

Figure 4

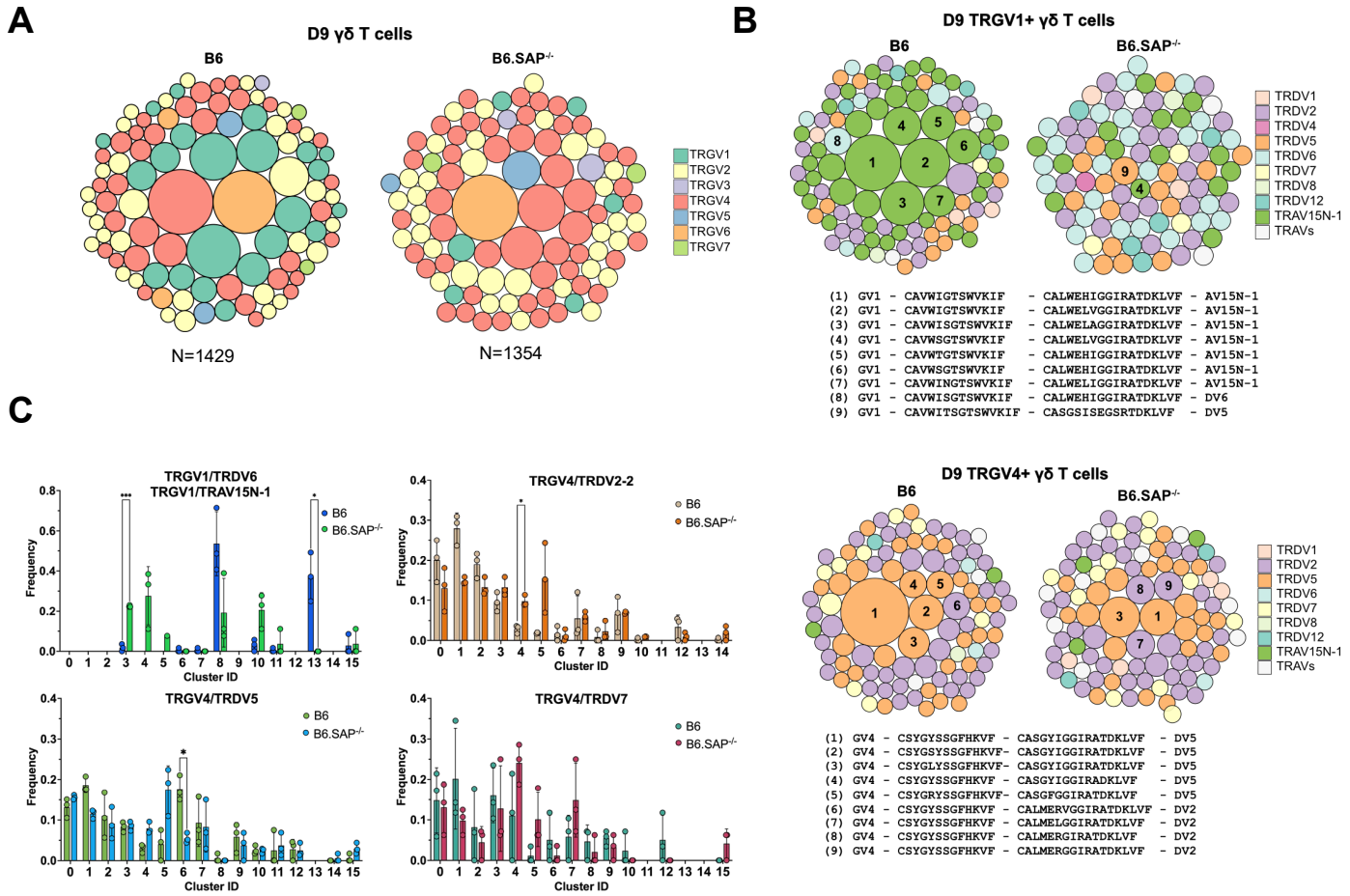
A
D9 γδ T cells
B6
B6.SAP-/-
TRGV1
TRGV2
TRGV3
TRGV4
TRGV5
TRGV6
TRGV7
N=1429
N=1354
B
D9 TRGV1+ γδ T cells
B6
B6.SAP-/-
TRDV1
TRDV2
TRDV4
TRDV5
TRDV6
TRDV7
TRDV8
TRDV12
TRAV15N-1
TRAVs
(1) GV1 - CAVWIGTSWVKIF - CALWEHIGGIRATDKLVF - AV15N-1
(2) GV1 - CAVWIGTSWVKIF - CALWELVGGIRATDKLVF - AV15N-1
(3) GV1 - CAVWISGTSWVKIF - CALWELAGGIRATDKLVF - AV15N-1
(4) GV1 - CAVWSGTSWVKIF - CALWELVGGIRATDKLVF - AV15N-1
(5) GV1 - CAVWTGTSWVKIF - CALWEHIGGIRATDKLVF - AV15N-1
(6) GV1 - CAVWSGTSWVKIF - CALWEHIGGIRATDKLVF - AV15N-1
(7) GV1 - CAVWINGTSWVKIF - CALWELIGGIRATDKLVF - AV15N-1
(8) GV1 - CAVWISGTSWVKIF - CALWEHIGGIRATDKLVF - DV6
(9) GV1 - CAVWITSGTSWVKIF - CASGSISEGSRTDKLVF - DV5
C
TRGV1/TRDV6
TRGV1/TRAV15N-1
TRGV4/TRDV2-2
TRGV4/TRDV5
TRGV4/TRDV7
B6
B6.SAP-/-
Frequency
Cluster ID
D9 TRGV4+ γδ T cells
B6
B6.SAP-/-
TRDV1
TRDV2
TRDV5
TRDV6
TRDV7
TRDV8
TRDV12
TRAV15N-1
TRAVs
(1) GV4 - CSYGYSSGFHKVF - CASGYIGGIRATDKLVF - DV5
(2) GV4 - CSYGSYSSGFHKVF- CASGYIGGIRATDKLVF - DV5
(3) GV4 - CSYGLYSSGFHKVF- CASGYIGGIRATDKLVF - DV5
(4) GV4 - CSYGYSSGFHKVF - CASGYIGGIRADKLVF - DV5
(5) GV4 - CSYGRYSSGFHKVF- CASGFGGIRATDKLVF - DV5
(6) GV4 - CSYGYSSGFHKVF - CALMERVGGIRATDKLVF - DV2
(7) GV4 - CSYGYSSGFHKVF - CALMELGGIRATDKLVF - DV2
(8) GV4 - CSYGYSSGFHKVF - CALMERGIRATDKLVF - DV2
(9) GV4 - CSYGYSSGFHKVF - CALMERGGIRATDKLVF - DV2

Figure 5

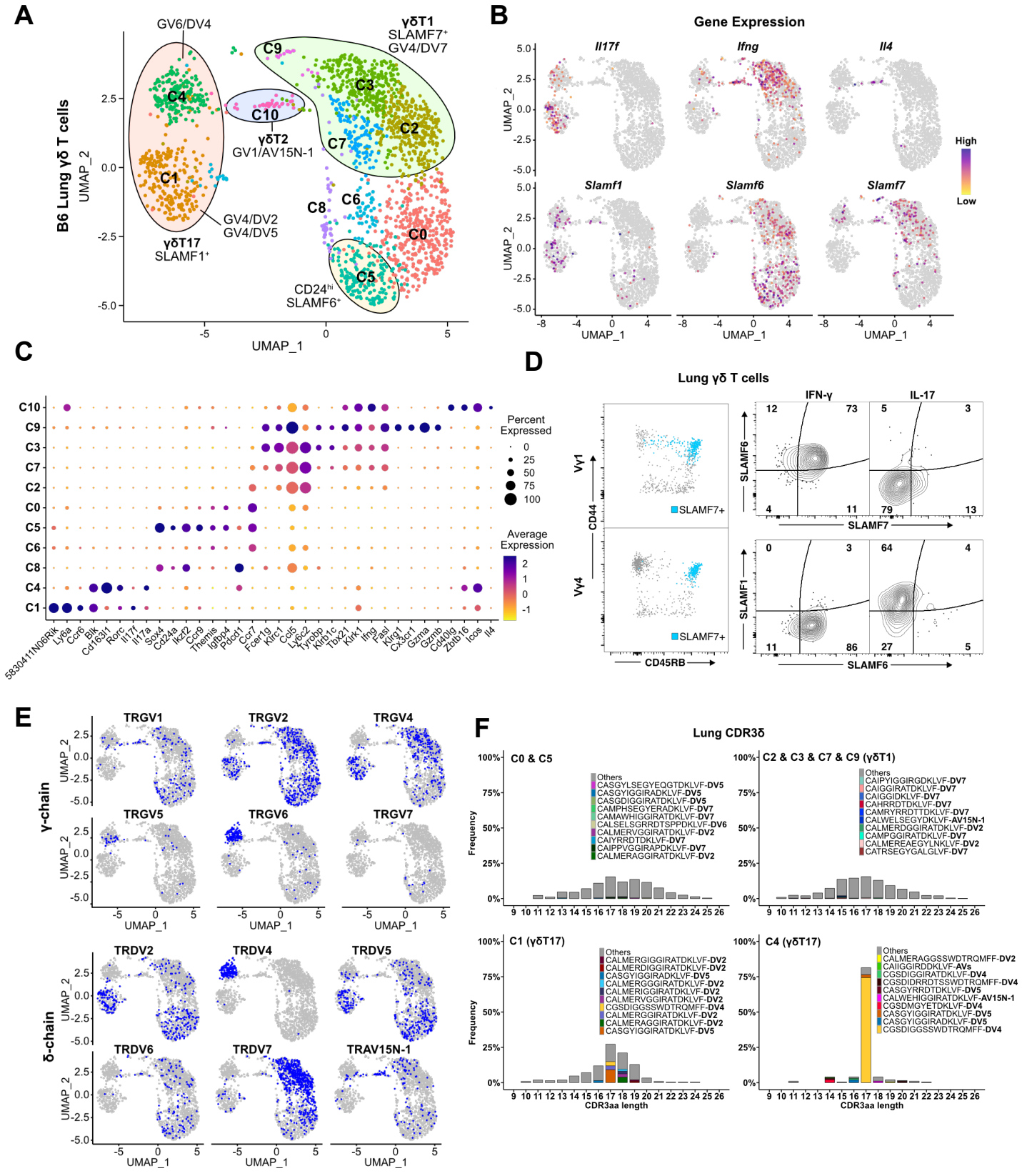
A
B6 Lung γδ T cells
GV6/DV4
γδT1
SLAMF7+
GV4/DV7
γδT2
GV1/AV15N-1
GV4/DV2
GV4/DV5
γδT17
SLAMF1+
CD24hi
SLAMF6+
C0
C1
C2
C3
C4
C5
C6
C7
C8
C9
C10
UMAP_1
UMAP_2
B
Gene Expression
Il17f
Ifng
Il4
Slamf1
Slamf6
Slamf7
High
Low
C
Percent Expressed
Average Expression
5830411N06Rik
Lyl6a
Ccr6
Blk
Cd163l1
Rorc
Il17f
Il17a
Sox4
Cd24a
Ikzf2
Ccr9
Themis
Igfbp4
Pdcd1
Ccr7
Fcer1g
Klrc1
Ccl5
Ly6c2
Tyrobp
Klrb1c
Tbx21
Klrk1
Ifng
Fasl
Klrg1
Cx3cr1
Gzma
Gzmb
Cd40lg
Zbtb16
Icos
Il4
D
Lung γδ T cells
IFN-γ
IL-17
Vγ1
Vγ4
CD44
CD45RB
SLAMF7+
SLAMF6
SLAMF7
SLAMF1
E
γ-chain
δ-chain
TRGV1
TRGV2
TRGV4
TRGV5
TRGV6
TRGV7
TRDV2
TRDV4
TRDV5
TRDV6
TRDV7
TRAV15N-1
F
Lung CDR3δ
C0 & C5
C2 & C3 & C7 & C9 (γδT1)
C1 (γδT17)
C4 (γδT17)
Frequency
CDR3aa length

Figure 6

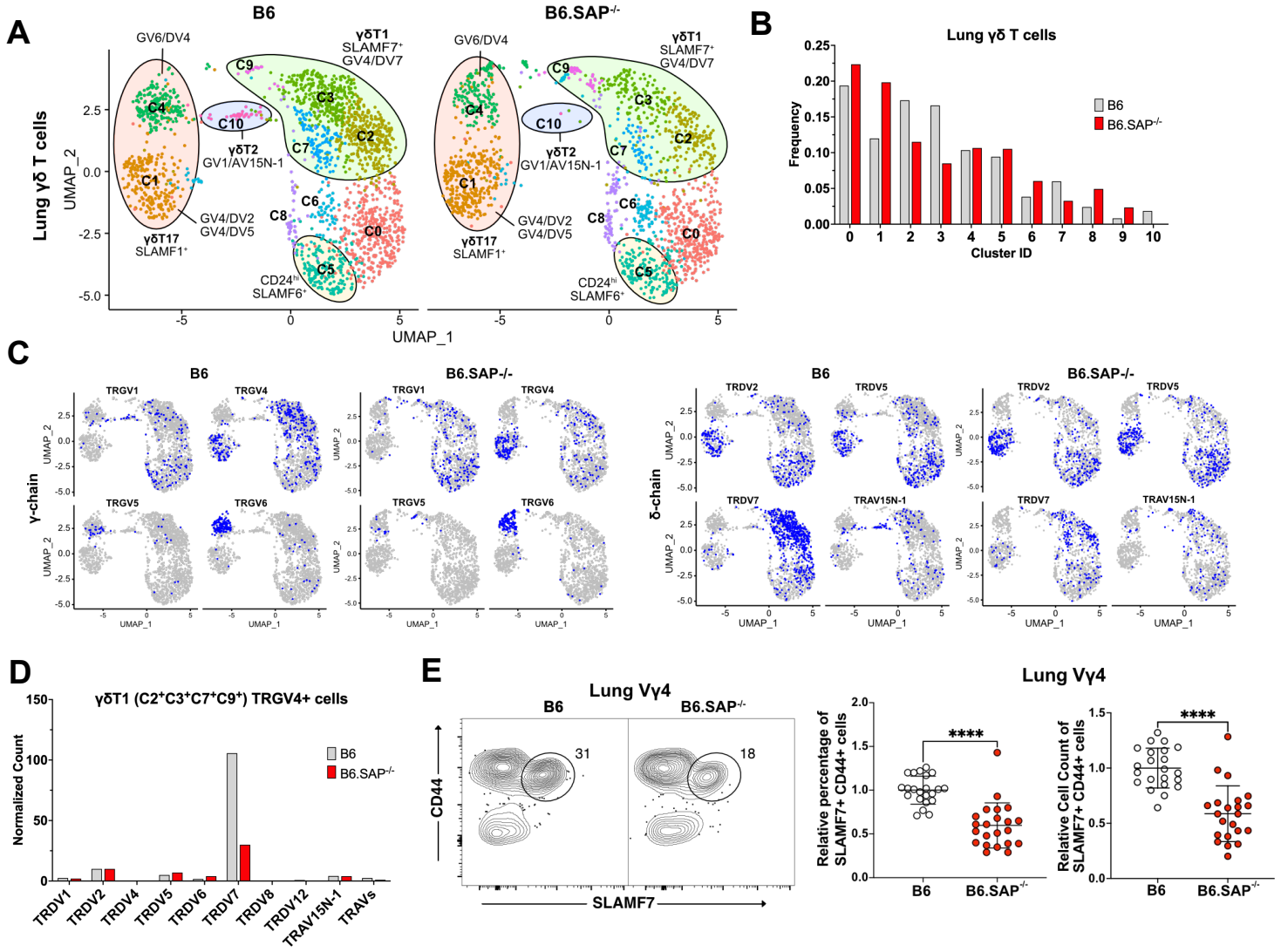
A
B6
B6.SAP-/-
Lung γδ T cells
UMAP_2
UMAP_1
GV6/DV4
γδT1
SLAMF7+
GV4/DV7
γδT2
GV1/AV15N-1
GV4/DV2
GV4/DV5
γδT17
SLAMF1+
CD24hi
SLAMF6+
C0
C1
C2
C3
C4
C5
C6
C7
C8
C9
C10
B
Lung γδ T cells
Frequency
Cluster ID
B6
B6.SAP-/-
C
γ-chain
δ-chain
TRGV1
TRGV4
TRGV5
TRGV6
TRDV2
TRDV5
TRDV7
TRAV15N-1
D
γδT1 (C2+C3+C7+C9+) TRGV4+ cells
Normalized Count
TRDV1
TRDV2
TRDV4
TRDV5
TRDV6
TRDV7
TRDV8
TRDV12
TRAV15N-1
TRAVs
E
Lung Vγ4
CD44
SLAMF7
31
18
Relative percentage of SLAMF7+ CD44+ cells
Relative Cell Count of SLAMF7+ CD44+ cells
****

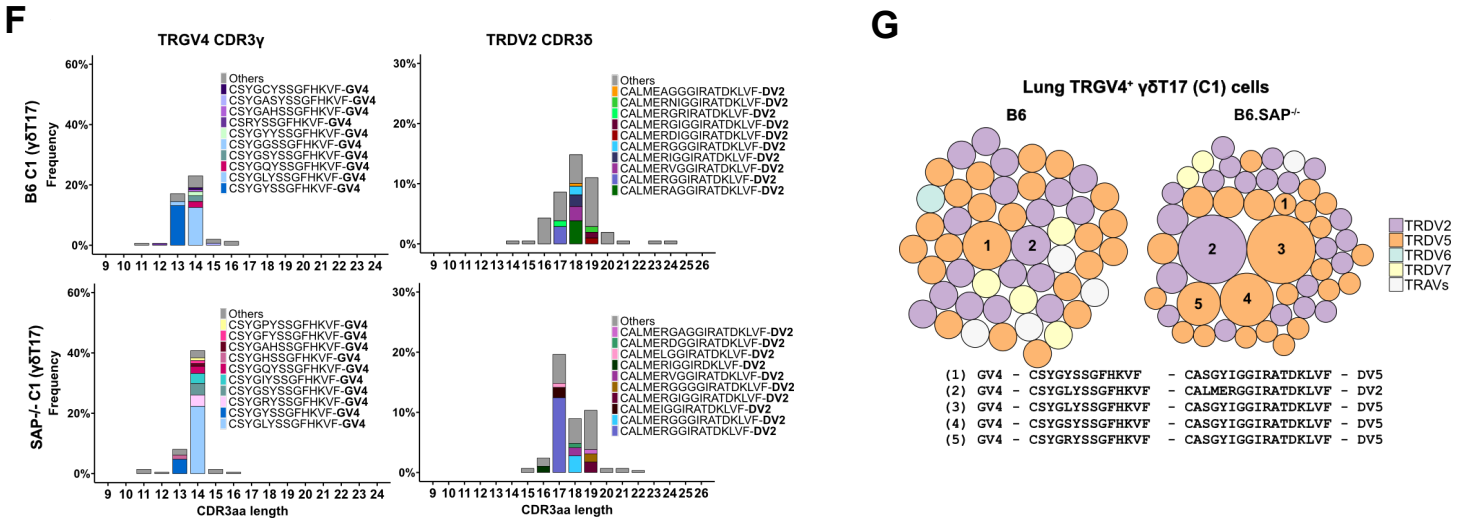
F
TRGV4 CDR3γ
TRDV2 CDR3δ
B6 C1 (γδT17) Frequency
SAP-/- C1 (γδT17) Frequency
Others
CSYGCYSSGFHKVF-GV4
CSYGASYSSGFHKVF-GV4
CSYGAHSSGFHKVF-GV4
CSRYSSGFHKVF-GV4
CSYGYYSSGFHKVF-GV4
CSYGGSSGFHKVF-GV4
CSYGSYSSGFHKVF-GV4
CSYGQYSSGFHKVF-GV4
CSYGLYSSGFHKVF-GV4
CSYGYSSGFHKVF-GV4
CALMEAGGGIRATDKLVF-DV2
CALMERNIGGIRATDKLVF-DV2
CALMERGRIRATDKLVF-DV2
CALMERGIGGIRATDKLVF-DV2
CALMERDIGGIRATDKLVF-DV2
CALMERGGGIRATDKLVF-DV2
CALMERIGGIRATDKLVF-DV2
CALMERVGGIRATDKLVF-DV2
CALMERGGIRATDKLVF-DV2
CALMERAGGIRATDKLVF-DV2
CSYGPYSSGFHKVF-GV4
CSYGFYSSGFHKVF-GV4
CSYGAHSSGFHKVF-GV4
CSYGHSSGFHKVF-GV4
CSYGQYSSGFHKVF-GV4
CSYGIYSSGFHKVF-GV4
CSYGSYSSGFHKVF-GV4
CSYGRYSSGFHKVF-GV4
CSYGYSSGFHKVF-GV4
CSYGLYSSGFHKVF-GV4
CALMERGAGGIRATDKLVF-DV2
CALMERDGGIRATDKLVF-DV2
CALMELGGIRATDKLVF-DV2
CALMERIGGIRDKLVF-DV2
CALMERVGGIRATDKLVF-DV2
CALMERGGGIRATDKLVF-DV2
CALMEIGGIRATDKLVF-DV2
CALMERGGGIRATDKLVF-DV2
CALMERGGIRATDKLVF-DV2
CDR3aa length
G
Lung TRGV4+ γδT17 (C1) cells
B6
B6.SAP-/-
TRDV2
TRDV5
TRDV6
TRDV7
TRAVs
(1) GV4 - CSYGYSSGFHKVF - CASGYIGGIRATDKLVF - DV5
(2) GV4 - CSYGLYSSGFHKVF - CALMERGGIRATDKLVF - DV2
(3) GV4 - CSYGLYSSGFHKVF - CASGYIGGIRATDKLVF - DV5
(4) GV4 - CSYGSYSSGFHKVF - CASGYIGGIRATDKLVF - DV5
(5) GV4 - CSYGRYSSGFHKVF - CASGYIGGIRATDKLVF - DV5

Figure 7

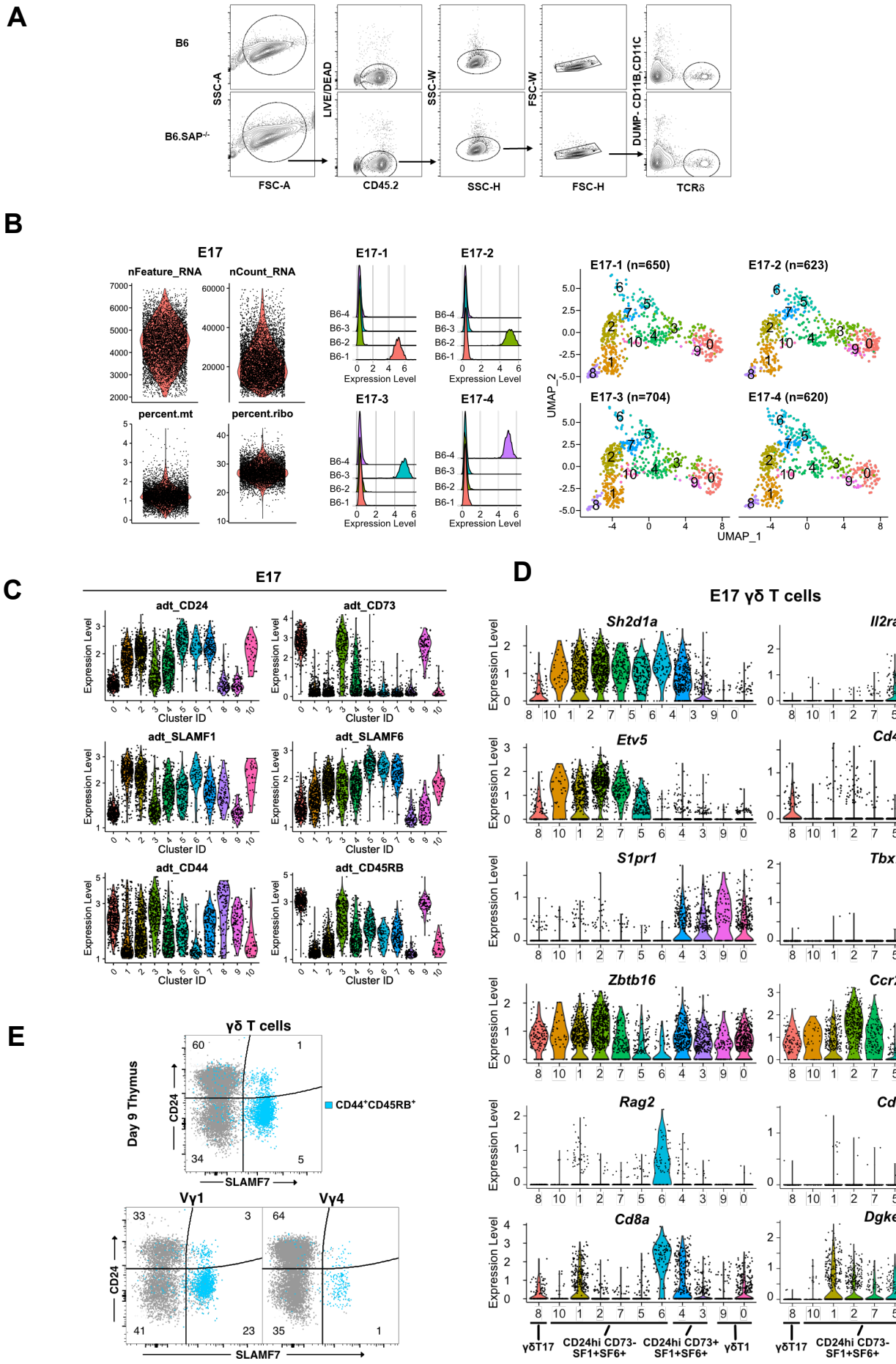

Supplemental Fig. 1

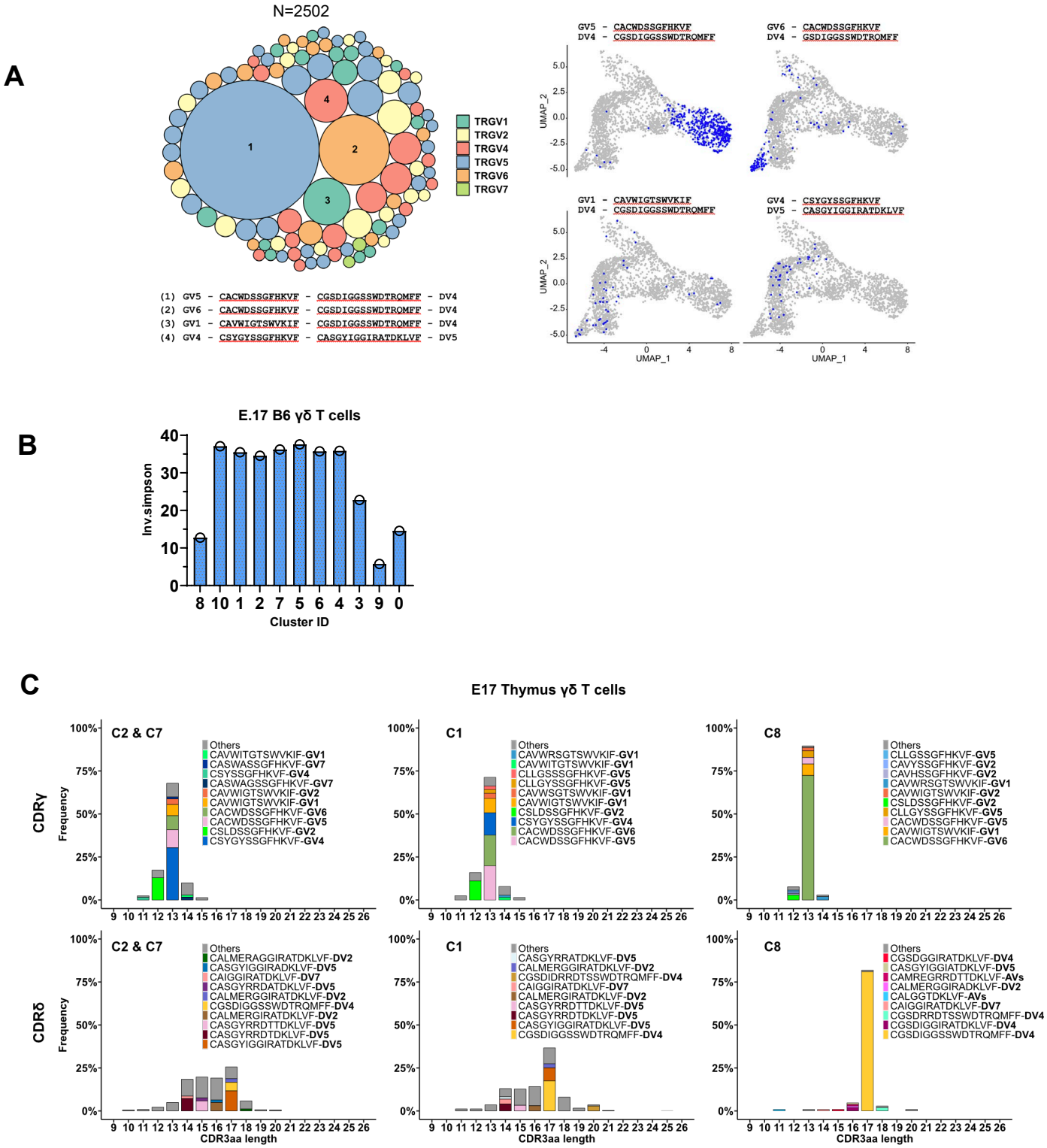

Supplemental Fig. 2

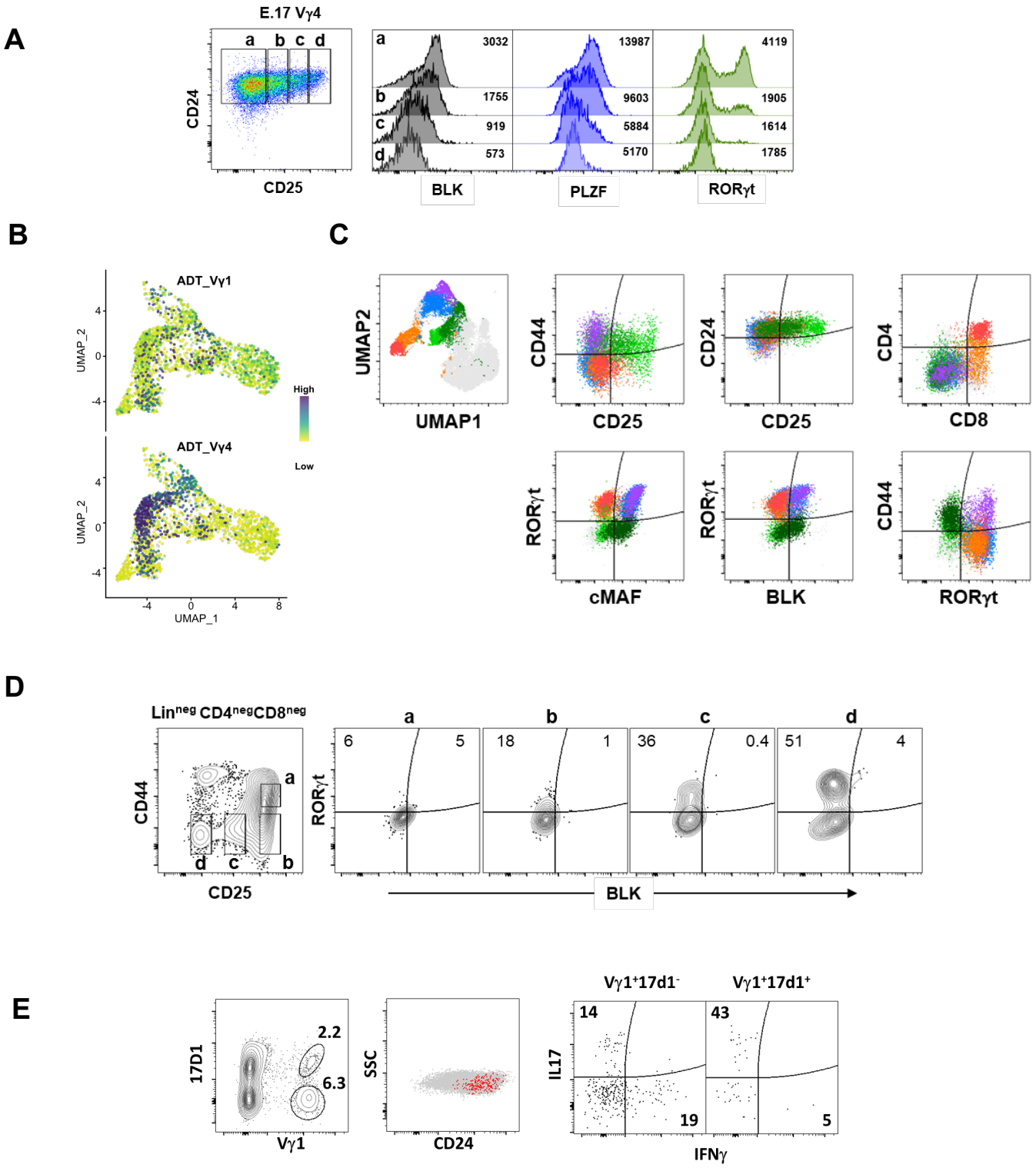

Supplemental Fig 3

A

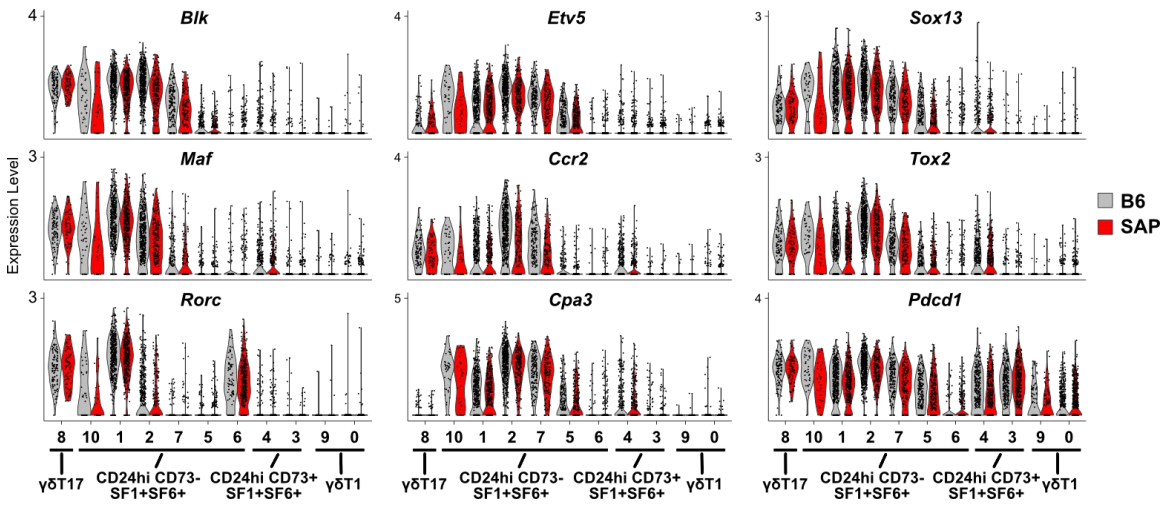

B

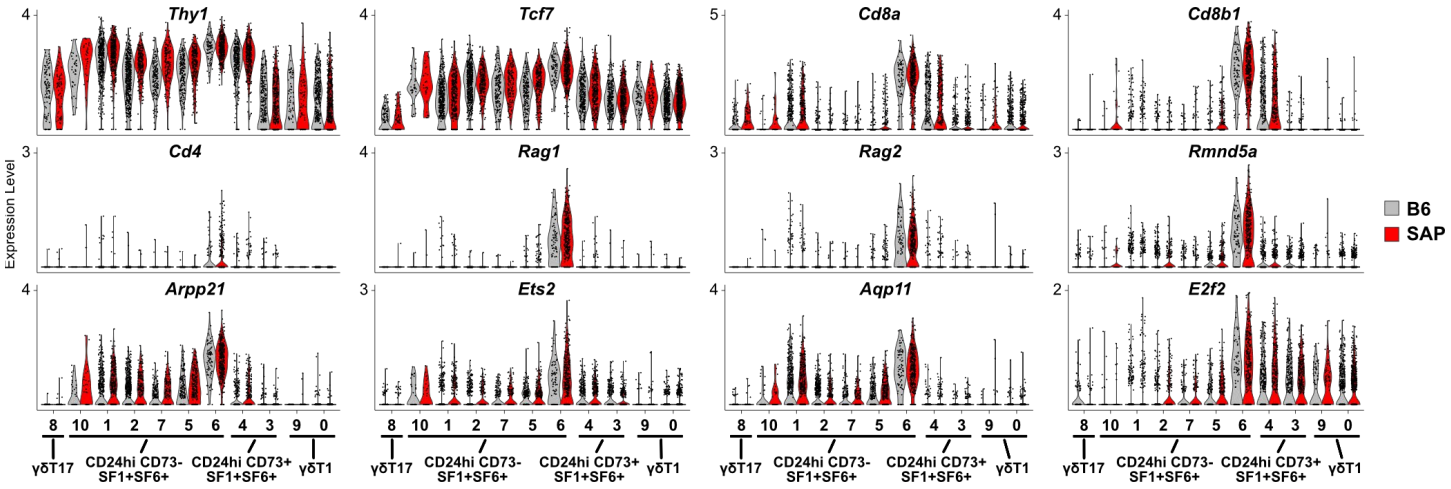

Supplemental Fig 4

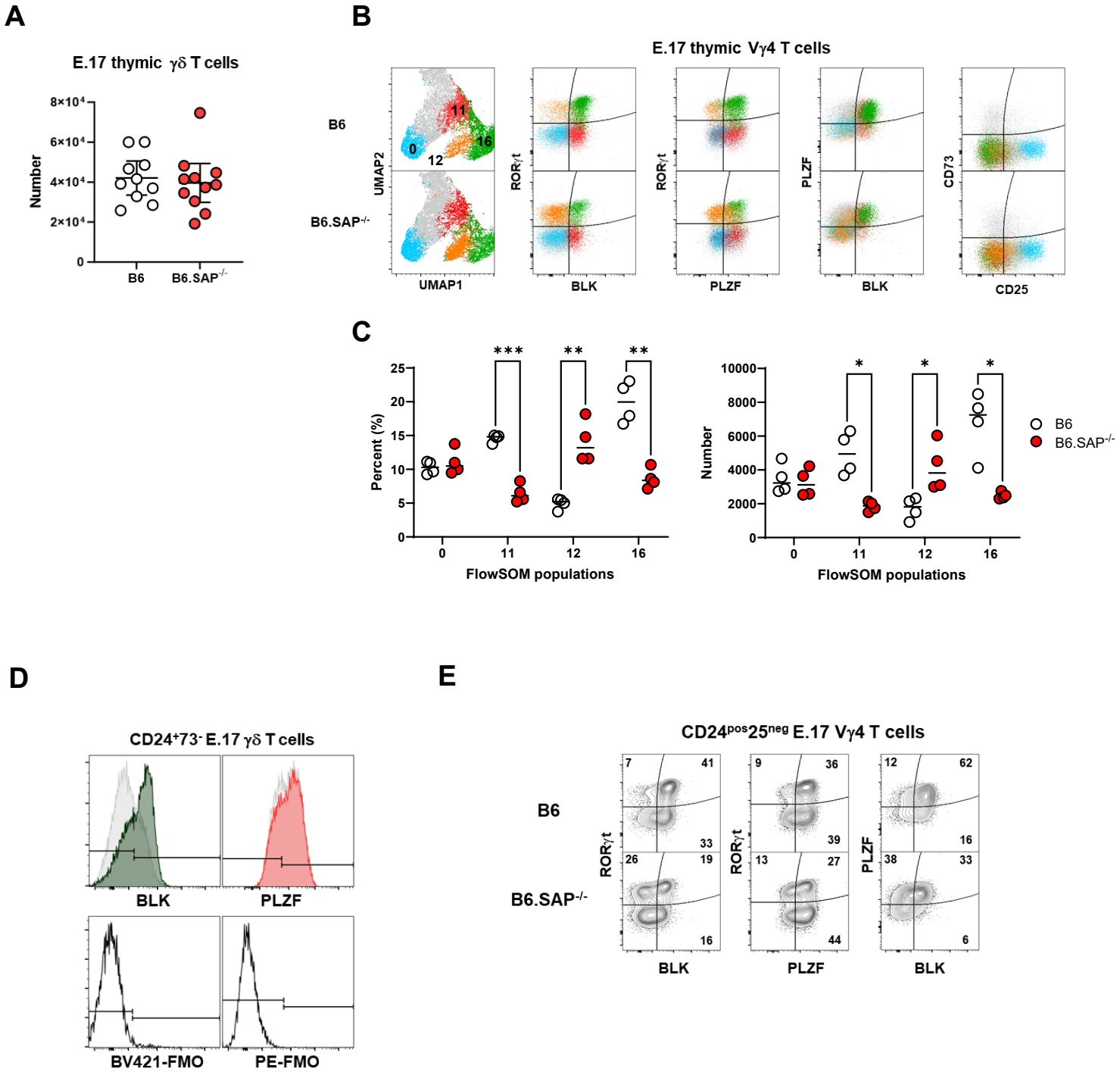
A
E.17 thymic γδ T cells
Number
8×10⁴
6×10⁴
4×10⁴
2×10⁴
0
B6
B6.SAP-/-
B
E.17 thymic Vγ4 T cells
B6
B6.SAP-/-
UMAP2
UMAP1
0
11
12
16
RORγt
BLK
PLZF
CD73
CD25
C
Percent (%)
Number
FlowSOM populations
***
**
*
B6
B6.SAP-/-
D
CD24+73- E.17 γδ T cells
BLK
PLZF
BV421-FMO
PE-FMO
E
CD24pos25neg E.17 Vγ4 T cells
B6
B6.SAP-/-
RORγt
PLZF
BLK
7
41
33
26
19
16
9
36
39
13
27
44
12
62
16
38
33
6

Suppl. Fig. 5

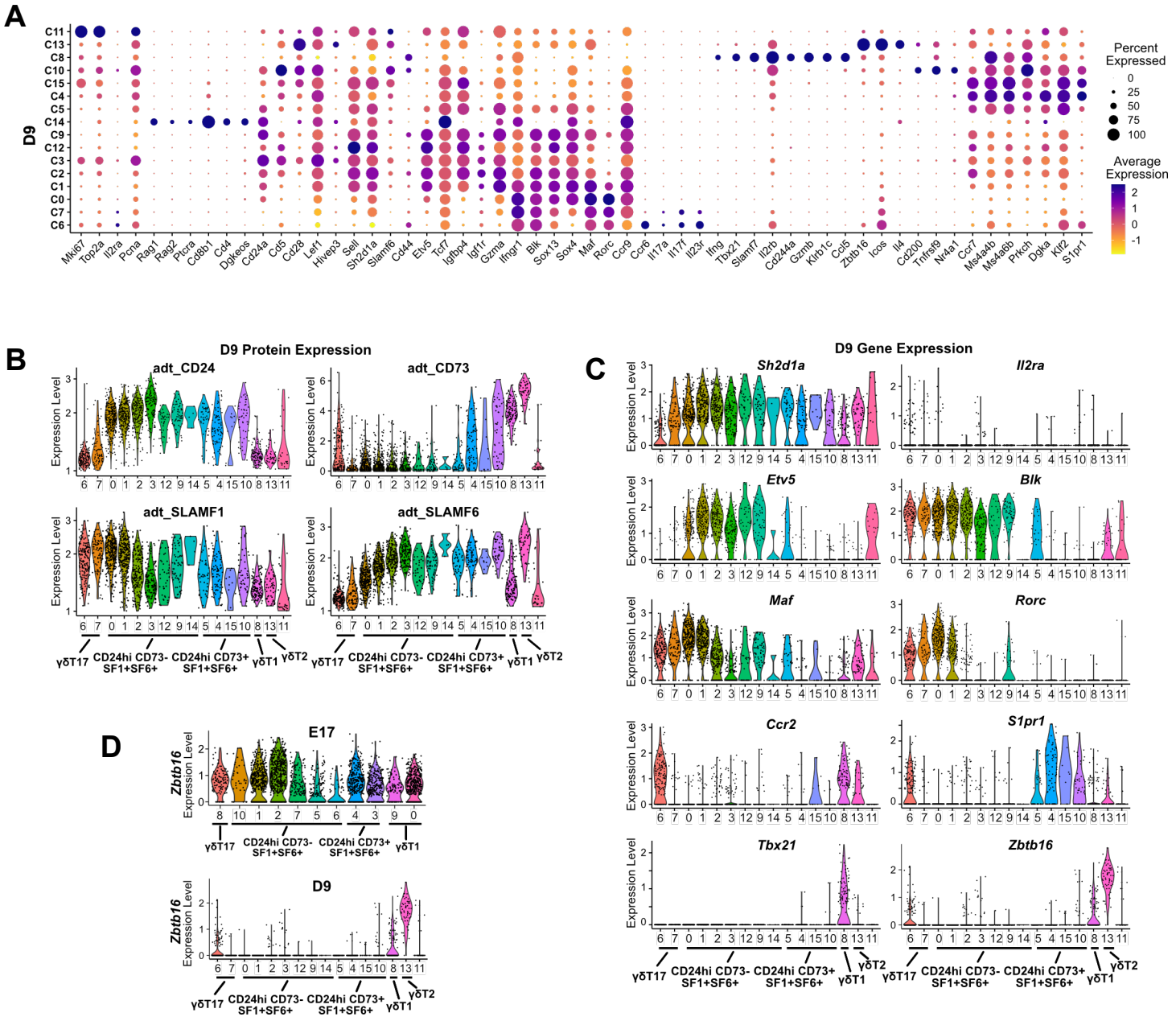
A
D9
C11
C13
C8
C10
C15
C4
C5
C14
C9
C12
C3
C2
C1
C0
C7
C6
Mki67 Top2a Il2ra Pcna Rag1 Rag2 Ptcra Cd8b1 Cd4 Dgkeos Cd24a Cd5 Cd28 Lef1 Hivep3 Sell Sh2d1a Slamf6 Cd44 Etv5 Tcf7 Igfbp4 Igf1r Gzma Ifngr1 Blk Sox13 Sox4 Maf Rorc Ccr9 Ccr6 Il17a Il17f Il23r Ifng Tbx21 Slamf7 Il2rb Cd244a Gzmb Klrb1c Cd6 Zbtb16 Icos Il4 Cd200 Tnfrsf9 Nr4a1 Ccr7 Ms4a4b Ms4a6b Prkch Dgka Klf2 S1pr1
Percent Expressed
0
25
50
75
100
Average Expression
2
1
0
-1
B
D9 Protein Expression
adt_CD24
adt_CD73
adt_SLAMF1
adt_SLAMF6
Expression Level
6 7 0 1 2 3 12 9 14 5 4 15 10 8 13 11
γδT17
CD24hi CD73- SF1+SF6+
CD24hi CD73+ SF1+SF6+
γδT1
γδT2
C
D9 Gene Expression
Sh2d1a
Il2ra
Etv5
Blk
Maf
Rorc
Ccr2
S1pr1
Tbx21
Zbtb16
D
E17
Zbtb16
Expression Level
8 10 1 2 7 5 6 4 3 9 0
D9

Suppl. Fig. 6

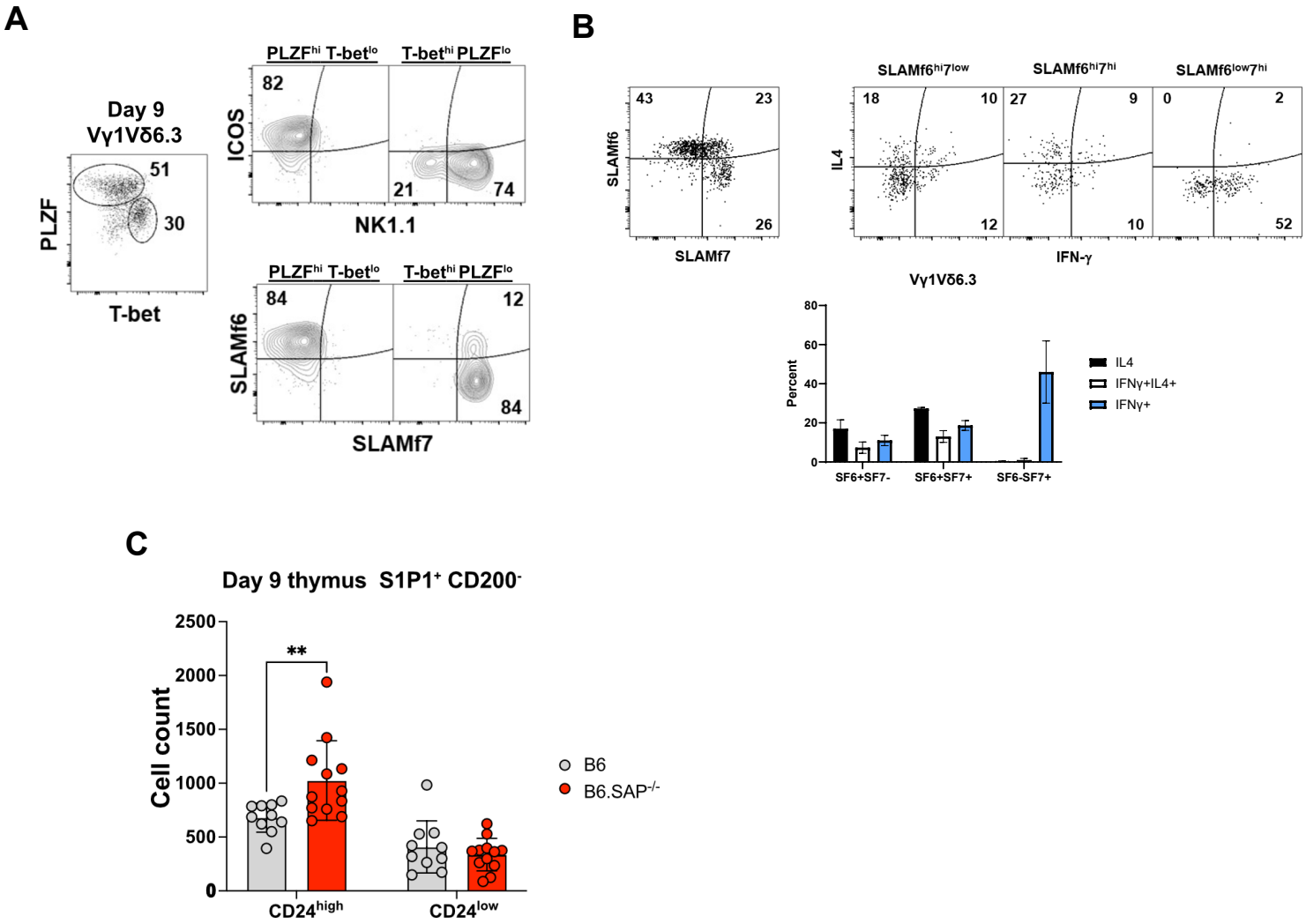
A
Day 9
Vγ1Vδ6.3
PLZF
T-bet
51
30
PLZFhi T-bethi
T-bethi PLZFlo
ICOS
NK1.1
82
21
74
SLAMf6
SLAMf7
84
12
84
B
SLAMf6
SLAMf7
43
23
26
SLAMf6hi7low
SLAMf6hi7hi
SLAMf6low7hi
IL4
IFN-γ
18
10
12
27
9
10
0
2
52
Vγ1Vδ6.3
Percent
IL4
IFNγ+IL4+
IFNγ+
SF6+SF7-
SF6+SF7+
SF6-SF7+
C
Day 9 thymus S1P1+ CD200-
Cell count
**
B6
B6.SAP-/-
CD24high
CD24low

Suppl. Fig. 7

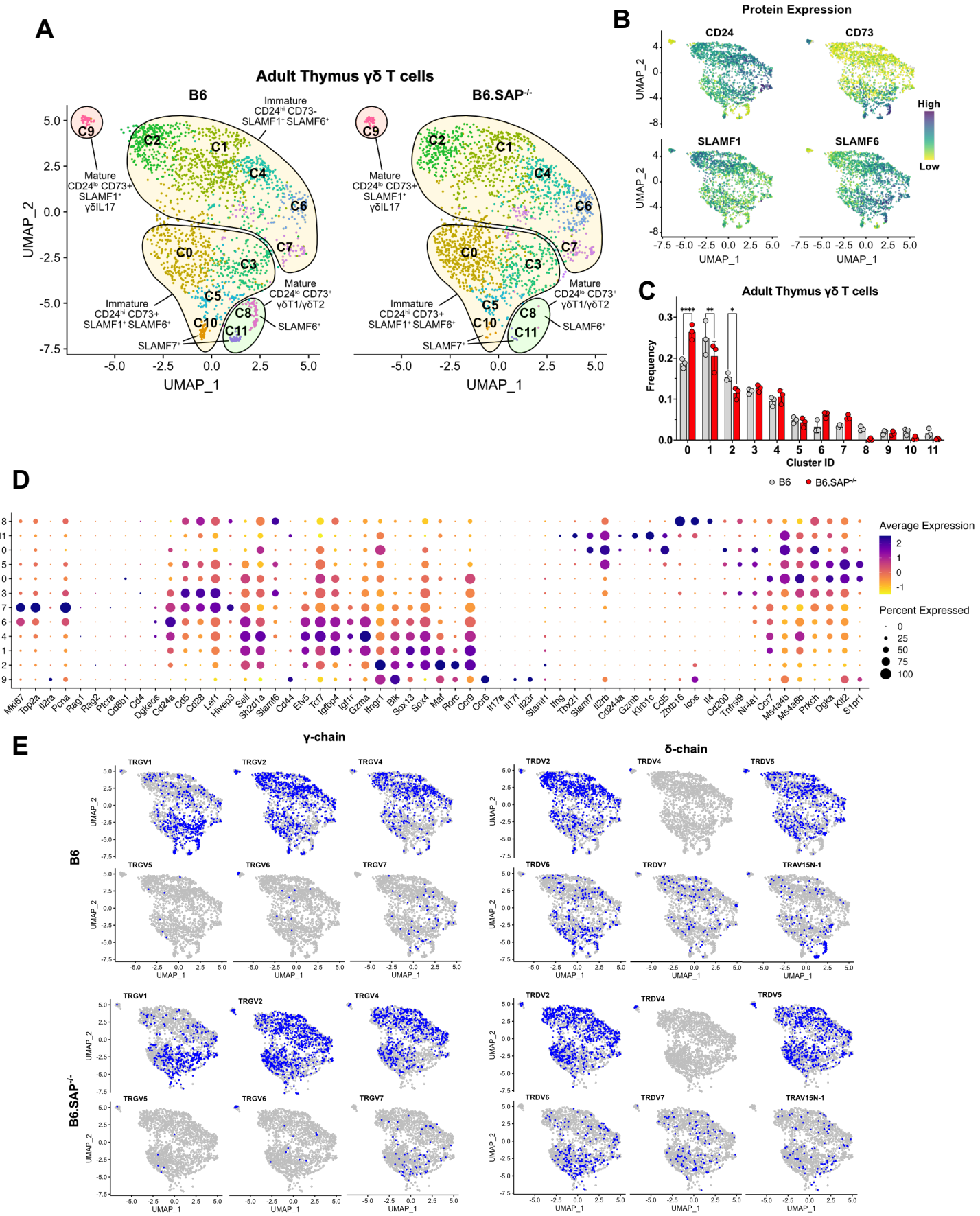

Supplemental Fig 8

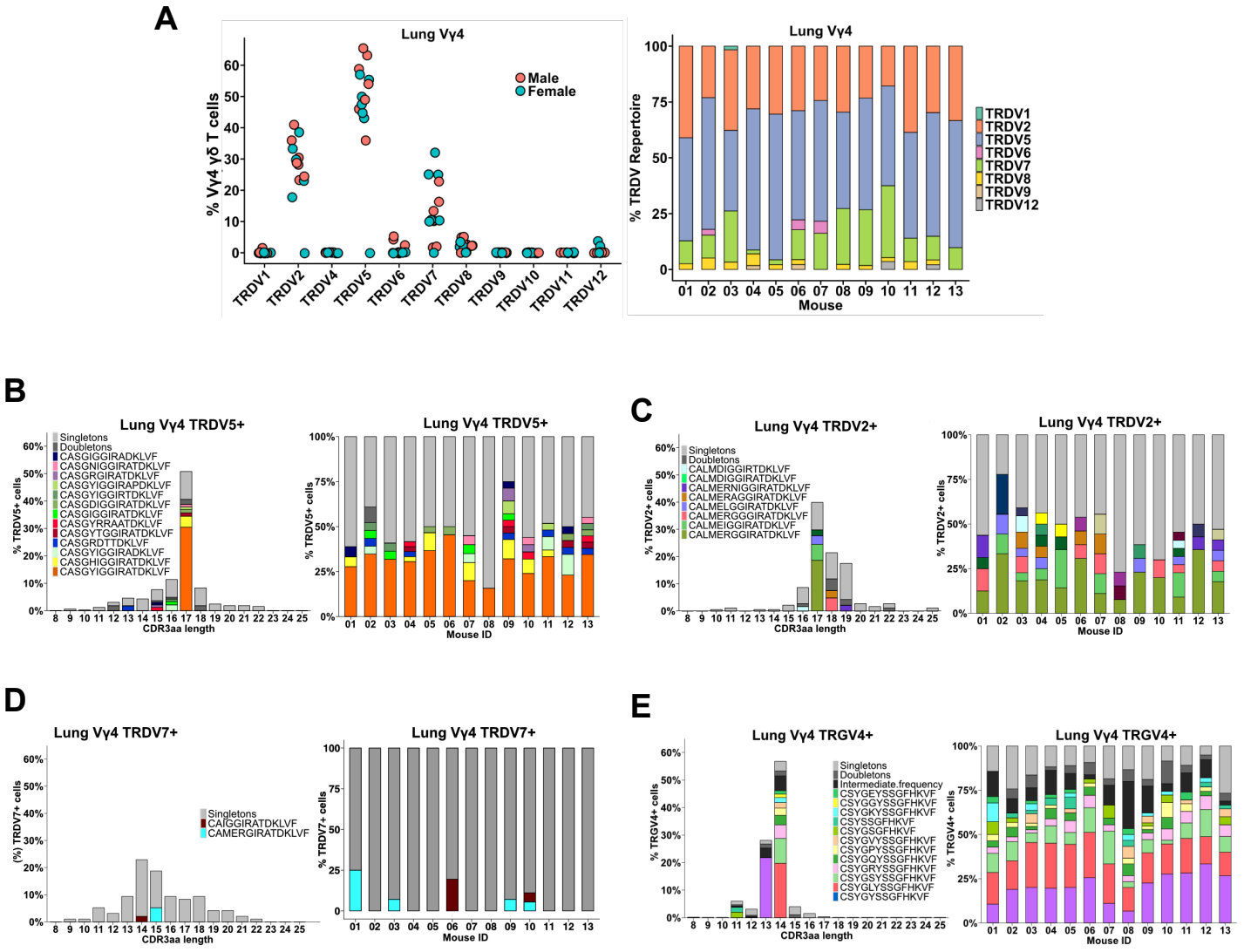

Supplemental Fig 9

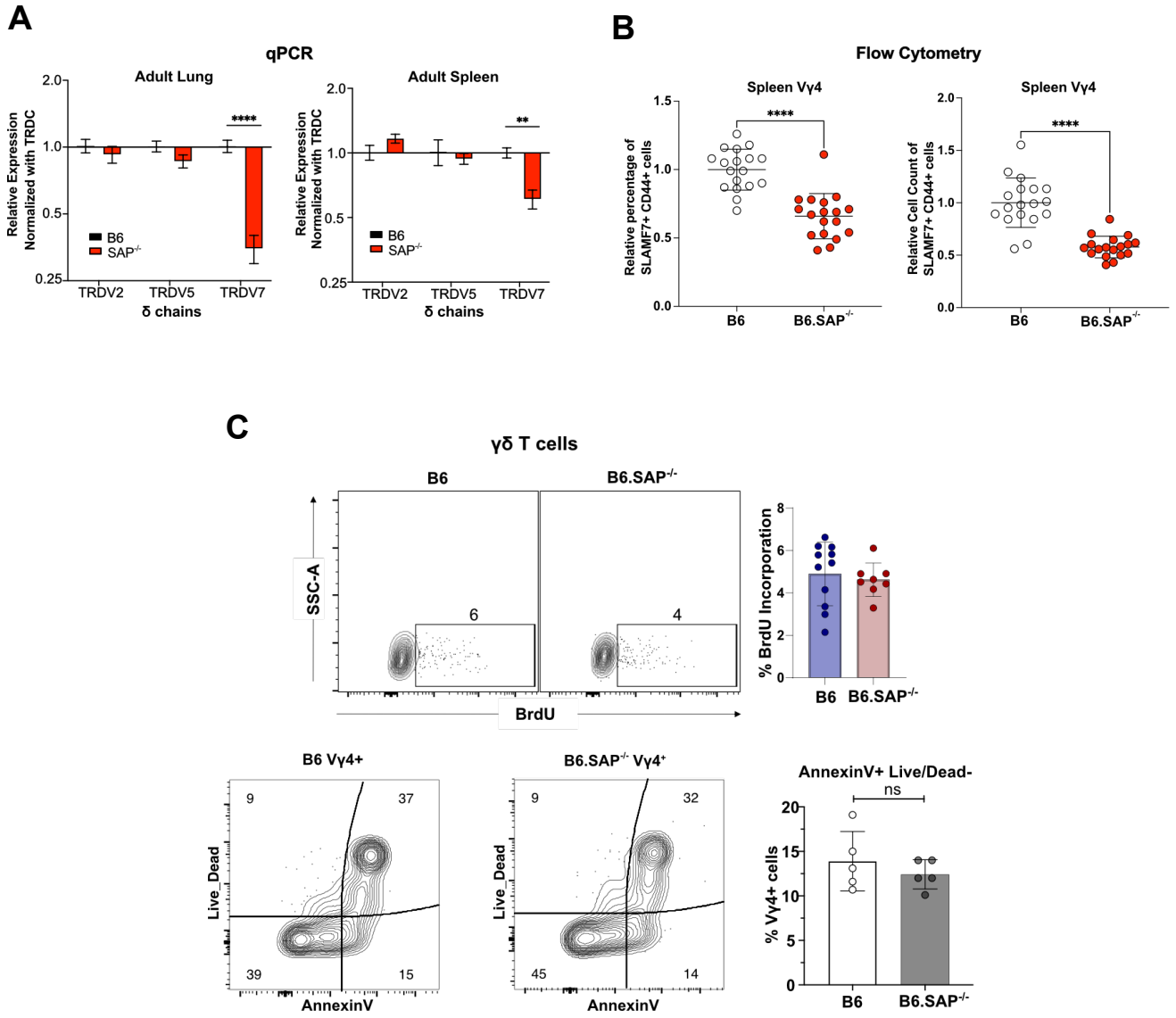

Supplemental Fig 10